Watershed Physical Processes Research Unit
National Sedimentation Laboratory
Oxford, MS 38655

Above Ground Plots at the MAFES-Holly Springs Experiment Station for Studying Impacts of Seepage on Erosion

G.V. Wilson[1], R.R. Wells[1], S.M. Dabney[1], H.G. Momm[1], A.J. Hudspeth[1], E.A. Gregory[1] and R. Saunders[2]

[1] Watershed Physical Processes Research Unit
[2] Mississippi Agricultural and Forestry Experiment Station

NSL Technical Report No. 78 March 2012

Table of Contents

LIST OF FIGURES

LIST OF TABLES

Above Ground Plots at the MAFES-Holly Springs Experiment Station for Studying Impacts of Seepage on Erosion

EXECUTIVE SUMMARY

Sediment is the most common contaminant causing impairment of streams in the United States. In many areas, the dominant source of sediment is gully erosion. Consideration for subsurface flow contributions to these erosion processes has largely been neglected in assessments and prediction technologies due to the lack of experimental observations and insufficient understanding of the governing processes. A common feature often associated with subsurface flow contributing to gully initiation is the occurrence of a water-restricting layer that perches water. The objective of this report is to describe facilities constructed at the North Mississippi Branch of the Mississippi Agriculture and Forestry Experiment Station (MAFES) at Holly Springs, Mississippi (HSES) to study seepage effects on runoff, erosion, and gully formation under a variety of topographic, soil, land use, and erosion control conditions. Six existing plots at HSES were selected for conversion into above ground seepage erosion plots because of existing runoff collection and measurement systems. By utilizing a common inner wall, the new above ground plots were enlarged to 5.49 m wide and elongated from the endplate upslope to 18.29 m to produce a 0.1 ha plot area. In addition, the sidewalls were elevated with distance from the endplate to change the slope from the original 3.1% to 10.0%. The back wall was designed to contain a water reservoir for inducing seepage into the plot center (convergent) area. A 15 cm thick compacted clay layer was placed above a base layer and extended from the back wall to 10.7 m downslope then tapered off to 0 m thick at 12.2 m downslope. Loess topsoil material was placed above the clay layer with the depth tapering off from between 45 to 60 cm thick at the back wall, depending upon the surface configuration, down to 0 cm thick where the clay layer reaches the surface at 10.7 m downslope. The above ground facilities described in this report were designed and constructed to fill the knowledge gap in the area of subsurface flow impacts on ephemeral gully erosion. Ephemeral gully erosion is a critical problem that significantly damages and deteriorates agricultural lands worldwide yet little mechanistic work has been done on subsurface flow processes contributing to gully initiation. Basic research and resulting prediction technology are still in the developmental stage. These facilities will enable the quantification of the impact of seepage on erosion rates and gully formation under controlled hydrologic conditions for a wide range of soil and land use conditions.

BACKGROUND

Soil erosion occurs over a continuum of scales ranging from interrill and rill to gully. Interrill erosion is the removal of a fairly uniform layer of soil by raindrop impacts and shallow surface flows. Rill erosion occurs on sloping fields in which numerous and randomly occurring "small" channels of only several centimeters in depth are formed. Gully erosion is caused by concentrated overland flow and/or subsurface flow during and immediately following heavy

rains (Soil Science Society of America, 2008). Ephemeral gullies are defined as small channels eroded by concentrated flow that can be easily filled by normal tillage, only to reform again in the same location by additional runoff events (Soil Science Society of America, 2008). In contrast, a gully (or classical gully) is defined as "deep enough (usually > 0.5 m) to interfere with, and not be obliterated by, normal tillage operations," (Soil Science Society of America, 2008).

According a US EPA report, sediment is the most common contaminant causing impairment of streams in the US (United State Environmental Protection Agency, 2000). In many areas, the dominant source of sediment is gully erosion. Poesen et al. (2003) estimated that, on average, 44% of the total soil erosion worldwide was by gullies, whereas, the USDA-Natural Resource Conservation Service (1997) estimated that 35% of the total soil loss in the United States was by gully erosion. Historically the emphasis of erosion research has been on sheet and rill erosion with the hydrologic focus on surface flow processes. Consideration for subsurface flow contributions to these erosion processes has largely been neglected in assessments and prediction technologies due to the lack of experimental observations and insufficient understanding of the governing processes.

Most gullies form by a combination of mechanisms, acting under varying conditions, sometimes synergistically, and varying magnitudes. One process that has received less attention than surface flow processes is subsurface flow. A common feature often associated with subsurface flow contributing to gully initiation is the occurrence of a water-restricting layer that perches water, sometimes termed a duplex soil (Faulkner, 2006). Gully erosion in high rainfall regions by subsurface flow may not be associated with shallow soils over bedrock but simply the occurrence of conductive layers residing over less permeable layers.

Duplex soils, layered soils with a shallow water-restricting horizon, are prone to seepage contributing to gully development. Numerous studies have shown that perched water tables develop over restrictive layers, resulting in preferential lateral flow (Wilson et al., 1990, 1991). Even in a simplistic sense, duplex soils have a limited soil water storage capacity that, once filled, will result in seepage at the surface contributing to surface runoff or affecting the erosion properties of the soil surface (Huang and Laflen, 1996; Darboux and Huang, 2005). In addition to the probability of subsurface flow directly affecting gully erosion in duplex soils, either by soil-piping or seepage, a water restricting layer near the surface is more likely to result in rainfall impacting the shear strength, s, of the soil surface and hydraulic shear stress, τ, applied to surface particles.

The role of subsurface flows in gully erosion has often been attributed to the decrease in soil shear strength, s, as the soil water tension, ψ, decreases as described by the Mohr-Coulomb equation (Fredlund et al., 1978):

$$s = c' + (\sigma - \psi_a) \tan\emptyset' + (\psi_a - \psi_w) \tan\emptyset^b \quad (1)$$

where c' is effective cohesion, $(\sigma - \psi_a)$ is the net normal stress [σ is total stress and ψ_a is pore-air pressure], $\emptyset'$ is effective angle of internal friction, $(\psi_a - \psi_w)$ is soil-water suction [ψ_w is pore-water pressure], and $\emptyset^b$ is effective angle of shearing resistance relative to an increase in soil suction.

The most universally accepted erosion prediction equation is the excess shear stress equation:

$$D_c = k_c(\tau - \tau_c)^b \quad (2)$$

where D_c is the flow detachment capacity, k_c is the concentrated flow soil erodibility, τ and τ_c are applied particle hydraulic shear stress and critical shear stress, respectively, and b is an exponent.

The relationship between D_c and τ - τ_c is typically assumed to be linear, b=1. Owoputi and Stolte (2001) found that seepage affects the rate of erosion by impacting the erodibility. Huang and Laflen (1996) and Gabbard et al. (1998) found that erosion rate significantly increased due to seepage exfiltration. It is not clear under what conditions exfiltration of seepage can be sufficient to entrain particles in runoff waters, thereby, directly causing gully development (Huang et al., 1999; Zheng et al., 2000). Exfiltration at the surface of hillslopes can increase the rate of surface runoff, which affects the shear stress and seepage increases surface soil erodibility. The removal of negative soil pore-water pressures by seepage reduces the soil shear strength and increases susceptibility to erosion. Howard and McLane (1988) proposed that increased erosion under seepage conditions was due to reduction of effective shear stress. Thoman and Niezgoda (2008) noted that many soil properties can affect soil erodibility and critical shear stress. They determined k_c and τ_c of channels using the in situ jet device and developed correlations between critical shear stress and soil cohesion properties. Similar type correlations need to be developed for conditions of seepage for soil erodibility (k_{se} and k_{sp}) and critical shear stress.

Therefore, the depth to a restrictive layer may be a critical variable in predicting gully locations. This restrictive layer may be a genetic feature of the soil, such as an argillic horizon, fragipan, caliche layer, or may be anthropogenic, such as a plow pan or depth of tillage. The increase in clay content with depth may not be large enough to qualify as an argillic horizon, yet lateral movement may occur. Wilson et al. (2007) found that just a 16% increase in clay content caused over two orders of magnitude decrease in saturated hydraulic conductivity (K_s), which resulted in seepage erosion at bank faces. Fox et al. (2010) showed that only one order of magnitude decrease in K_s between layers was sufficient to cause seepage. Subsurface flow can contribute to gully formation and growth in ways not necessarily represented by surface

topography, such as gully sidewall failure (Collison, 2001; Wilson et al., 2007) due to seepage, particle entrainment in runoff due to seepage forces, and enhanced erodibility or reduced critical shear due to loss of cohesion.

Despite the general understanding of the subsurface flow processes involved in soil erosion, very little field or plot scale work has been done to measure the impact of seepage on erosion or gully formation due in part to the difficulty in controlling the hydrology. The lead author attempted to induce seepage using the C-plots (described by Cullum et al., 2007) at the Holly Springs Experiment Station (HSES) but without success. These plots were selected because of the presence of a fragipan horizon. The plot sides were isolated to prevent lateral inflow-outflow by trenching the plot sides and inserting a plastic barrier. An injection trench was installed at the upslope end. However, sufficient inflow to induce seepage at the surface was never obtained due to the weakness and significant (> 0.6-m) depth of the fragipan horizon at this location.

An alternative approach, based upon observations by the lead author during his travels in China, was to build above ground plots such that the soil and hydrologic conditions inducing seepage could be more easily controlled. Above ground runoff plots are quite common at research stations in China, Figure 1. Such plots provide complete restriction on lateral flow into and out of the plot sides in the same sense that conventional runoff plots are bermed to prevent runon and runoff from the surface which is essential to mass balance. Unlike the plots observed in China, these would need to include a water-restricting layer and a means of injecting water under controlled conditions in order to induce seepage.

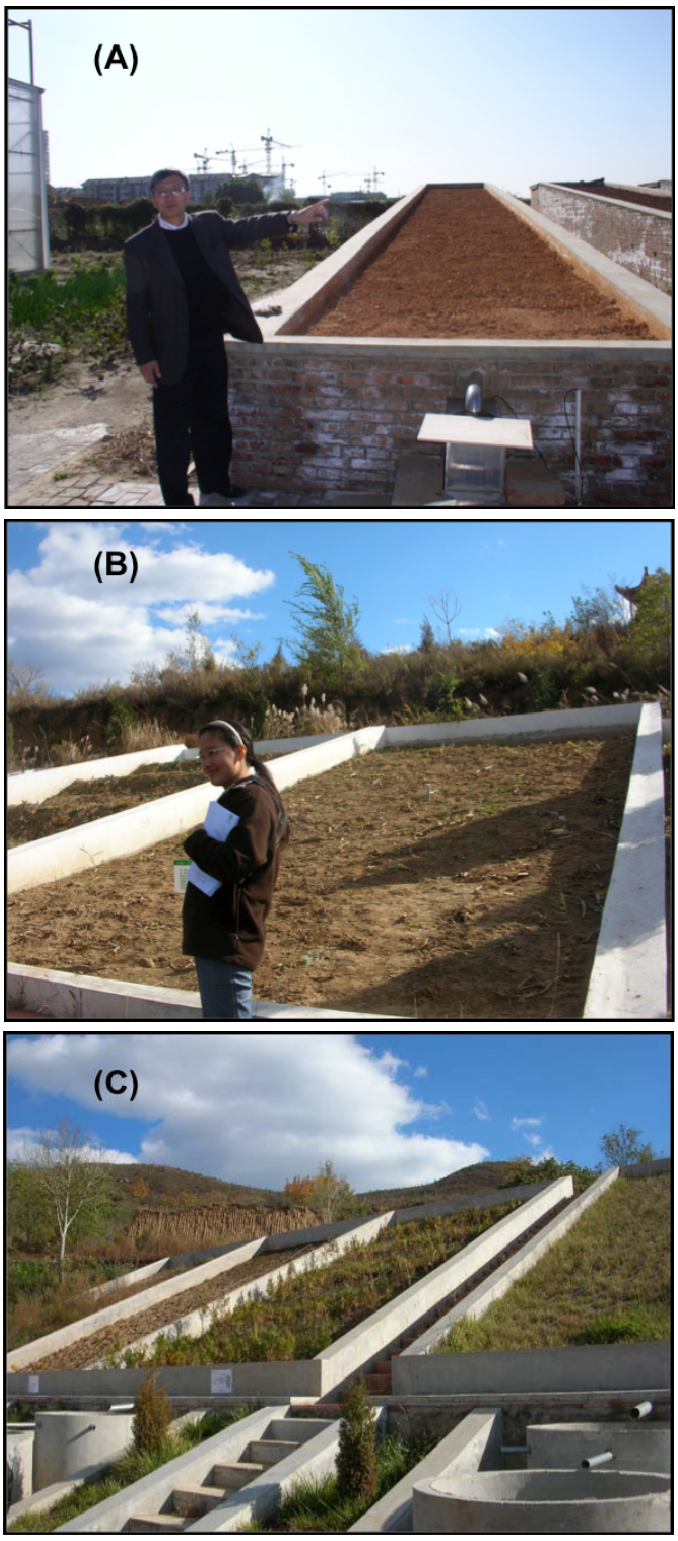

Figure 1. Above ground erosion research facilities in China. (A) Dr. Baoyuan Liu at above ground plots at Fangshan Experiment Station of Beijing Normal University; (B) graduate student, Ms. Yang Yang, at Shangxinzhuang Soil and Water Experimental Station; (C) additional above ground plots at same location for studying roadside hillslope stability.

The objective of this report is to describe the facilities constructed at the North Mississippi Branch of the Mississippi Agriculture and Forestry Experiment Station (MAFES) at Holly Springs, Mississippi (HSES) to study seepage effects on runoff, erosion, and gully formation under a variety of topographic, soil, land use, and erosion control conditions.

BED CONSTRUCTION

Natural-soil field plots at HSES used by Wilson et al. (2008), historically called the L plots, were selected for conversion into above ground repacked-soil plots for future seepage experiments because of the existing runoff collection and measurement systems. The lower end of each L plot had an endplate and runoff collector that routed water into an H-flume equipped with an FW-1 water level recorder and an N-1 Coshocton wheel sampling device. Soils on the L-plots were classified as Loring silt loam (fine-silty, mixed, active, thermic Oxyaquic Fragiudalfs). The L-plots were arranged in three blocks with three plots per block; each 0.01-acre plot was 3.66-m (12 ft) wide and 10.67-m (35 ft) long. The slopes of all plots ranged from 2 to 4.5% with a mean slope of 3.1%.

Two blocks (3 plots each) were selected for conversion into above ground plots, Figure 2. The original plots were spaced 1.83-m (6 ft) apart. By utilizing a common inner wall, the new above ground plots were enlarged to 5.49-m (18 ft) wide and elongated from the endplate upslope to 18.29-m (60 ft) to produce a 0.1-ha plot area. In addition, the sidewalls were elevated with distance from the endplate to change the slope from the original 3.1% to 10.0% (Figure 3).

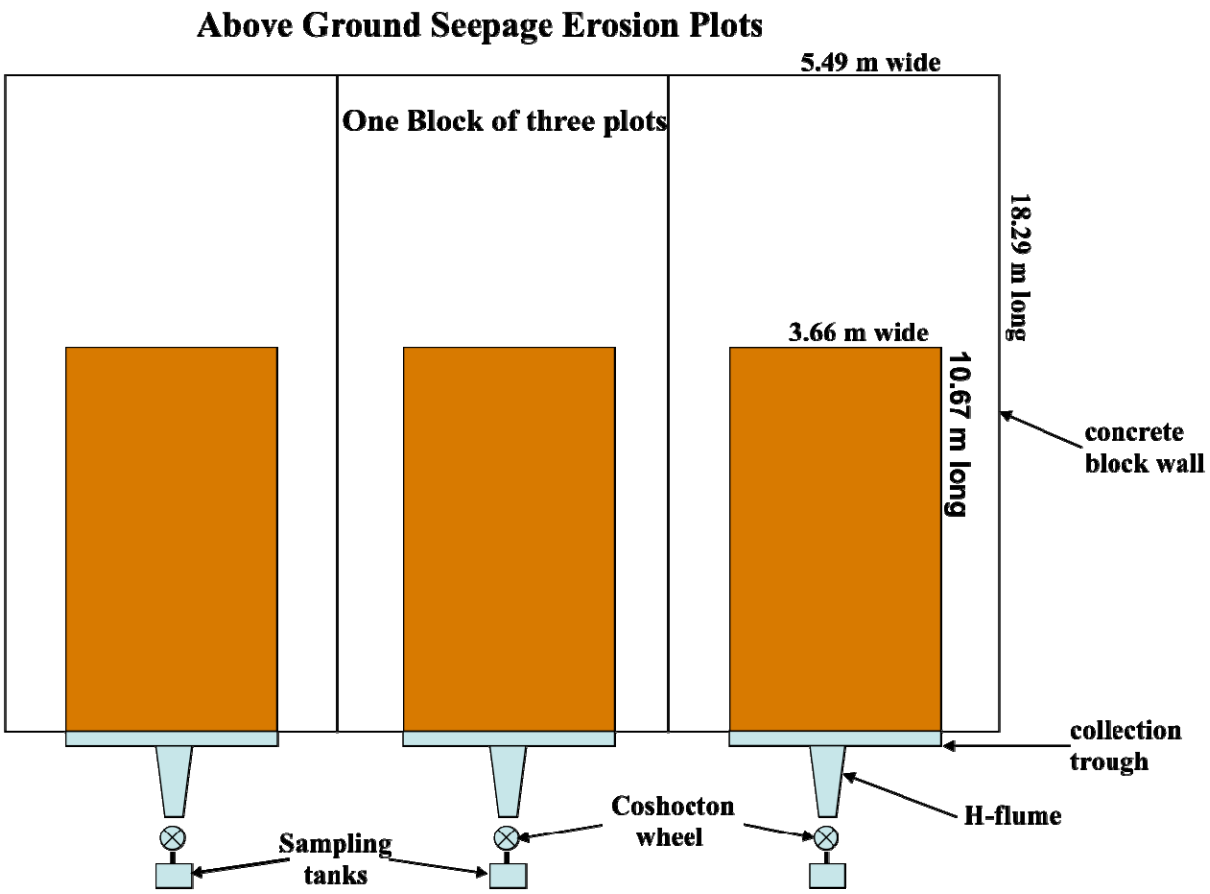

Figure 2. Each original L-plot, identified as the orange area) was 10.67 (35 ft) long by 3.66 m (12 ft) wide with a 1.83 m (6 ft) gap between them. These plots were enlarged to 18.29 m (60 ft) long by 5.49 m (18 ft) wide with concrete block walls installed to separate the new plot areas. The new plots will have a 10% slope.

The front was designed with a sloping concrete block wall from the sidewall height of 0.61-m at the lower end of the sidewall to a 0.3-m height at the flow collection flume of the original plot area (Figure 4). The original plot contained an endplate down to 0.46-m deep along its entire width. The 0.3-m deep footer served as an extension to the endplate across the entire plot width. Plots were designed such that they could have a swale to the new soil surface to foster convergent flow to the plot centerline. For swale-surface plots, the concrete block walls in the front serve as an aboveground endplate but this can be extended with removable metal endplates to allow access inside the plots with machinery.

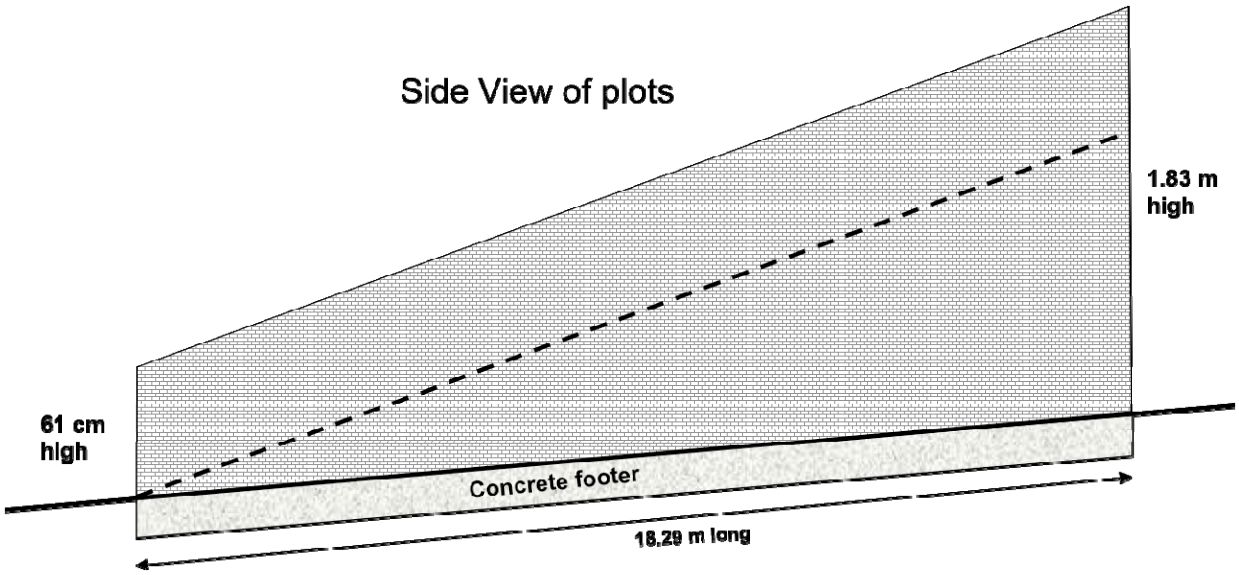

Figure 3. Side view of plot wall resting on the concrete and rebar reinforced footer illustrating the original soil surface (solid line) with a slope of 3.1 % and the new soil surface (dotted line) with a slope of 10 %.

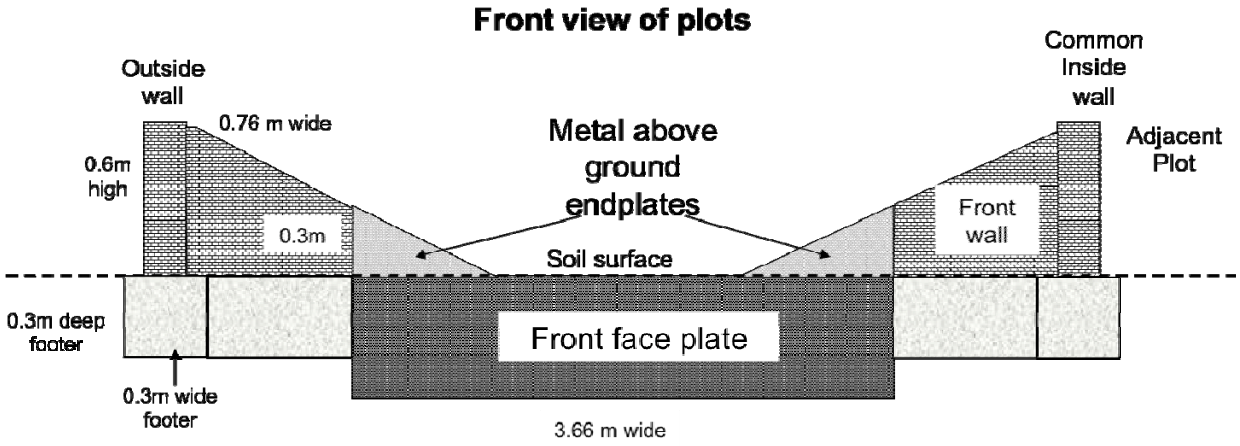

Figure 4. Front view of plots illustrating the endplate of the original plot and above ground retractable endplate for plots with a swale-surface, as well as the concrete block walls resting on the concrete and rebar reinforced footer.

The back wall (Figure 5) was designed to contain a water reservoir for inducing seepage in the plot center (convergent) area. Between January and March 2010, six water reservoirs (tanks) were built for installation in the back walls. These tanks were fabricated from 1.9 cm (3/4 in) thick plexiglass. The inner reservoir size was 1.05-m (41.5 in) wide inside by 1.12-m (44.25 in) deep inside but the outer walls extended 0.063-m (2.5 in) on the left and right sides and 0.07-m (3 in) on the bottom side for overlapping the concrete block walls. Thus, the front and

backsides were 1.22-m (48 in) wide by 1.22-m high. The inside of the tank was made to fit snuggly on the plot walls and were, therefore, slightly larger than the width (8 inches) of concrete blocks. Measurements were made of all plot wall openings to make sure what width the tanks needed to be for proper fitting. The tanks were reinforced with three vertical plexiglass braces spaced 0.25-m (10 in) apart. These were perforated with 0.013-m (1/2 in) holes spaced 0.076-m (3 in) apart to allow free water movement inside the tank. The outer edge of the backside of the plexiglass had holes drilled and tapped for screws to hold the tank in place on the walls (Figure 6). Drain plugs were drilled at levels of 0, 15, 30, 45, 60, and 90 cm for maintaining a constant head at these levels within the tanks.

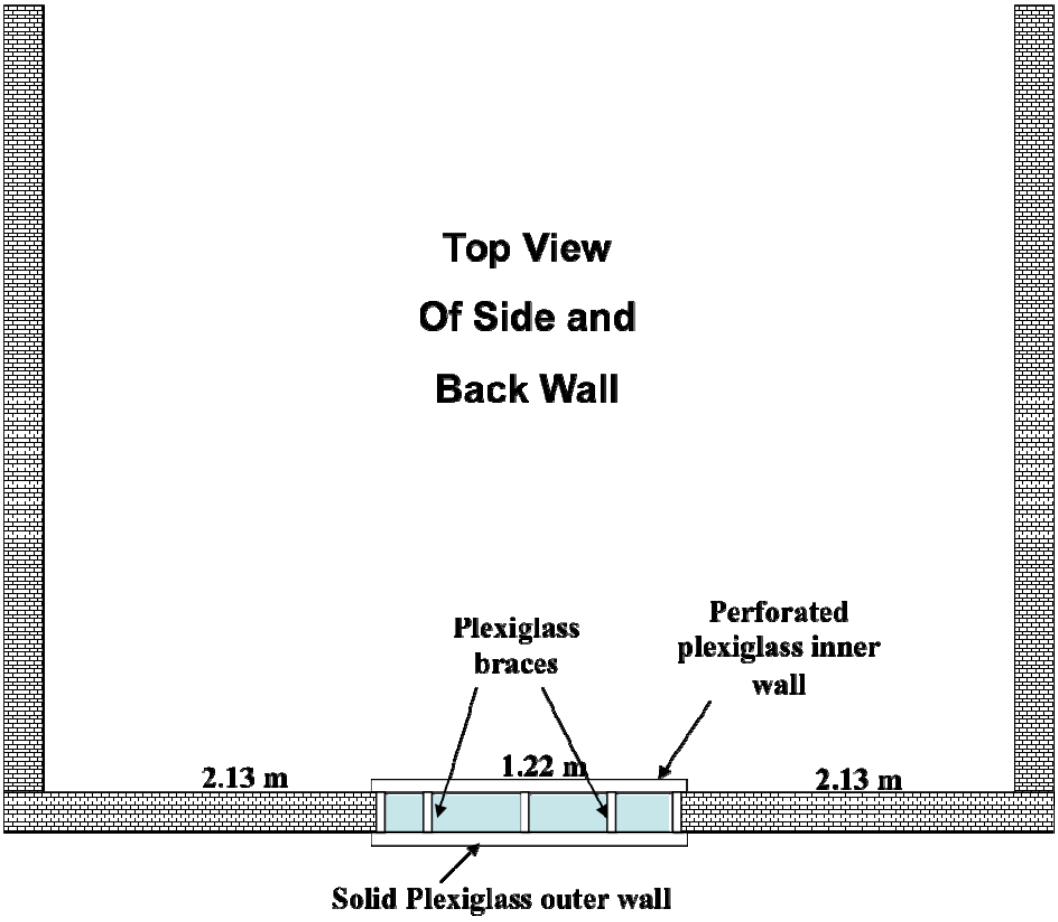

Figure 5. Top view of back wall with water reservoir inserted into center.

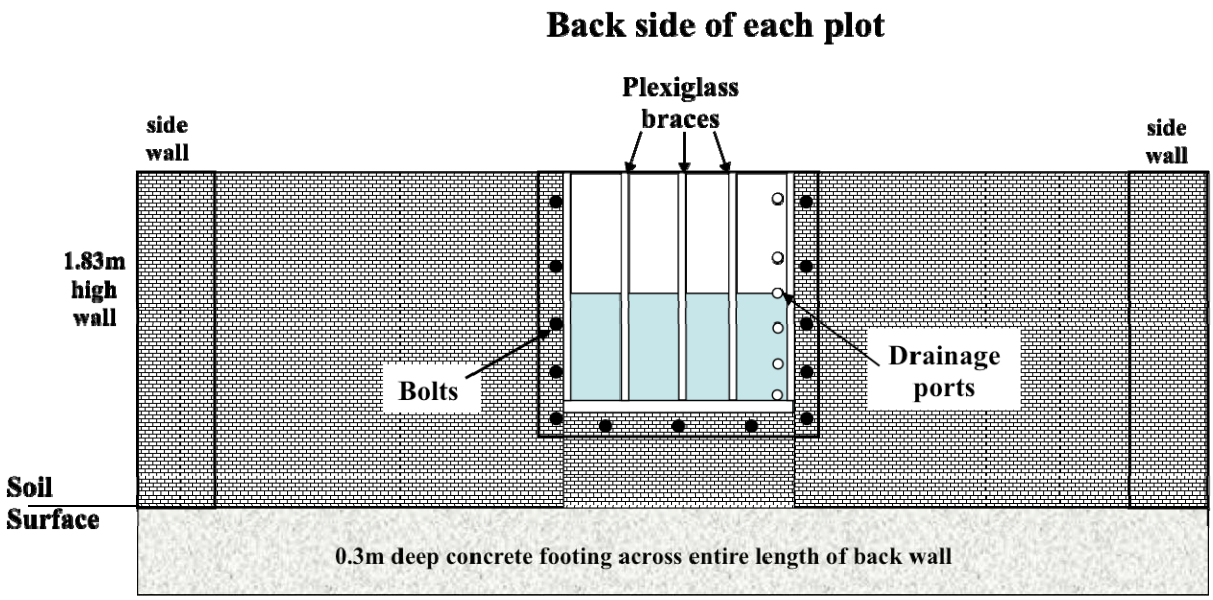

Figure 6. Water reservoir in back wall is 1.05m wide and 1.12m deep by 0.2m wide. Reservoir has three inner braces that are perforated. Drainage ports on back side to control the water level in reservoir. Bottom 0.3m of reservoir's inner wall is has perforated for injection into soil bed immediately above the clay layer.

Excavation for the wall footers was dug on 29 September 2009. Wall footers were made of rebar reinforced concrete and concrete block walls were reinforced with rebar according to standard footer and block wall requirements. The plot walls were constructed between 6 to 22 October 2009 by Gene Stewart Contractors. Cracks and other defects in the walls were sealed on 24-26 May 2010 and walls were sealed with water sealant paint on 26 May - 2 June 2010 (Figure 7).

The soil used for filling plots was excavated from the Long-Term Erosion plots (described by McGregor et al., 1999) during 19-21 October, 2010 by Jon L. Woods Construction Co. using a soil pan (Figure 8a). The soil from this location was the same loess material as the L plots (Loring SiL) and managed as no-till soybean since 1983. The soil pan removed topsoil from the no-till plot areas down to the level of the eroded conventional till plots (topsoil above the fragipan). Woods Construction also supplied the clay material for creating a water restrictive layer. The clay, a weather shale residuum, was obtained from a local borrow pit. The

clay was stored in three piles (Figure 8b) while the loess topsoil was stored in two large piles, one on each side of the plots.

Figure 7. Backside view of plot walls after construction and during initial soil before filling but before installation of water reservoirs in back walls. Inner walls of plots were lined with polyethylene sheets to limit seepage out of plots after filling. One of the piles of excavated loess soil is seen in the background.

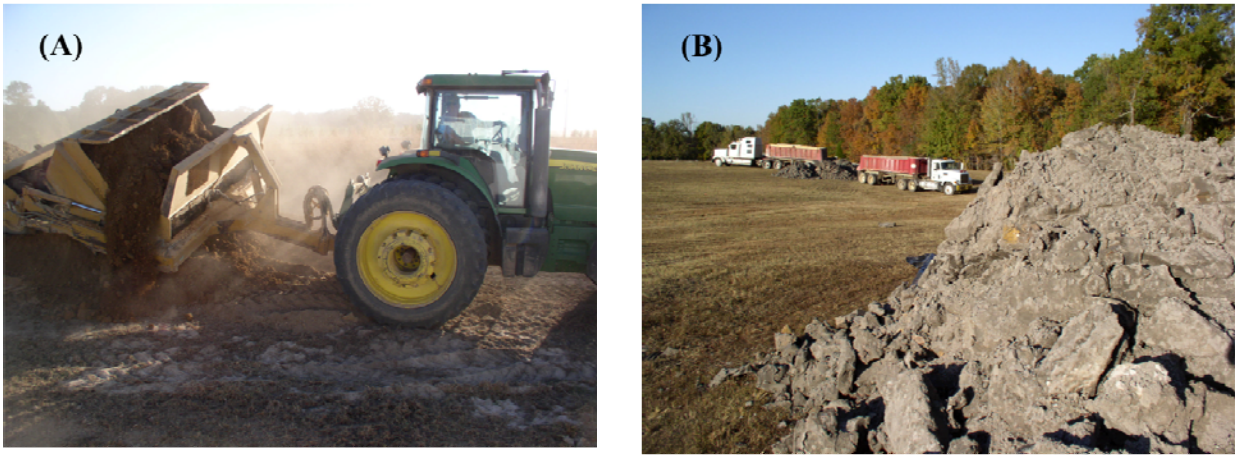

Figure 8. (A) Loess soil material being unloaded from soil pan. (B) Clay material stored in three piles for future use as a water restrictive layer.

The initial plot plan included three plots with a uniform (flat) sloped surface and three plots with a swale shaped surface to facilitate convergent flow to the plot middle with these two

treatments randomly assigned to the six plots (Figure 9). Uniform plots had the same depth laterally across the plot, whereas swale plots had a lateral slope to cause convergent flow to the plot centerline. Plots were named "seepage erosion plots", i.e. SEP, and numbered 1 to 6 from left to right looking upslope. Thus, plots SEP 1, 2, and 5 contain a uniform-sloped surface, and plots SEP 3, 4, and 6 have a swale-shaped surface topography. Plots were designed to contain a water restrictive layer that extends from the back wall to 10.7-m downslope where it surfaces and remains at the surface to 12.2-m downslope at which point the base material surfaces. The base layer of each plot consists of "compacted" loess soil that extends from the back wall to the front endplate. The thickness of the "compacted" loess base layer decreases from 0.6-m at the back wall to 0 cm at the endplate. The 0.15-m thick "compacted" clay layer above the base layer extends from the back wall to 10.7-m downslope then tapers off to 0-m thick at 12.2-m downslope (Figure 10). For the uniform-sloped plots, the loose surface material above the clay layer is 0.47-m deep over the clay layer (total depth of 1.22-m over the original soil surface) at the back wall and tapers off to 0-m thick where the clay layer reaches the surface at 10.7 m downslope (Figure 10). For the swale plots, an additional 0.3-m of topsoil was applied along each plot sidewall that tapers off laterally to the uniform-sloped plot surface dimensions at 2.13-m laterally from each sidewall (Figure 11). Thus, the swale has approximately a 14% slope towards the plot middle in addition to the 10% slope length-wise. The middle 1.22-m of the plot has a uniform slope similar to the uniform-sloped plots.

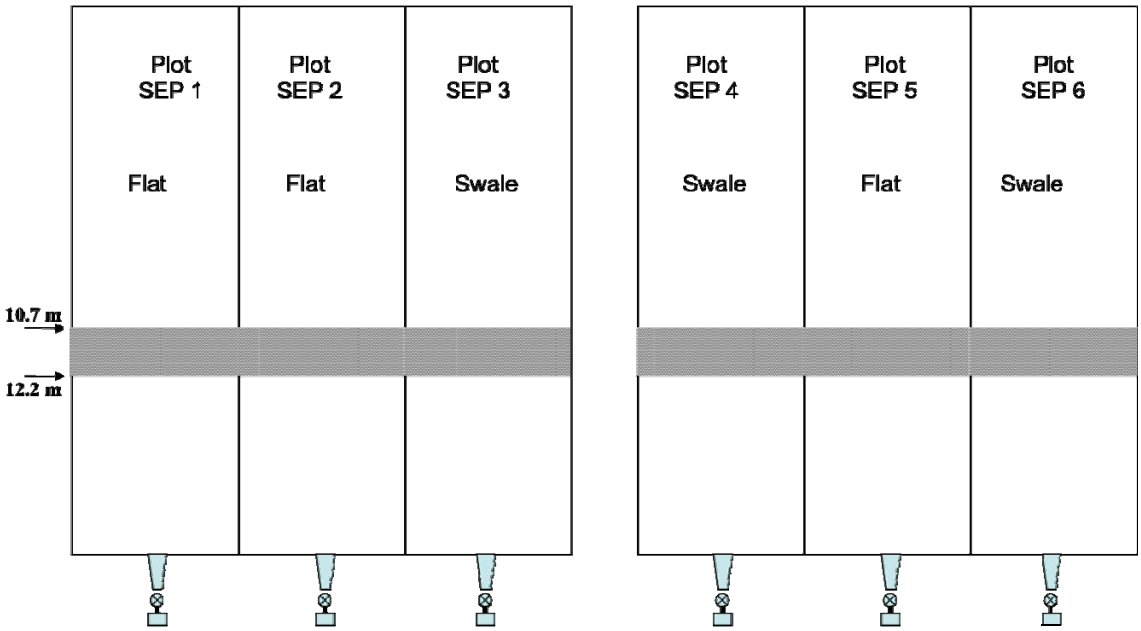

Figure 9. The wall is 1.83-m high at the back wall and 1.16-m high at the 12.2-m downslope location. The clay layer has a uniform depth laterally along the width of the plot. The clay layer will be exposed to the surface from 10.7-m downslope to 12.2-m downslope. The clay layer is 1.07-m to 1.22-m (15 cm thick layer) below the top of the back wall and 0.61 m below top of wall at 12.2-m downslope, i.e. 0-m thick. The clay layer is full 0.15-m thick at 10.7-m from back wall with 0-m of soil covering. The upper 10.7-m has the full 0.15-m thick clay layer after compacting.

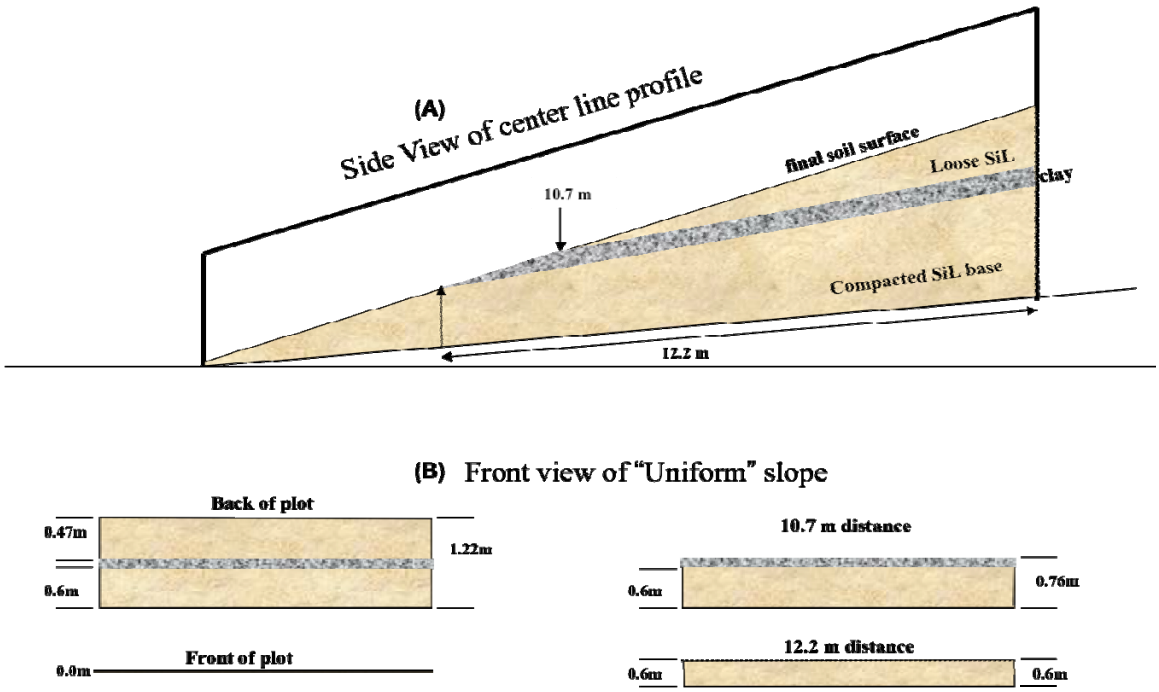

Figure 10. Final soil profile after filling for the three "Uniform-sloped" plots with 0.15-m thick clay layer surfacing 10.7-m downslope and ending 12.2-m downslope.

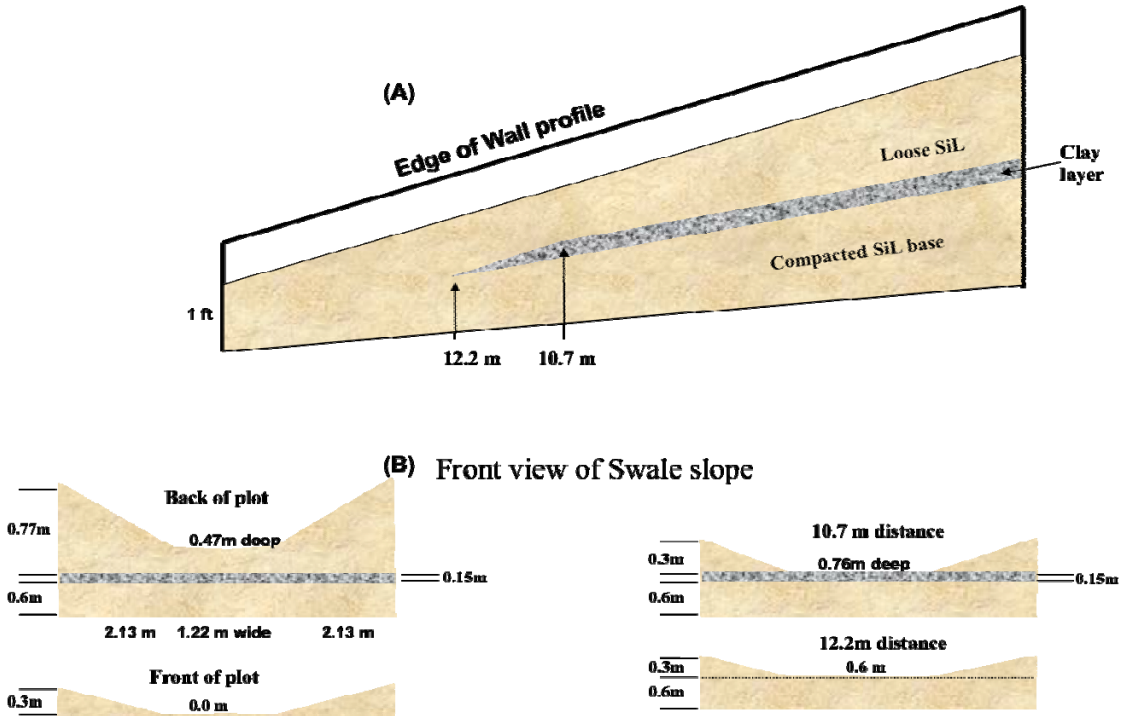

Figure 11. Final soil profile after filling for three "Swale" plots with clay layer that is buried at plot edge but surfaces between 10.7 to 12.2-m downslope from back wall at plot center line.

Plots were partially filled with topsoil on 19-28 October 2010. The inner walls of the plots were first lined with polyethylene sheets to prevent seepage into or out of plots. The desired level for filling was marked with spray paint on the inner wall sheets of the plots. Plots SEP4 and SEP5 were the first to be filled. The original soil surface was first scarified using the bucket teeth to provide good continuity between the original soil surface and the base layer material. The base layer material was added by dumping soil over the plot walls with a tractor frontend loader and using a S175 Bobcat skid-steer front end loader (Figure 12a,b). Soil was redistributed within the plot with a mini-excavator (Fig 12c) and by manually moving soil. Later, it was decided that the process of redistributing the soil with the mini-excavator was too slow so for the remainder of the plots, the Bobcat was maneuvered into the plots and used to redistribute the soil (Figure 12d). This worked much better and also the 6300 lb Bobcat compacted the soil laid down for the base

layer. The Bobcat loader was run over the entire surface off all plots several times to compact the base material. In addition, the soil was left exposed during the winter to allow time for settling.

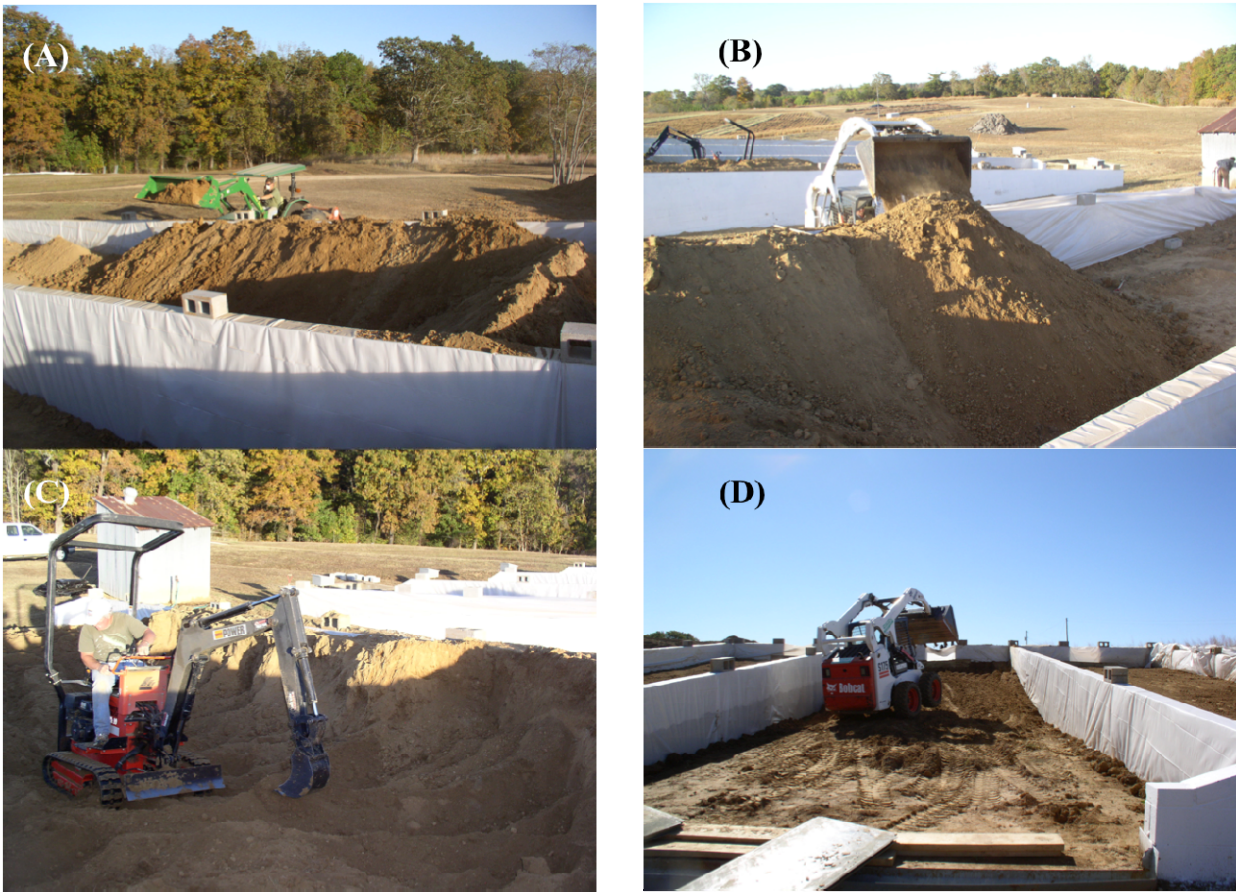

Figure 12. Filling plots with loess soil material by (A) Alan Hudspeth and (B) Randy Saunders. Redistributing the soil within the plots by (C) Glenn Wilson and (D) Randy Saunders.

Water tanks (Figure 13) were installed in the plots during the week of May 18-20, 2011. The water tanks were installed by lowering the tanks into place using the frontend loader of the tractor. The tanks were sealed by inserting foam along the inside walls and bottom edge, then pulling the tanks tight against the wall using the screws on the backside of the tanks. The edges were then sealed with silicon sealant. A rain shield was placed over the tanks.

Figure 13. Back side of plot with the water tank installed but prior to clay layer or final filling.

The clay layer was installed and compacted between 27 May and 9 June 2011. Measurements were made of the depth to the top of the filled soil. Excess soil (soil above the design level) was dug out and dumped out of the plots or pushed to the lower end of the plots using the Bobcat. It was noted that plots with the base layer soil spread out by the mini-excavator (SEP4 and SEP5) were less compacted and wetter in the subsurface than the others. To alleviate this problem, the Bobcat was run several times over these plots then used to open up the surface with the bucket's teeth to facilitate drying. This process was repeated for several days until dried out and then compacted like the other four plots using the Bobcat and had a base layer as firm as the other four plots. The depth of the top of the 0.15-m thick clay layer was marked on the inner plot sidewalls prior to filling with clay. The clay material was prepared for filling by first spreading out the clay piles using the Bobcat and tractor's frontend loader (Figure 14a).

Figure 14. (A) Clay pile spread out for preparation prior to installation in plots. (B) Large clods of clay were broken down by roto-tiller. (C) Tianyu Zhang applying water to clay material to obtain optimum water content for compacting. (D) Compacting of the clay layer using a vibrating plate compactor.

Then the clay was roto-tilled (Figure 14b) to break it into smaller (2 inch or less) aggregates and to unify the moisture content. Clay was allowed to dry for a couple of days while being roto-tilled periodically to get it dry enough for compacting. When the moisture was right, it was hauled to the plots using the tractor frontend loader. The clay material was loaded into and spread out within the plots using the tractor and Bobcat, respectfully. Once the clay material was in place and to the desired depth and compacted by the Bobcat, the clay was further compacted using a Wacker 1550 AW vibratory plate compactor with water tank (Figure 14d). The vibratory plate compactor weighed 86.2 kg, provided maximum force (without water) of 15 kN to a base area of 0.23 m^2 (23" x 15.5") to provide a compaction pressure of 65.3 kPa. The compactor was

run over the entire area twice. In some instances, moisture was added back to the clay to obtain better moisture content for compacting (Figure 14c). Once compacted, the clay layer was watered down and covered with a plastic barrier. The clay was maintained moist by periodic wetting until time for final plot filling with topsoil. The plastic cover over the clay layer was removed from the plots and the surface of the clay layer on each plot was surveyed using a TOPCON GLS 1500 laser scanner.

Final plot filling was done the week of 5 to 7 October, 2011 for the uniform-slope plots and 10 to 11 October 2011 for the swale plots. The sidewalls of each plot were marked for the desired depth to fill the plots. Loess soil from the storage pile was loaded into the plots using the tractor's front-end loader. The soil within the plots was redistributed to the desired depth, which was uniform laterally, using the Bobcat (Figure 15a). All 6 plots were filled to the desired depth for a uniform slope. The filling of the plots with the Bobcat tended to compact the soil, so after the final desired level was acquired, the teeth of the Bobcat bucket were used to break up and scarify the surface (Figure 15b). A rear-tine tiller was then used to till up the soil surface (Figure 15c) to either 0.15-m depth or maximum depth of penetration depending upon the depth to the clay layer which surfaces between 10.7 to 12.2-m (35 to 40 ft) downslope of the back wall. The three uniform-slope plots (SEP1, SEP2, SEP5) were then smoothed at the surface using a rake (Figure 15d). For the Swale plots, it was determined that the Bobcat was not able to create the swale, therefore, the mini-excavator was operated within these plots to move soil from one side to the other within the plot to create the swale (Figure 16a). The mini-excavator stayed within the 1.22-m (4 ft) wide level middle area and primarily moved soil dumped on the exposed side to the other (inner wall) side. The remaining shaping of the loose soil was done manually by shovel. The plots were shaped to have a 0.3-m (1 ft) higher soil at the edge that sloped down over 2.13-

m (7 ft) lateral length to a level middle area (Figure 16b). Thus, the edge of the plots had a surface that was 0.3-m (1 ft) below the top of the wall and a middle that was 0.6-m (2 ft) below the top. The surfaces were raked smooth (Figure 16c). The final surfaces of all six plots were laser scanned using a TOPCON GLS-1500 laser scanner (Figure 16d). Plots then had a metal triangular endplate installed at the lower end on each side of the plot to create an above ground endplate that matched the swale configuration.

Figure 15. (A) Loose soil added to all plots to the level of the uniform-sloped plots using Bobcat. (B) Compaction of surface by Bobcat removed before exiting each plot using the Bobcat's teeth on the bucket. Plot surfaces were tilled (C) and then racked smooth (D).

Three undisturbed soil cores, 3.5-inch diameter, were taken per plot on 26 October 2011, one at each of three positions. The positions were 0.91-m, 1.82-m, and 2.74-m from the sidewall approximately 4.57-m below the back wall. All plots were sampled and bulk density determined.

It was decided that the V-shaped collection trough (Figure 17) needed to be replaced with a flat-bottomed (rectangle-shaped) sediment-settling trough to prevent the flume section from being over-whelmed with excessive sediment loads (Figure 18). The original 3.66-m (12 ft) section of the V-shaped collection trough was replaced with a 0.25-m (10 in) wide and 0.46-m (18 in) deep rectangular collection trough. The trough extends 0.2-m (8 in) below the bottom of the flume. Troughs on plots SEP 1, 2, and 3 were replaced January 3 to 5 and plots SEP 4, 5, and 6 were replaced February 9-10, 2012. Sediment in troughs are recovered after storm events and recorded separately from that measured by the Coshocton wheel-tank system (Figure 19). Runoff can be recorded by summing the volume in the trough with that measured by the tanks after splitting by the Coshocton wheel. Plans are to install pressure transducers in troughs for measuring runoff dynamics by knowing the trough dimensions and flume stage rating.

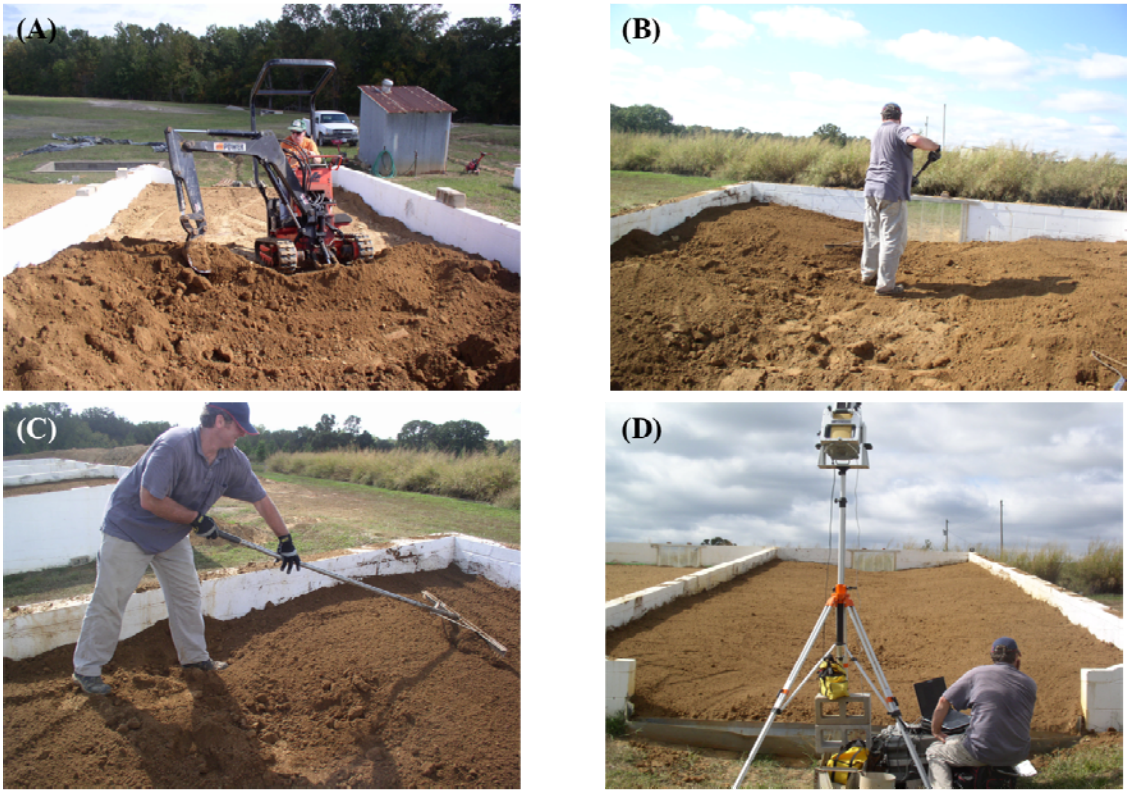

Figure 16. Swale plot had the soil creating the convergent slope redistributed using the mini-excavator (A) and by hand (B). The desired slope was manually shaped using hand rakes (C) and the surfaces of all plots were laser scanned by Rob Wells (D).

Figure 17. Final soil shape for one of the three uniform-sloped plots (A) and one of the swale-shaped plots (B).

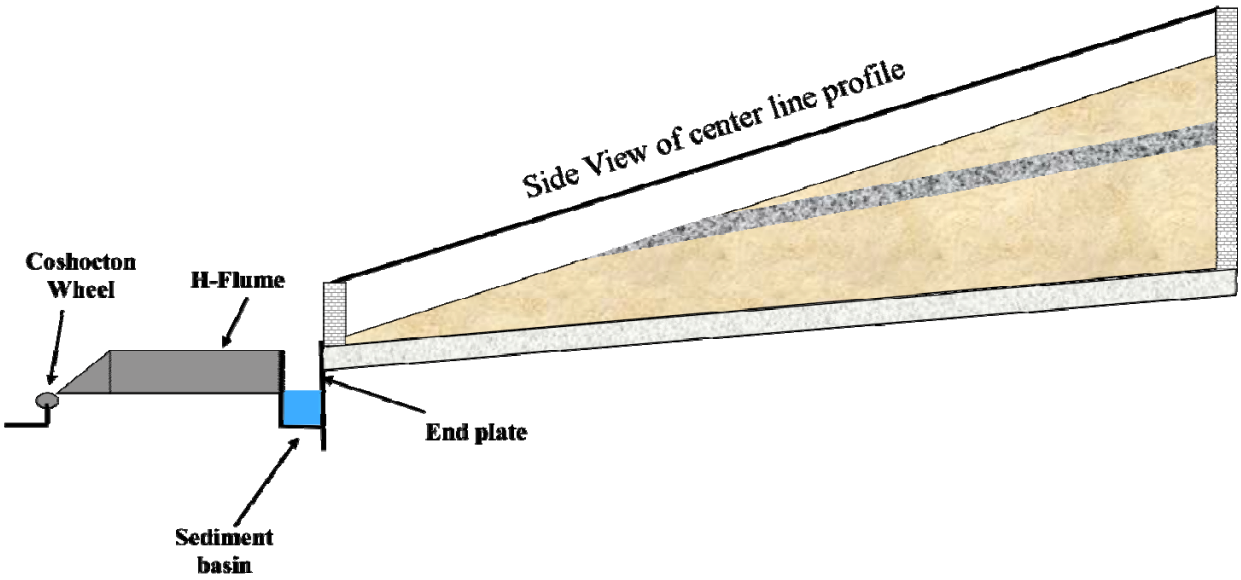

Figure 18. Flat-bottomed sediment basin made to width of square shovel for ease of excavation. Water level maintained at top between storms. Attached directly to existing flume with Coshocton wheel.

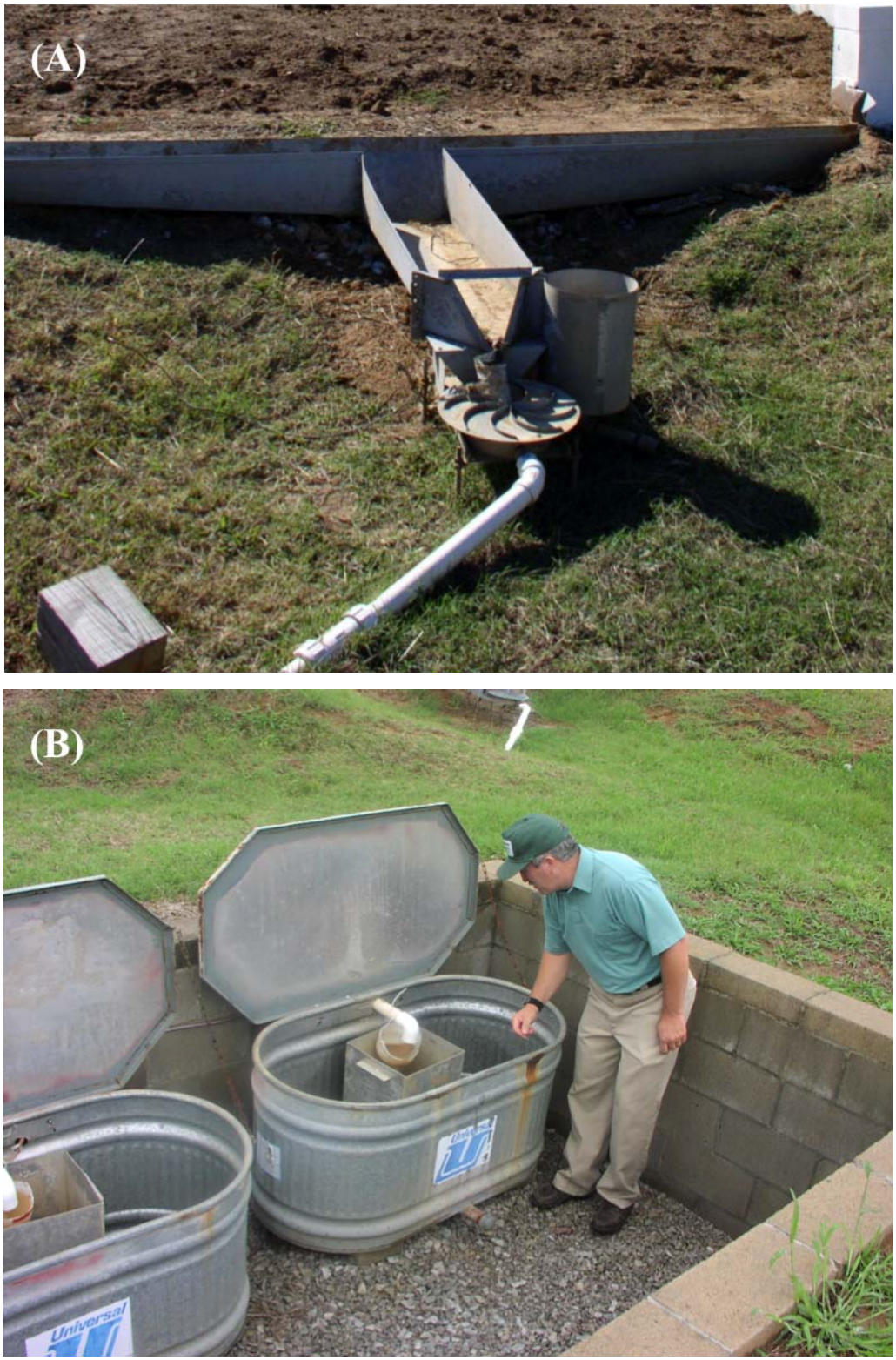

Figure 19. Soil water flow and sediment concentration samples are obtained using a Coshocton wheel splitter at the end of the flume (A) that routes one hundredth of the flow to a collection tank for measuring the depth of flow and taking a sediment sample (B).

BED SURVEYS

LiDAR technology, measures the laser pulse travel time from the transmitter to the target and back to the receiver allowing the distance to be calculated (Wehr and Lohr, 1999). In this process, a very accurate timing system is needed to guarantee an accurate resolution since laser pulses are sent at the rate of thousand times per second. Additionally, the transmitter and the receiver must be located at the same physical location, which is a single-ended system because the phase of the incoming signal is compared to phase of internal clock at the same location (Measures R. M., 1984). Ground-based LiDAR is a simplified system because the sender/receiver's location is known. They operate in a similar fashion to a reflectorless total stations. For each pulse, these systems can measure: (1) x, y, z coordinates values with respect to the position of the laser sensor; (2) the intensity of the returned signal as reflectance; and (3) RGB values from an integrated digital camera within the instrument.

These systems are capable of collecting information with a wide range of ground sampling densities as a result of operator controlled factors such as the scan angles (area covered by individual scans), average point density of scans, and degree of overlap between scans. Higher point density can be achieved by higher sensor resolution, smaller vertical field of view angles, and multiple scans of the same ground location. The instrument resolution is often controlled by an imaginary plane located at the middle range of the vertical field of view and is orthogonal to the sensor's normal sight. The vertical field of view angles also influence the point density as point sampling becomes sparser as vertical scan angles tend to the horizon. Multiple scans can be used to collect data over the same geographical location resulting in increased sampling density and overcomes problems such as shadowing and limited coverage due to vegetation.

For a more detailed accounting of the technical background, implementation of site survey and post-survey data processing using the TOPCON GLS survey equipment, see Momm *et al.*, 2011. The equipment used to scan the SEP beds (Fig. 20) was a TOPCON GSL-1500 series that has a 4 mm single point accuracy distance (Table 1). Surveys were conducted on October 5 and 6, 2011 for the clay layer scans and October 11, 2011 for the final soil surface scans. Surveys were subset to the same extent (SEP bed only) to remove unwanted laser points regarding sidewalls. A contour plot (upstream boundary of the beds is on the right edge of figure) of each SEP bed resulting from the final soil surface scans is shown in Figure 21. The survey dataset is too large (gigabytes) to provide in this report but these data may be available, on an as needed basis, upon request to the authors responsible, i.e. Drs. Rob Wells and Henrique Momm. To describe the baseline topography, a set of cross-sections were generated using a user-provided centreline (Momm et al., 2011). Cross-sections at different locations were computed (Figures 23-24; SEP 1) based on various parameters (Table 2). A total of 69 transverse cross-sections (0.25-m spacing) and 3 longitudinal cross-sections (1.3-m spacing) were generated for each SEP bed (Figure 22) varying in extent and number of points as a result of the non-uniform distribution of laser points. All cross-sections for each SEP bed are given in the Appendix.

Table 1. General specifications of the TOPOCON GLS-1500 laser scanner.

Parameter	Value	Unit	Condition
Single point accuracy distance	4.0	(σ) mm	1 to 150 meters
Single point accuracy vertical angle	6.0	seconds	1 to 150 meters
Single point accuracy horizontal angle	6.0	seconds	1 to 150 meters
Maximum scan rate	30000	pts/second	
Scan density spot size	6.0	mm	1 to 40 meters
Scan maximum sample density	1.0	mm	up to 100 meters
Laser wavelength	1535	Nm	
Laser pulse duration	3.6	nano second	

Table 2. Parameters considered in the generation of the cross-sections for multi-temporal morphological analysis of gully evolution in croplands.

Parameter	**Value**
Cross-section size	5.0 meters
Distance between points in the cross-section	2.5 centimeters
Distance between cross-sections	25.0 centimeters
Power used in IDW	2.0
Search radius	5.0 centimeters

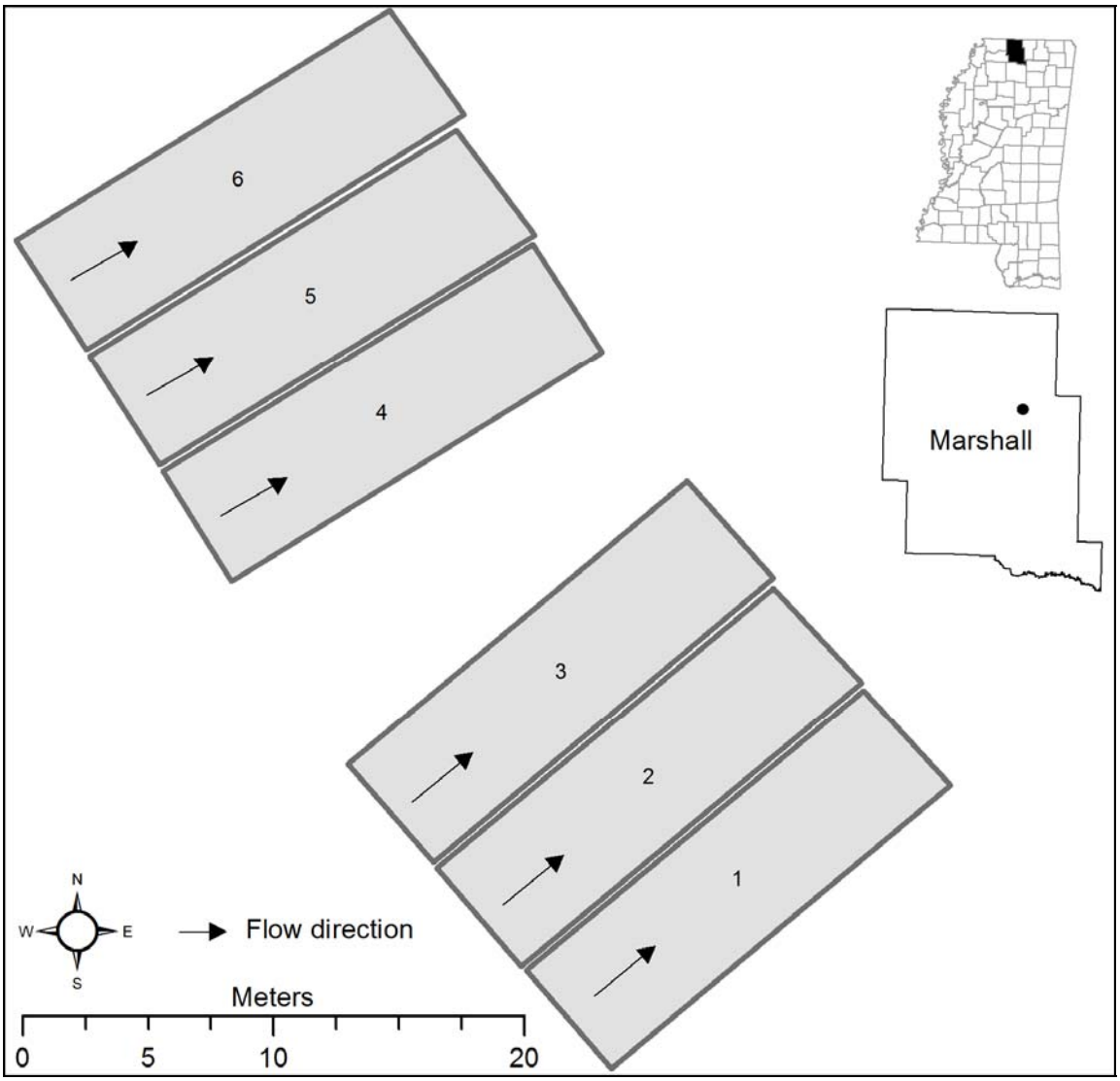

Figure 20. Geographic location and nomenclature adopted for study plots.

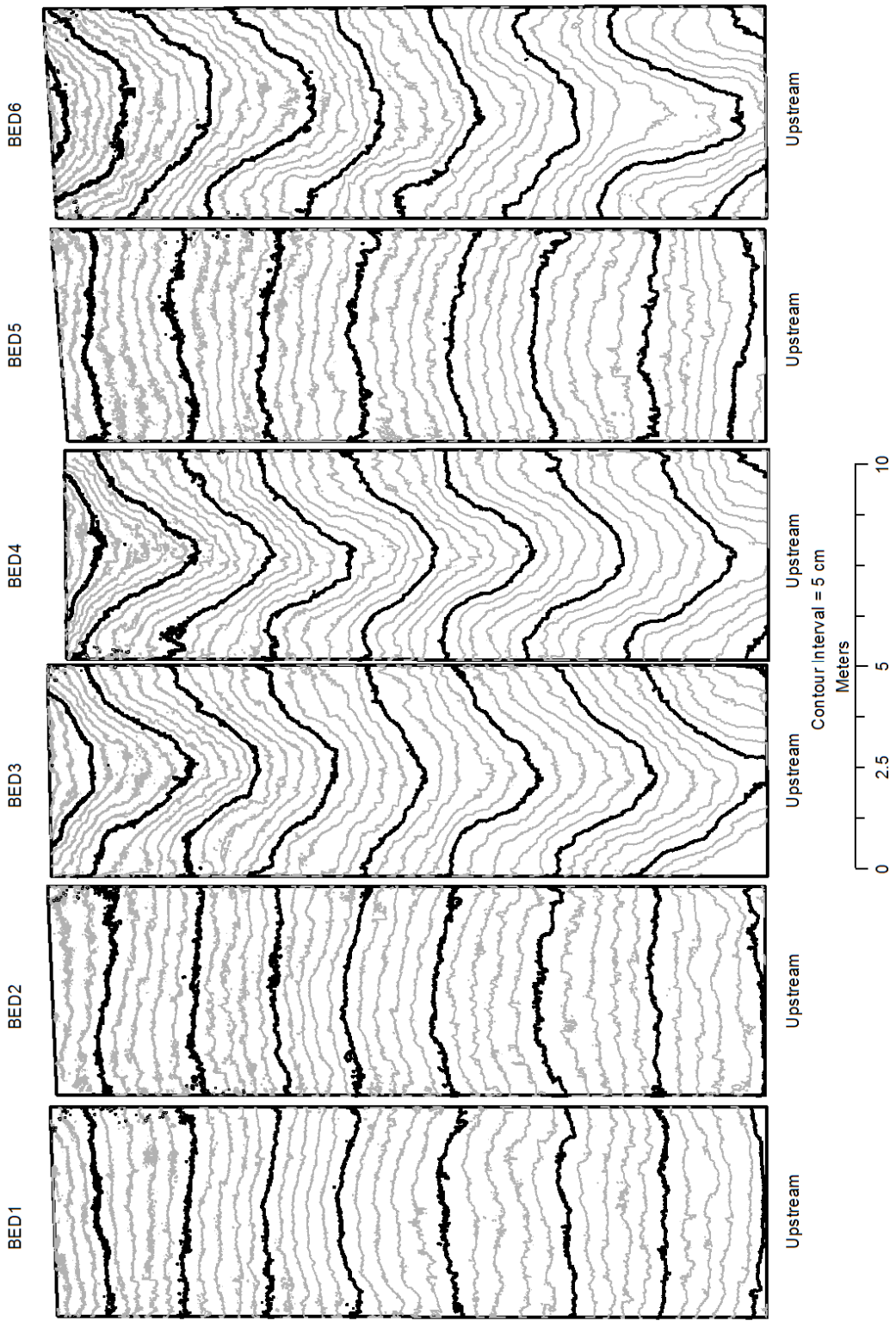

Figure 21. Contour plots of SEP 1 – 6 based upon surface laser scan data.

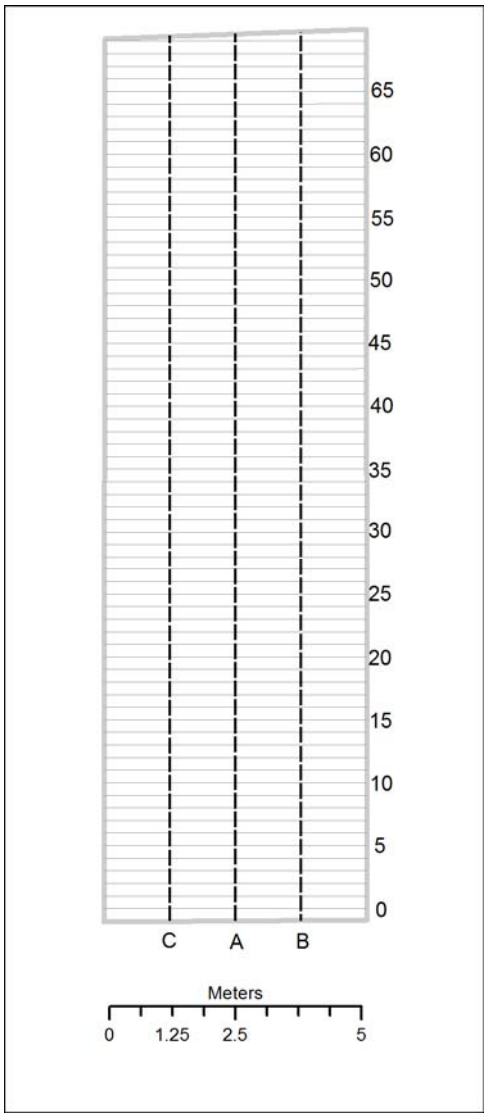

Figure 22. General cross-section schema used in all six beds. Transverse cross-sections are represented by gray lines and numbered from zero to 69. Zero represents the most upstream transect. Longitudinal cross-sections are represented by dashed black lines (A, B and C). Transverse cross-sections are spaced at 25 cm and longitudinal cross-sections at 130 cm.

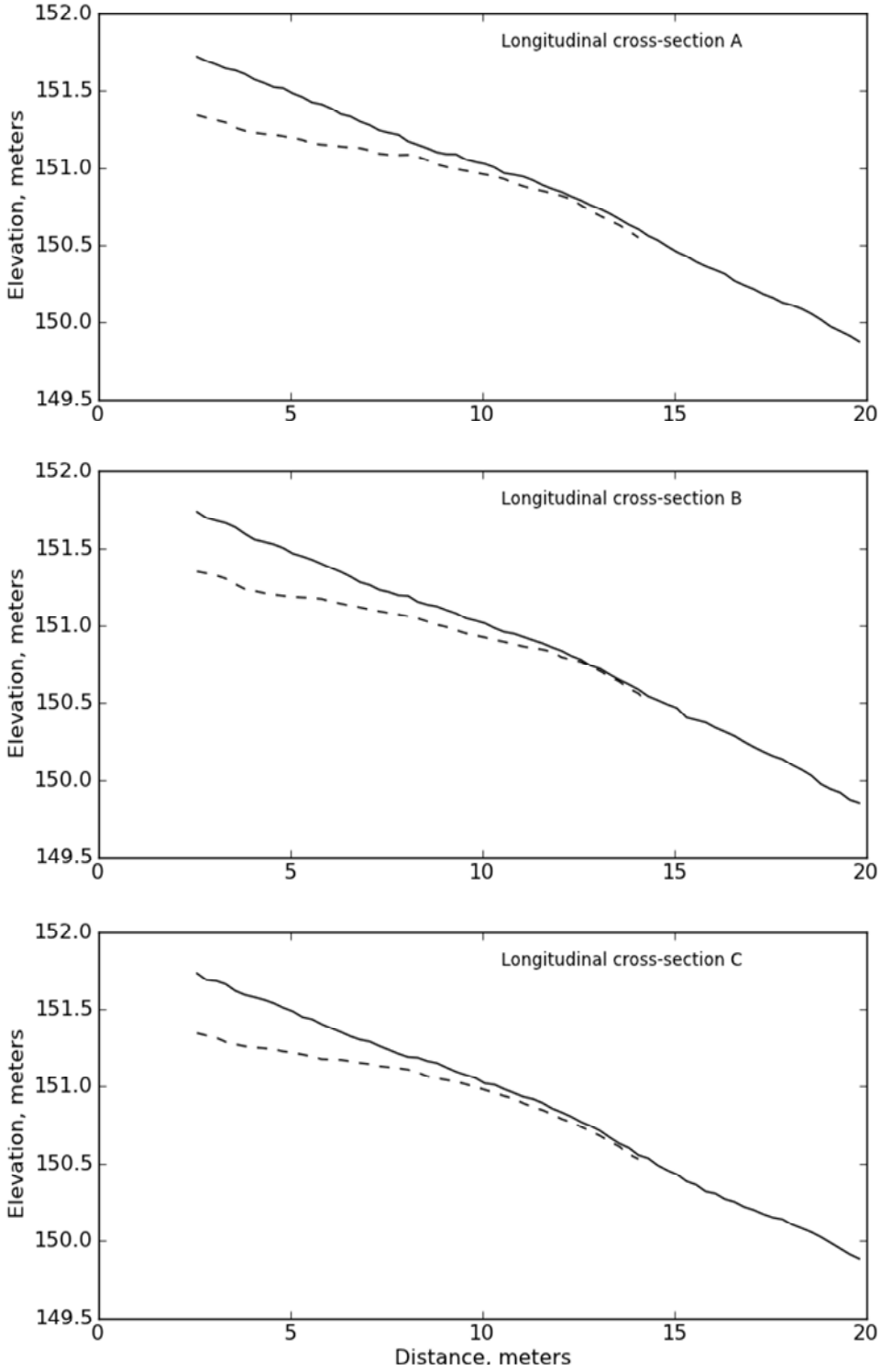

Figure 23. Longitudinal cross-sections for SEP 1 of the top of the compacted clay layer (dashed line) and the soil surface (solid line).

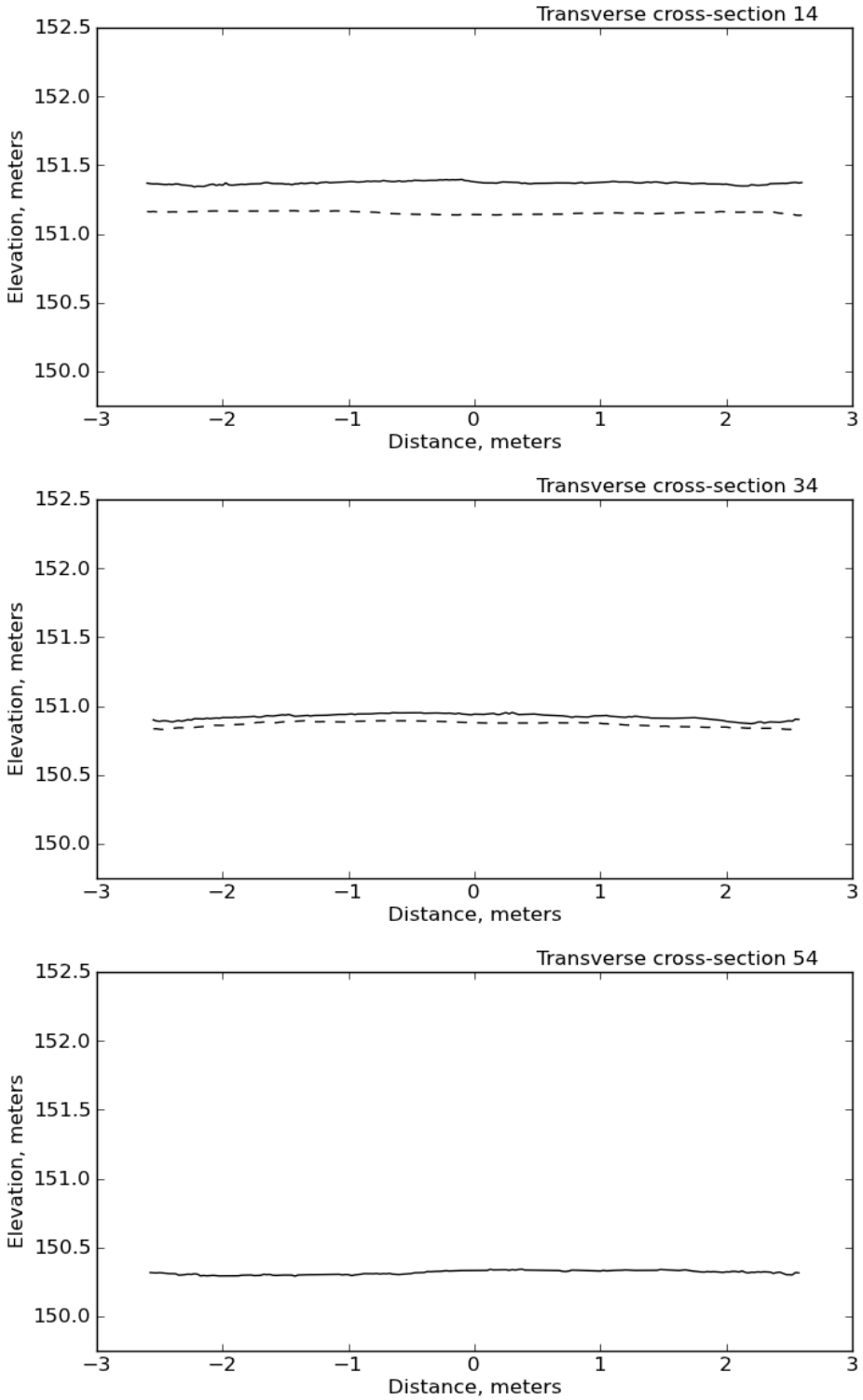

Figure 24. Transverse cross-sections 14, 34 and 54 for SEP 1 (see Fig. 22). Dashed line represents the clay layer and solid line represents the initial soil surface.

CONCLUSIONS

Ephemeral gully erosion is a critical problem that significantly damages and deteriorates agricultural lands worldwide yet little mechanistic work has been done on the subsurface flow processes contributing to gully initiation. The basic research and resulting prediction technology are still in the developmental stage. Quantification of the impact of seepage on erosion rates and gully formation are needed under controlled hydrologic conditions for a wide range of soil and land use conditions. The above ground facilities described herein were designed and constructed to fill the knowledge gap in this area of ephemeral gully erosion.

REFERENCES

Collison, A.J.C. 2001. The cycle of instability: stress release and fissure flow as controls on gully head retreat. Hydrol. Proc., 15:3-12.

Cullum, R.F., G.V. Wilson, K.C. McGregor, and J.R. Johnson. 2007. Runoff and soil loss from ultra narrow-row cotton plots with and without stiff-grass hedges. J. Soil and Tillage Res. 93(1):56-63.

Darboux, F, and C.H. Huang. 2005. Does soil surface roughness increase or decrease water and particle transfer. Soil Sci. Soc. Am. J. 69:748-756.

Faulkner, H. 2006. Piping hazard on collapsible and dispersive soils in Europe. In: Soil Erosion in Europe, J. Boardman, J. Poesen (Editors) John Wiley & Sons, Ltd.

Fredlund, D.G., N.R. Morgenstern, and R.A. Widger. 1978. The shear strength of unsaturated soils. Canadian Geotechnical J. 15:313-321.

Fox, G.A., Herren, D.M., G.V. Wilson, E.J. Langendoen, A.K. Fox, and *M.L. Chu-Agor***.** 2010. Numerically predicting seepage gradient forces and erosion sensitivity to soil hydraulic properties. J. Hydrol., 389:354-362.

Gabbard, D.S., C.H. Huang, L.D. Norton, and G.C. Steinhardt. 1998. Landscape position, subsurface hydraulic gradients and erosion processes. Earth Surface Proc. Land., 23: 83-93.

Howard, A.D., and C.F. McLane, III. 1988. Erosion of cohesionless sediment by ground water seepage. Water Resour. Res., 24(10): 1659-1674.

Huang, C.H., and J.M. Laflen. 1996. Seepage and soil erosion for a clay loam soil. Soil Sci. Soc. Am. J. 60:408-416.

Huang, C.H., L.K. Wells, and L.D. Norton. 1999. Sediment transport capacity and erosion processes: Model concepts and reality. Earth Surface Processes and Landforms 24 (6): 503-516.

McGregor, K.C., R.F. Cullum, and C.K. Mutchler. 1999. Long-term management effects on runoff, erosion, and crop production. Transactions of ASAE, Amer. Soc., Agroic. Eng., St. Joseph, MI. 42(1): 99-105.

Measures R. M., 1984. Laser Remote Sensing Fundamentals and Applications. John Wiley & Sons, Inc.

Momm, H.G., R. Bingner, R. Wells, and S. Dabney. 2011. Methods for Gully Characterization in Agricultural Croplands using Ground-Based Light Detection and Ranging. Sediment Transport / Book 2. Dr. ABM Faruk Bhuiyan (Ed.), ISBN: 979-953-307-248-6, InTech.

Owoputi, L.O., and W.J. Stolte. 2001. The role of seepage in erodibility. Hydrol. Proc., 15:13-22.

Poesen, J., J. Nachtergaele, G. Verstraeten, and C. Valentin. 2003. Gully erosion and environmental change: importance and research needs. Catena 50, pp. 91–133.

Soil Science Society of America. 2008. Glossary of Soil Science Terms. Soil Science Society of America, Madison, WI.

Thoman, R.W., and S.L. Niezgoda. 2008. Determining erodibility, critical shear stress, and allowable discharge estimates for cohesive channels: Case study in the Powder River Basin of Wyoming. J. Hydraulic Eng., 134: 1677-1687.

U.S. Environmental Protection Agency. 2000. Atlas of America's Polluted Waters, EPA 840-B-00-002. Office of Water (4503F). United States Environmental Protection Agency, Washington, D.C.

USDA-NRCS. 1997. America's Private Land: A Geography of Hope. USDA-Natural Resources Conservation Service, Washington, DC.

Wehr, A. and U. Lohr, 1999. Airborne laser scanning – An introduction and overview, ISPRS Journal of Photogrammetry and Remote Sensing, 54(2-3): 68-82.

Wilson G.V., P.M. Jardine R.J. Luxmoore, and J.R. Jones. 1990. Hydrology of a forested watershed during storm events. Geoderma, 46: 119-138.

Wilson G.V., P.M. Jardine R.J. Luxmoore, L.W. Zelazny D.A. Lietzke, and D.E. Todd. 1991. Hydrogeochemical processes controlling subsurface transport from an upper subcatchment of Walker Branch Watershed during storm events: 1. Hydrologic transport process. J. Hydrol., 123: 297-316.

Wilson G.V., R.K. Periketi, G.A. Fox, S.M. Dabney, F.D. Shields, Jr., and R.F. Cullum. 2007. Seepage erosion properties contributing to streambank failure. Earth Surf. Proc. Land., 32(3): 447-459.

Wilson, G.V., K.C. McGregor, and D. Boykin. 2008. Residue impacts on runoff and soil erosion for different corn plant populations. J. Soil and Till. Res. 99(2): 300-307

Zheng, F.L., C.H. Huang, and L.D. Norton. 2000. Vertical hydraulic gradient and run-on water and sediment effects on erosion processes and sediment regimes. Soil Science Society of America Journal, 64(1): 4-11.

APPENDIX

REPRESENTATION OF INITIAL TOPOGRAPHIC CONDITIONS
See Fig. 22 for reference to cross section locations.

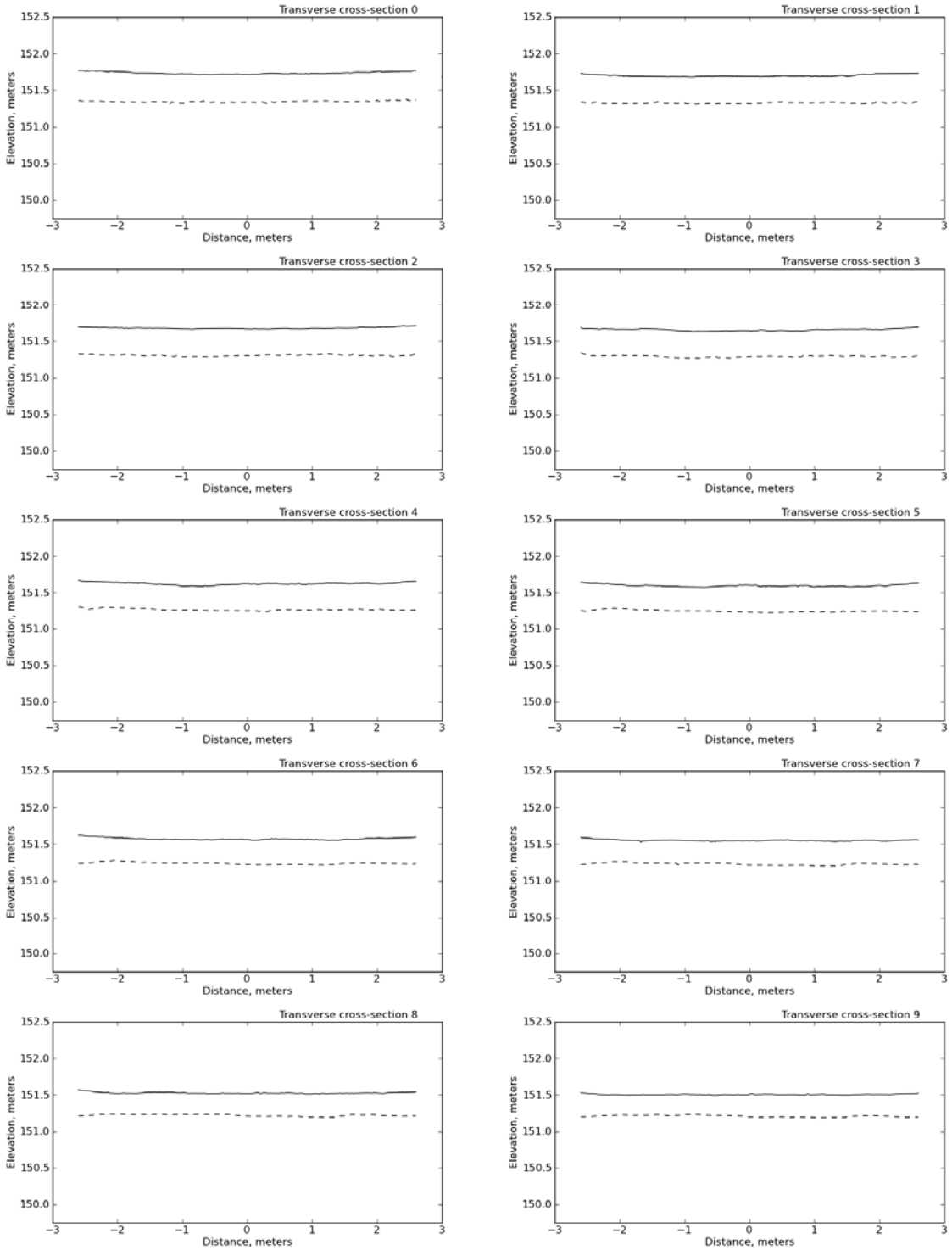

Figure A1. Transverse cross-sections 0 to 9 for SEP 1. Dashed line represents the clay layer and solid line represents the soil surface.

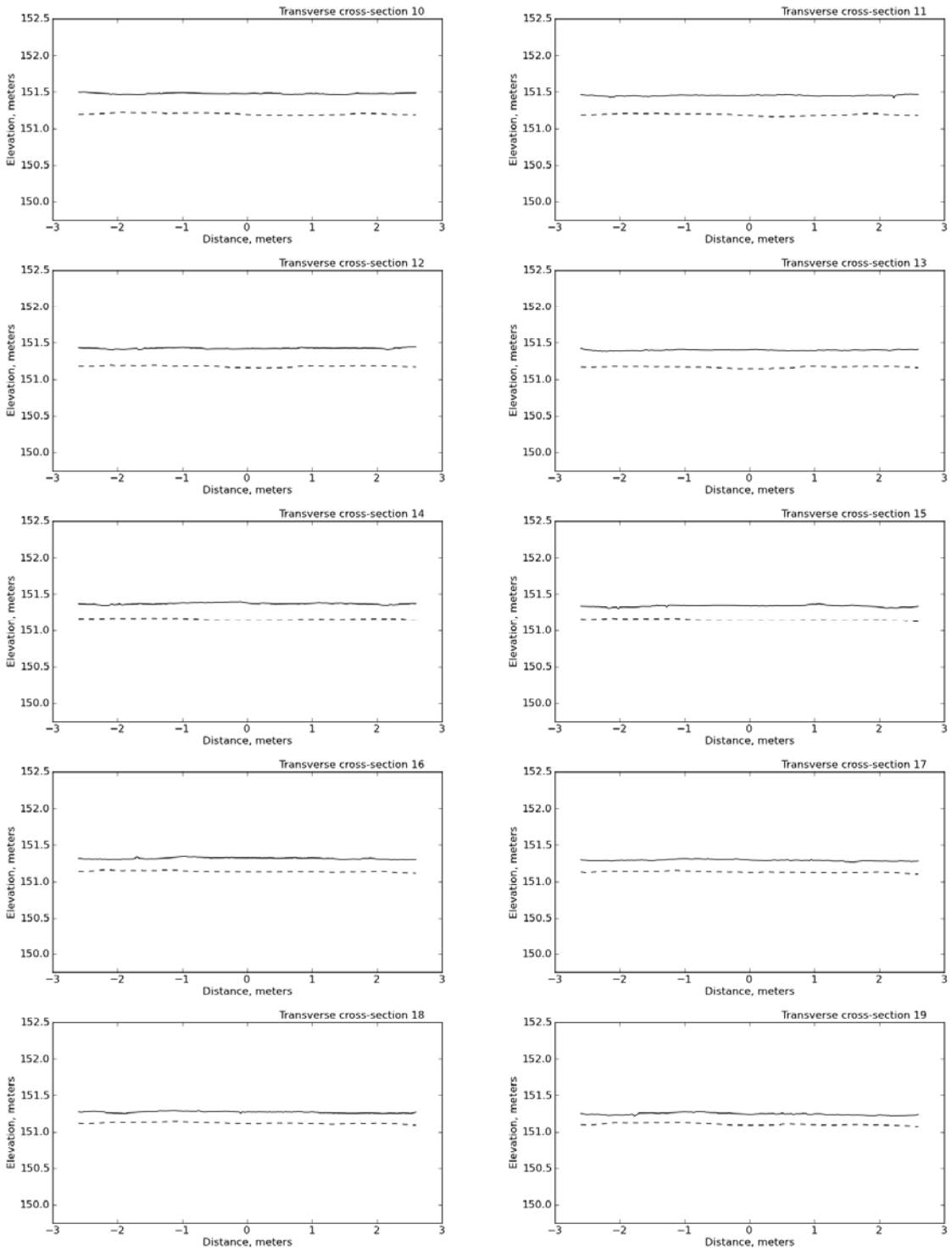

Figure A2. Transverse cross-sections 10 to 19 for SEP 1. Dashed line represents the clay layer and solid line represents the soil surface.

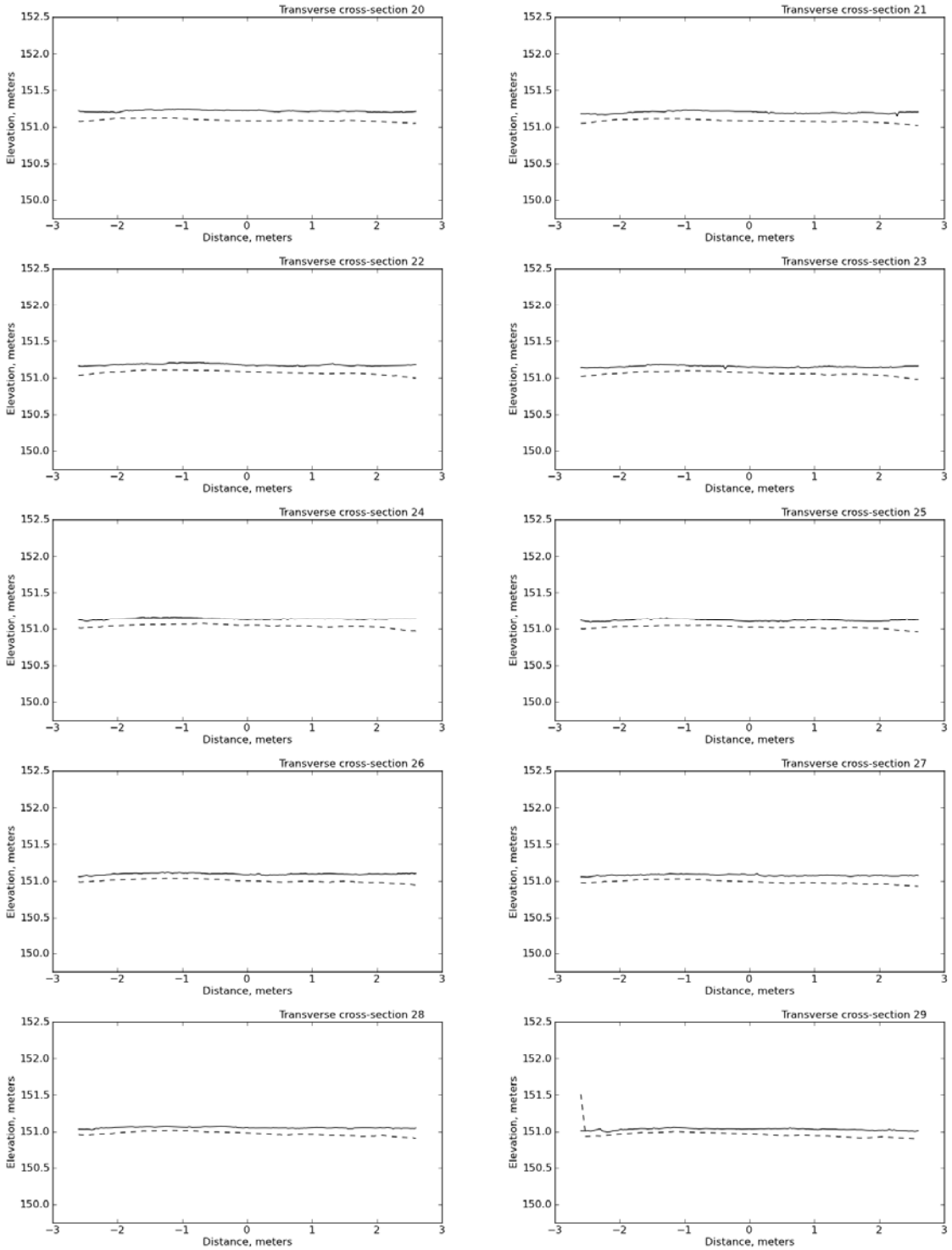

Figure A3. Transverse cross-sections 20 to 29 for SEP 1. Dashed line represents the clay layer and solid line represents the soil surface.

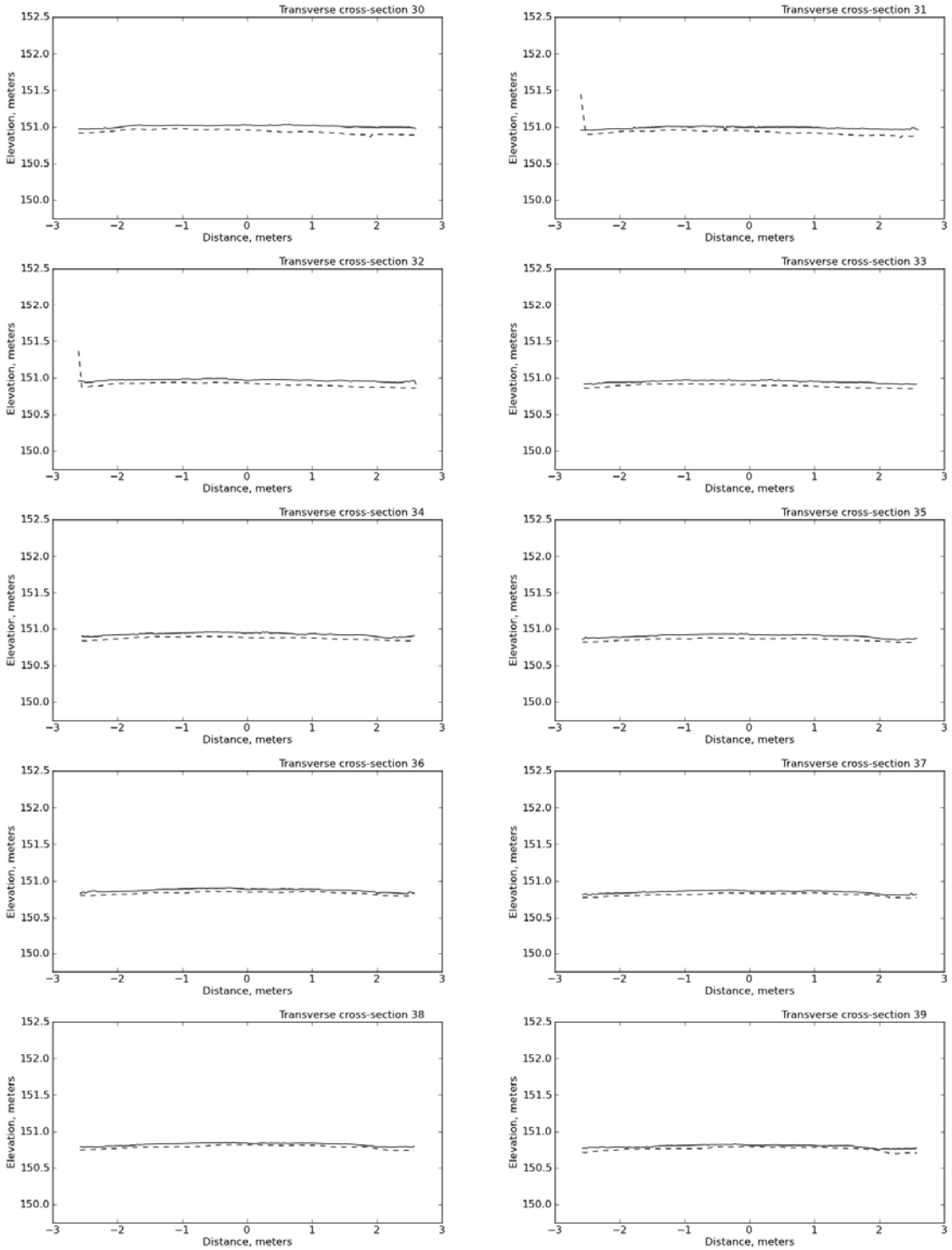

Figure A4. Transverse cross-sections 30 to 39 for SEP 1. Dashed line represents the clay layer and solid line represents the soil surface.

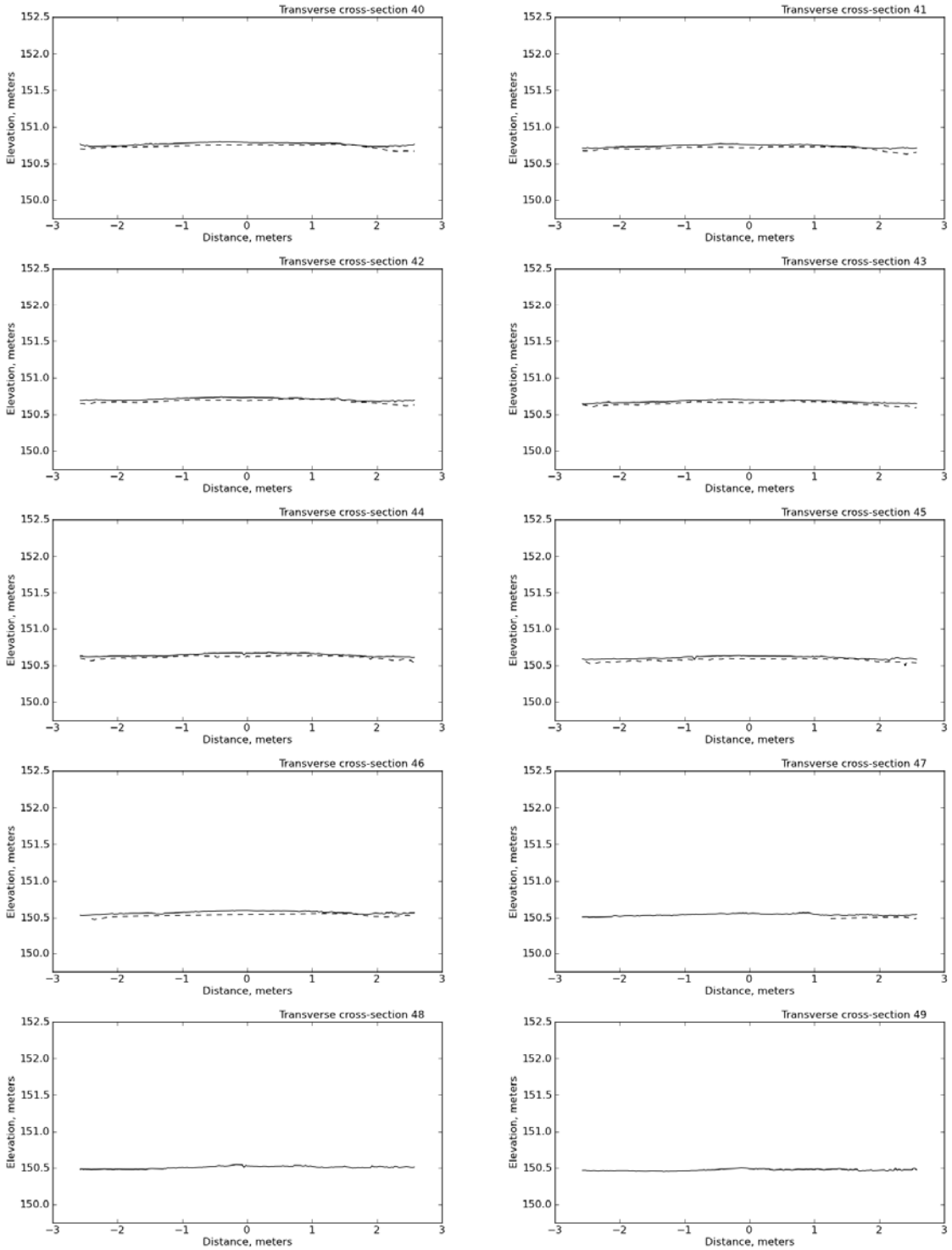

Figure A5. Transverse cross-sections 40 to 49 for SEP 1. Dashed line represents the clay layer and solid line represents the soil surface.

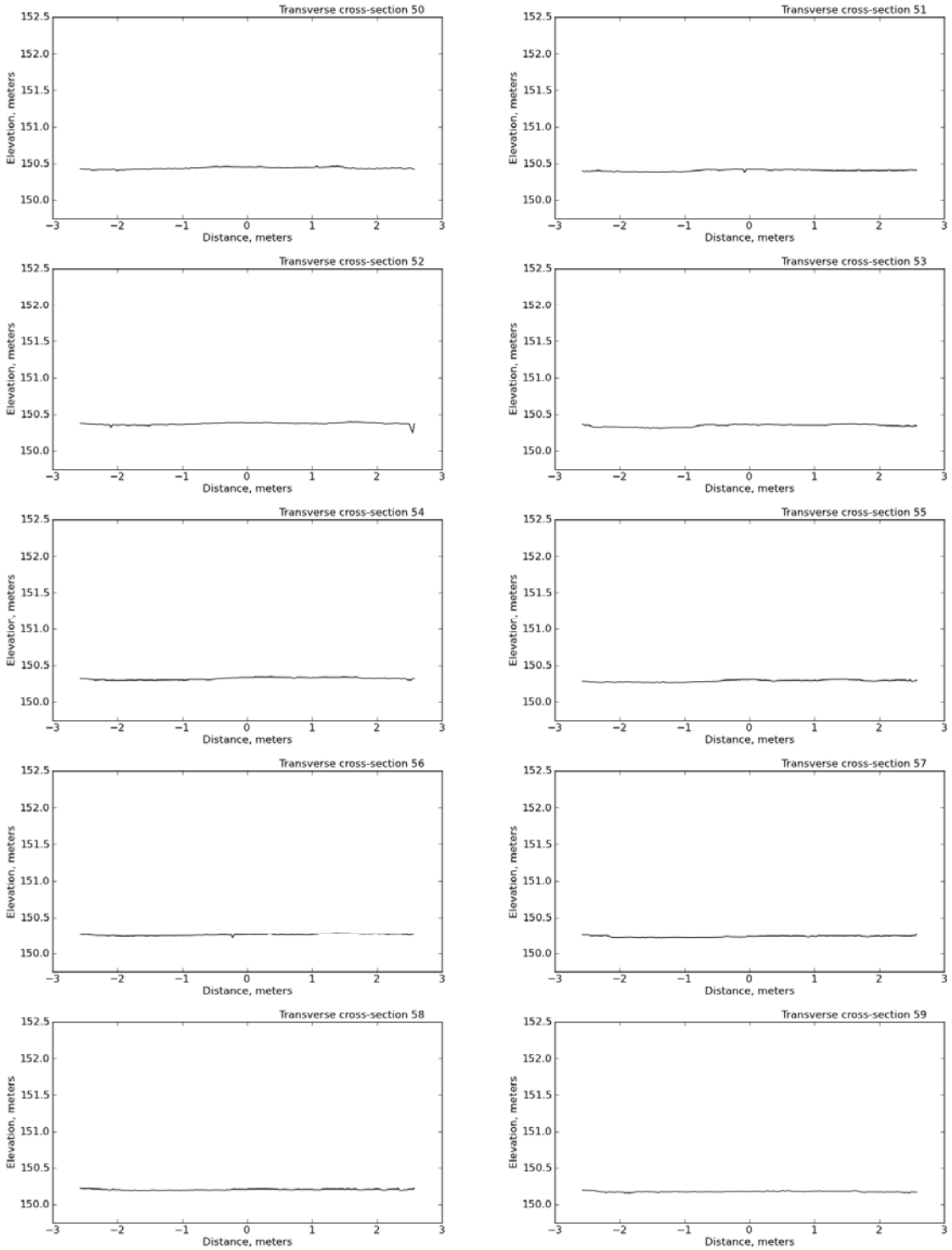

Figure A6. Transverse cross-sections 50 to 59 for SEP 1. Dashed line represents the clay layer and solid line represents the soil surface.

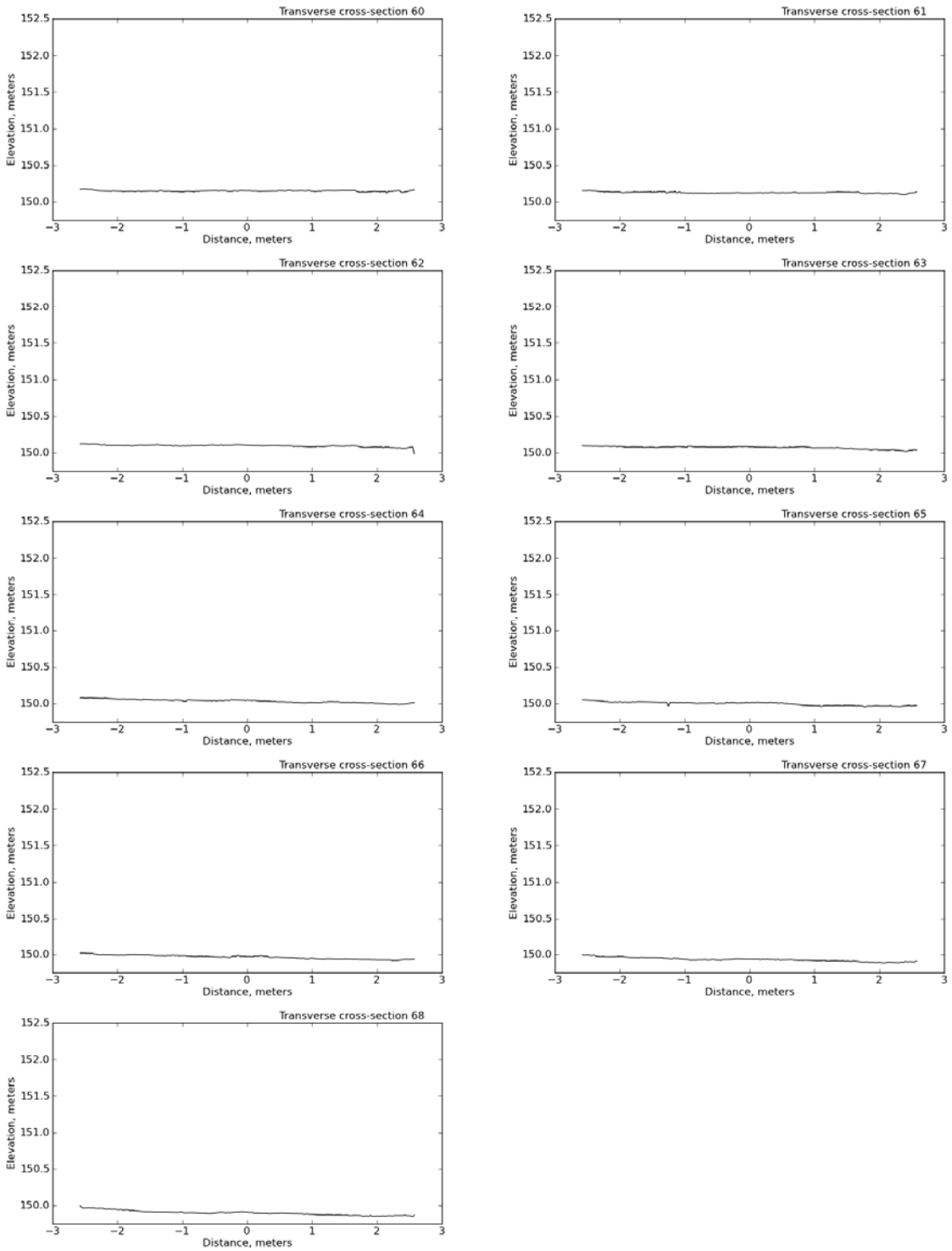

Figure A7. Transverse cross-sections 60 to 68 for SEP 1. Dashed line represents the clay layer and solid line represents the soil surface.

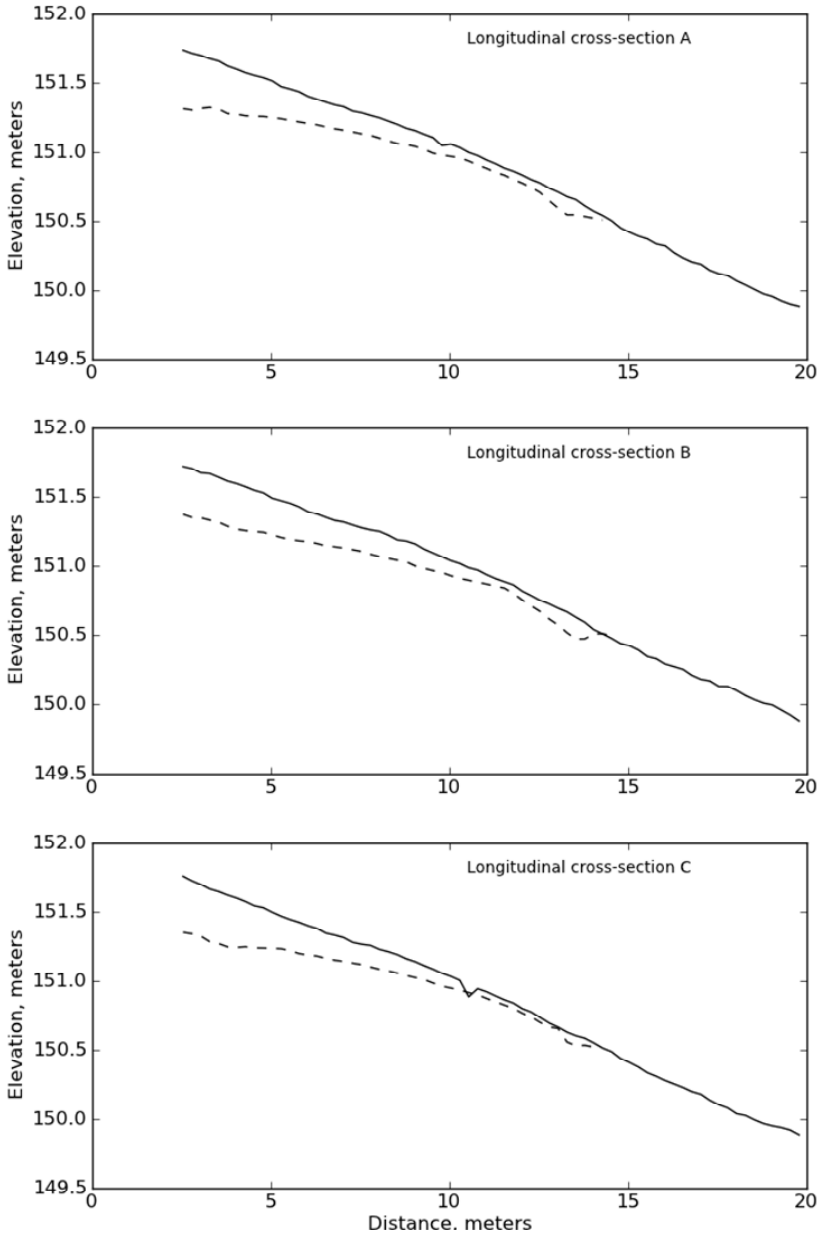

Figure A8. Longitudinal cross-sections for SEP 2.

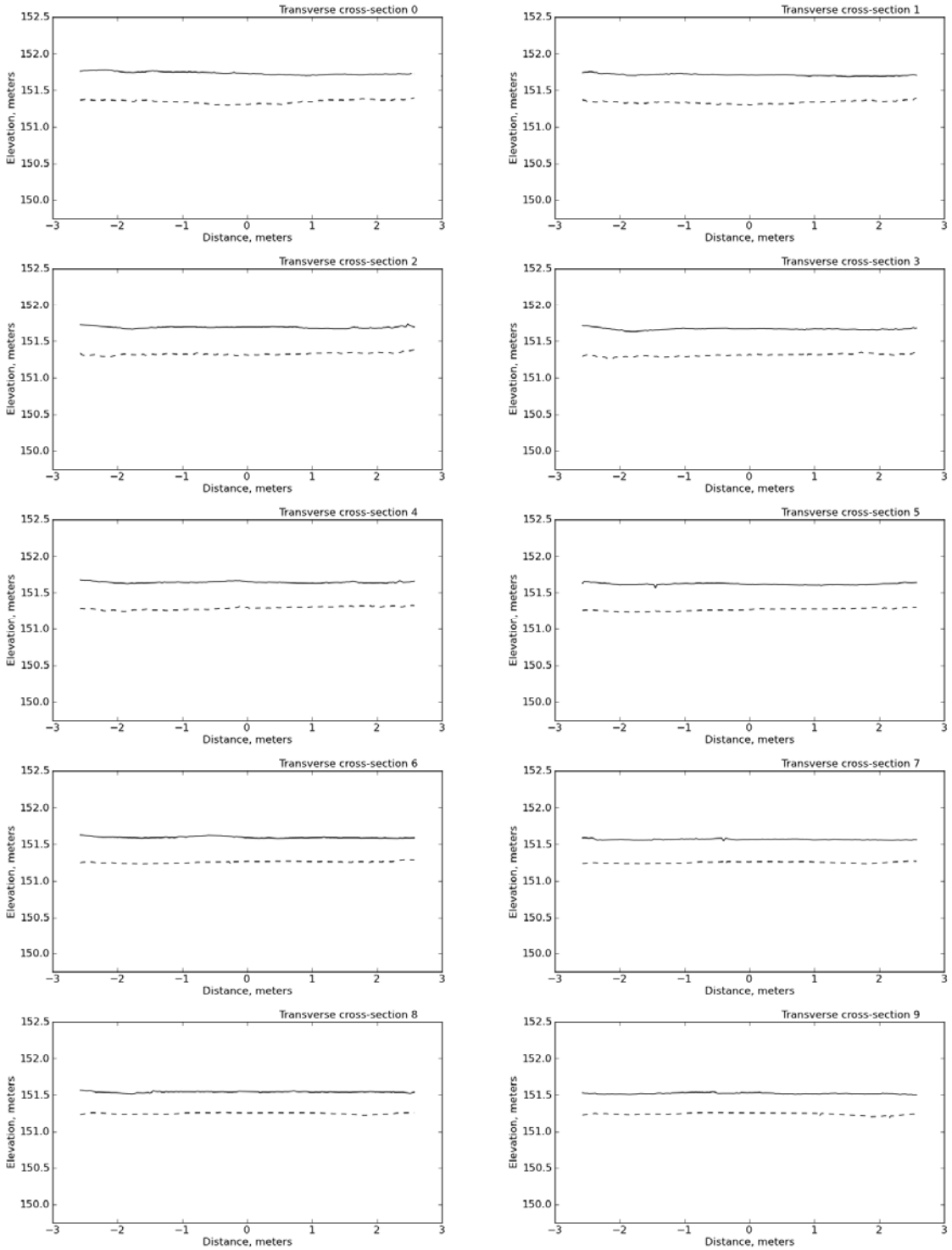

Figure A9. Transverse cross-sections 0 to 9 for SEP 2. Dashed line represents the clay layer and solid line represents the soil surface.

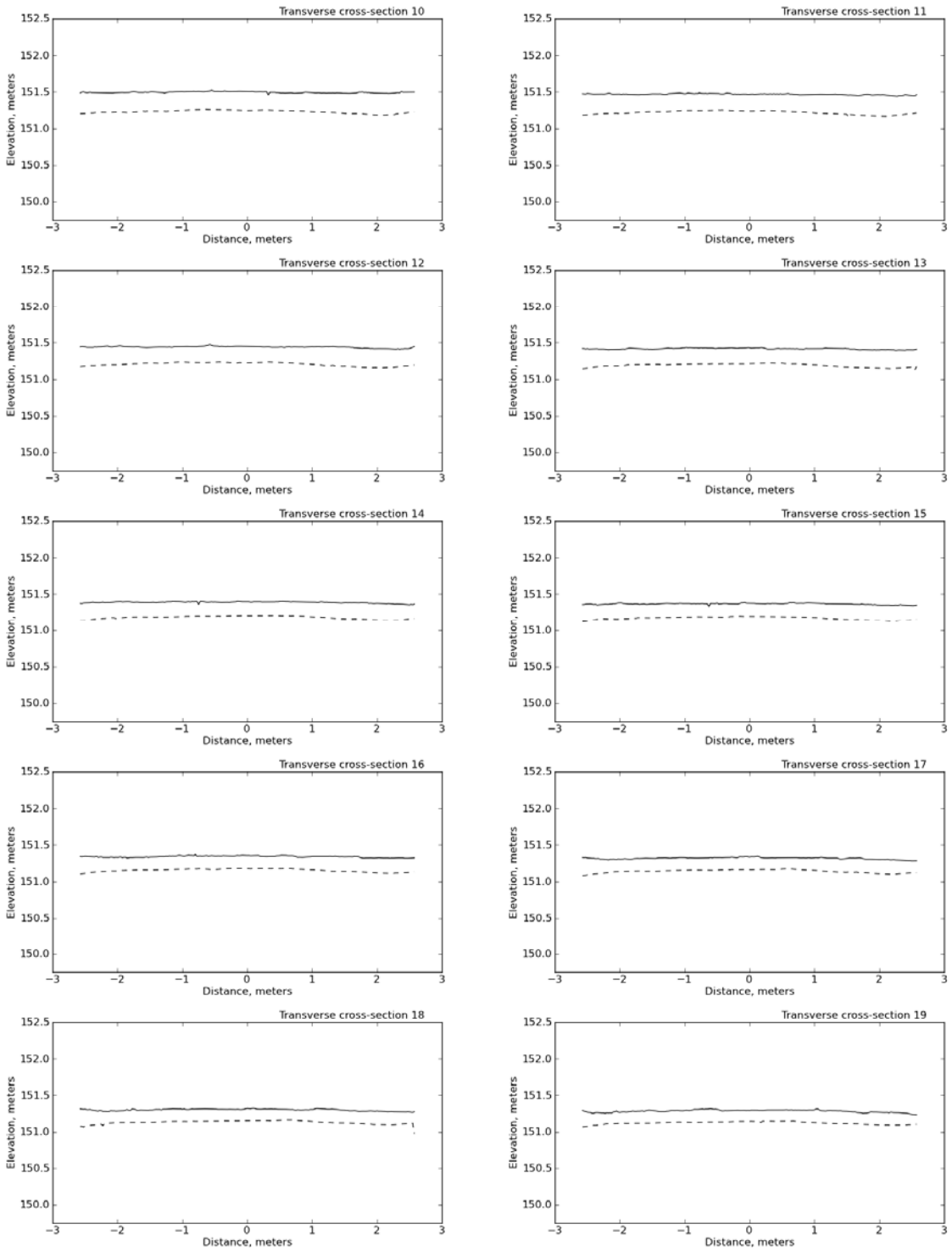

Figure A10. Transverse cross-sections 10 to 19 for SEP 2. Dashed line represents the clay layer and solid line represents the soil surface.

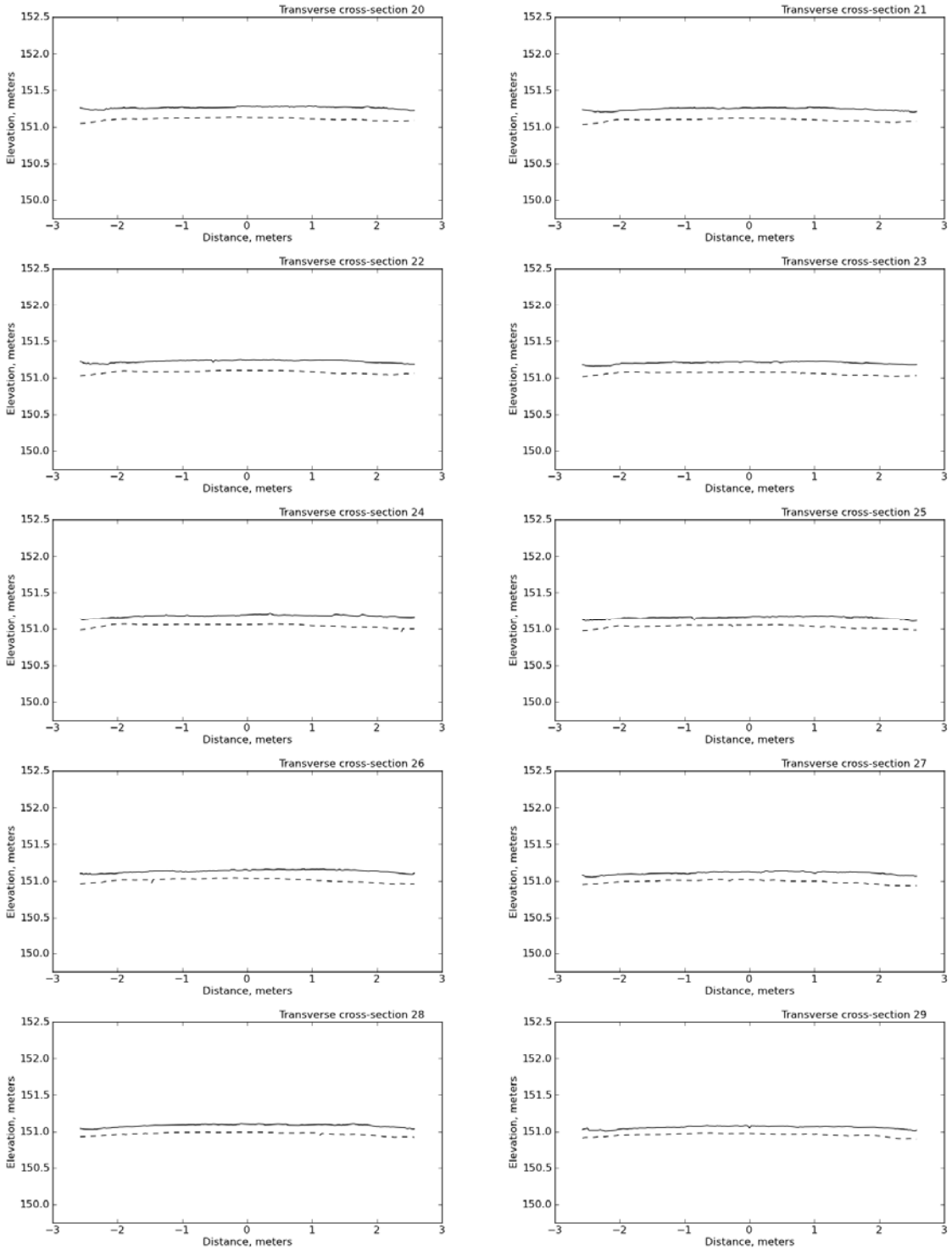

Figure A11. Transverse cross-sections 20 to 29 for SEP 2. Dashed line represents the clay layer and solid line represents the soil surface.

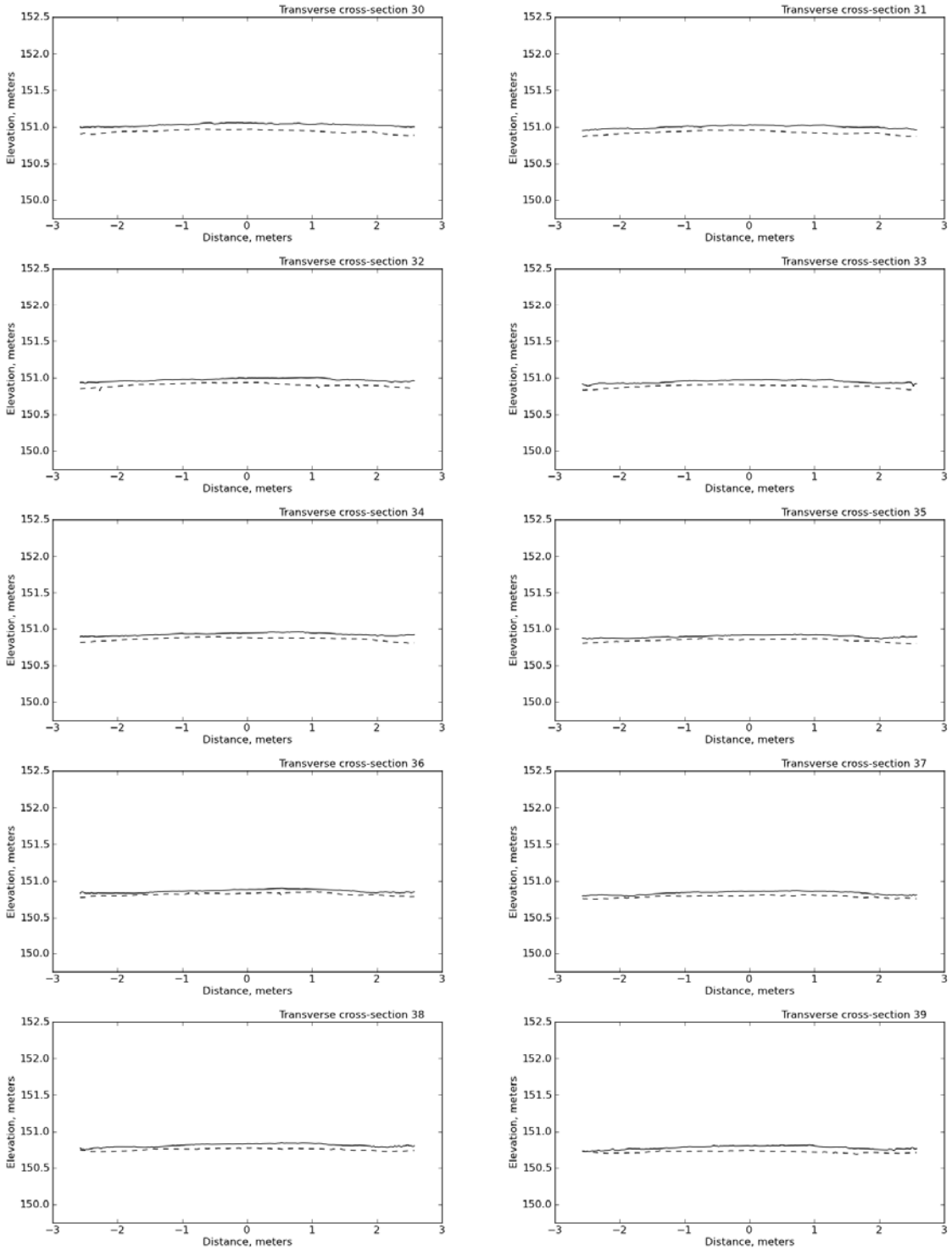

Figure A12. Transverse cross-sections 30 to 39 for SEP 2. Dashed line represents the clay layer and solid line represents the soil surface.

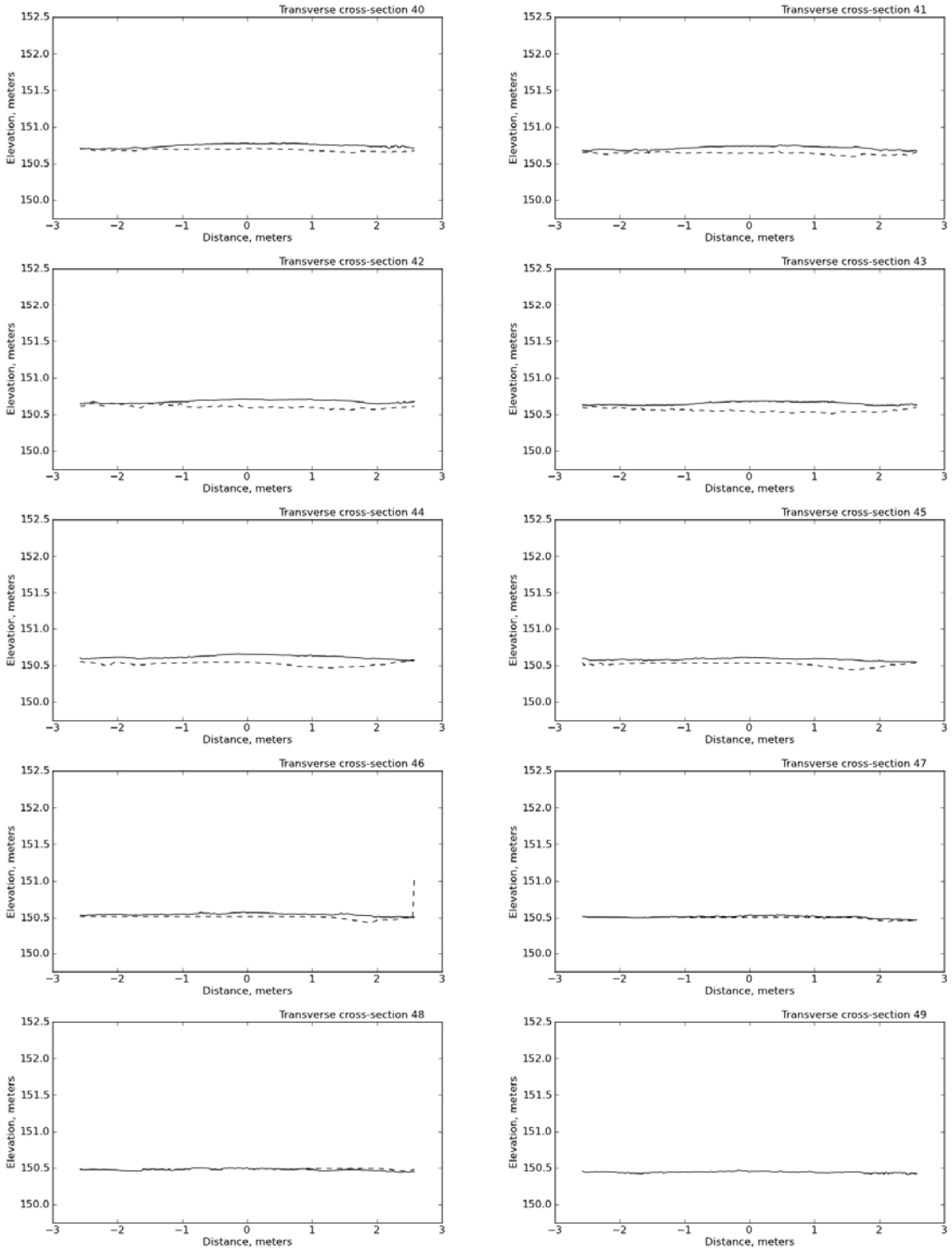

Figure A13. Transverse cross-sections 40 to 49 for SEP 2. Dashed line represents the clay layer and solid line represents the soil surface.

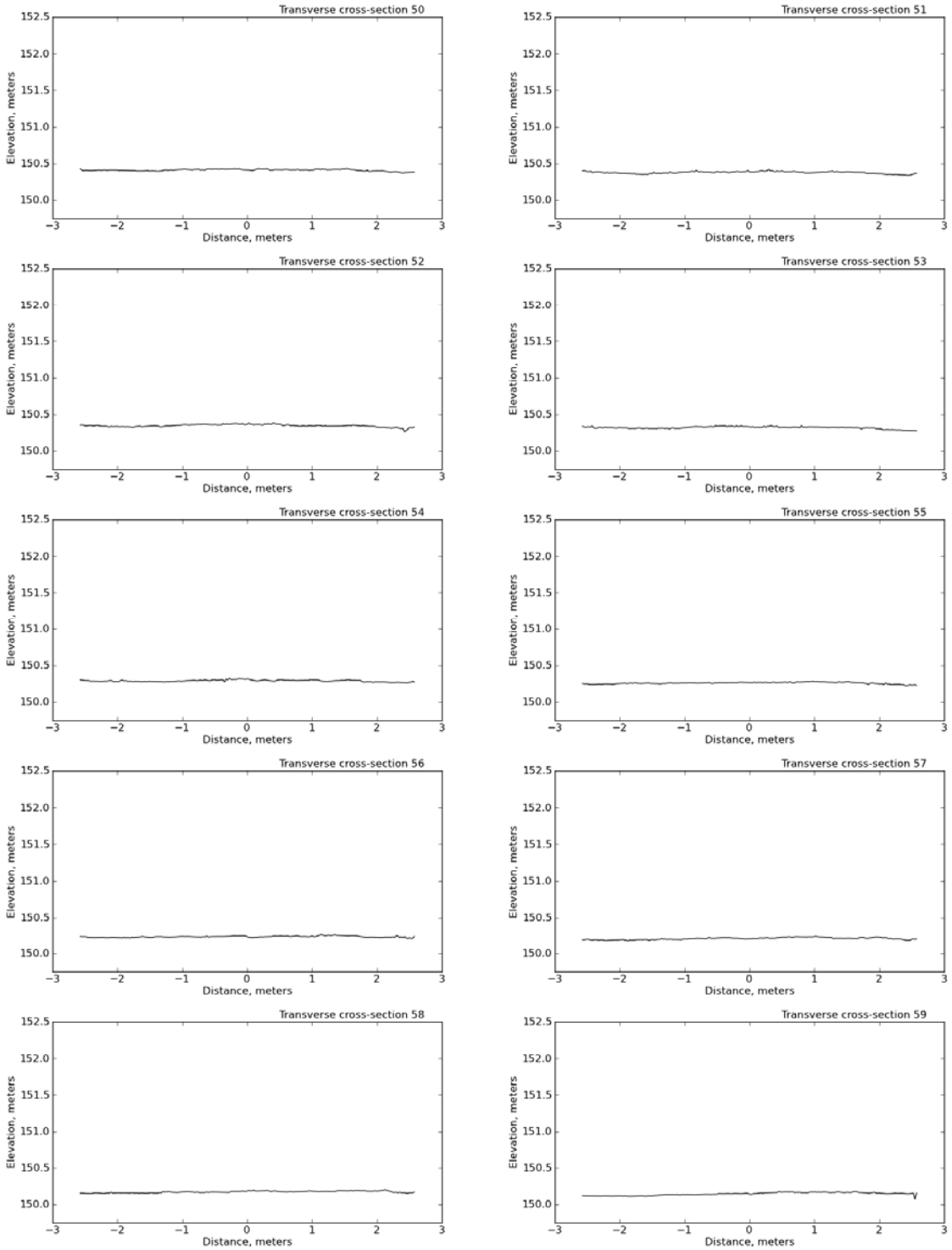

Figure A14. Transverse cross-sections 50 to 59 for SEP 2. Dashed line represents the clay layer and solid line represents the soil surface.

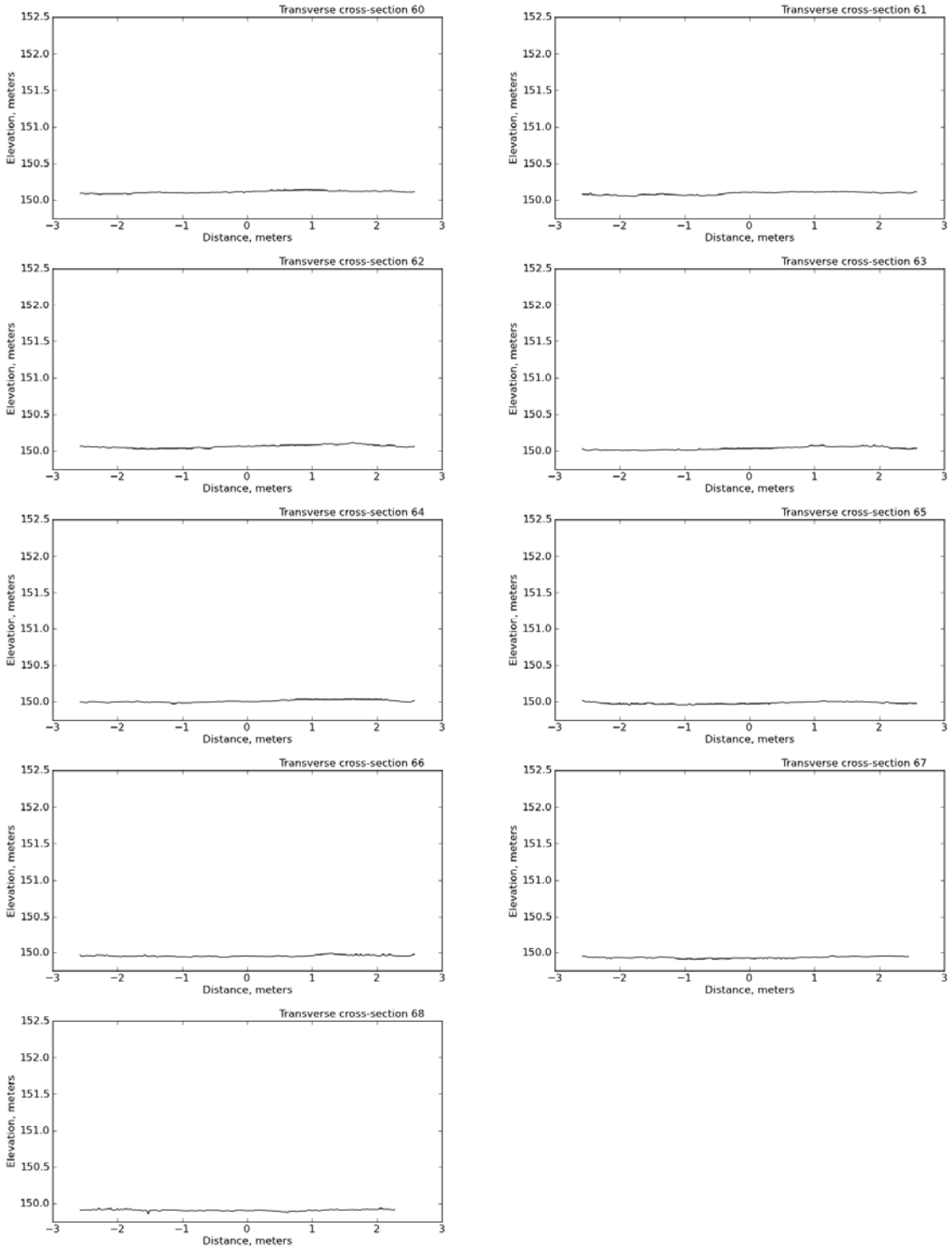

Figure A15. Transverse cross-sections 60 to 68 for SEP 2. Dashed line represents the clay layer and solid line represents the soil surface.

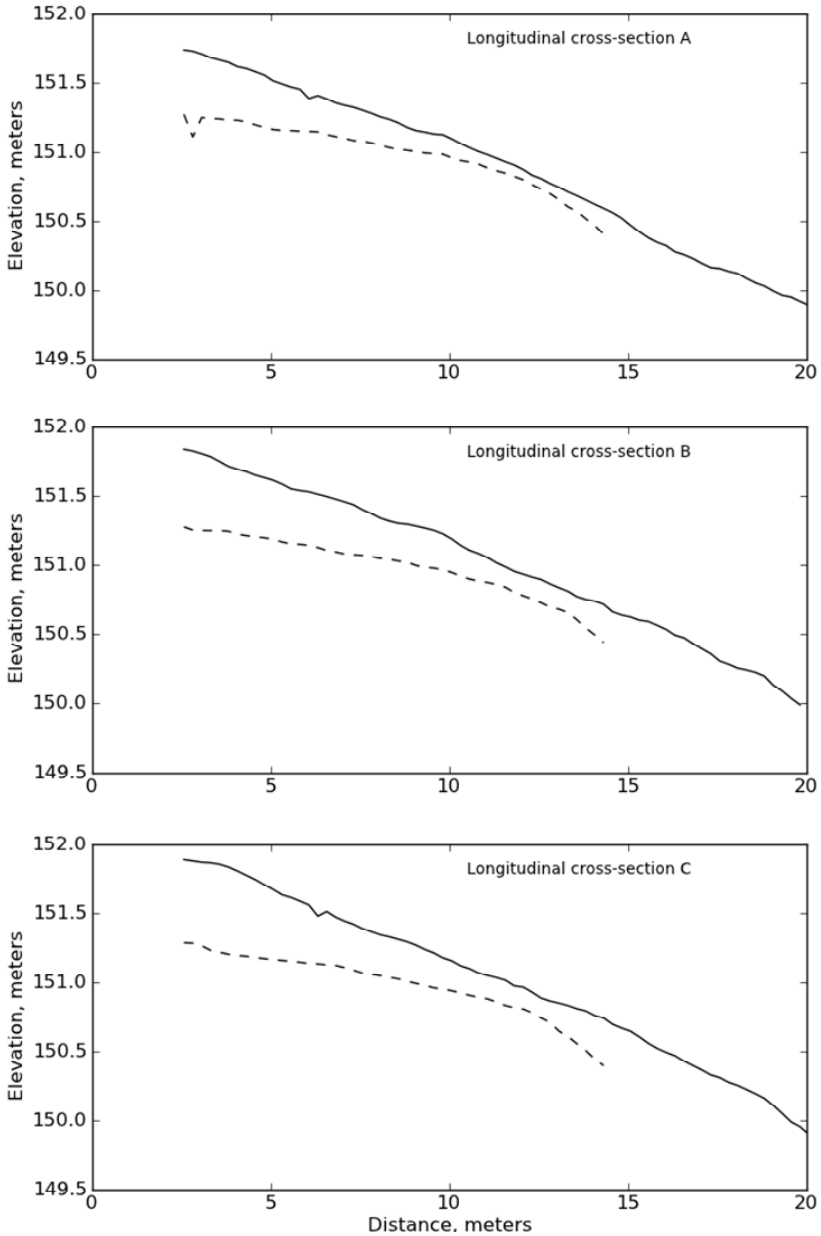

Figure A16. Longitudinal cross-sections for SEP 3.

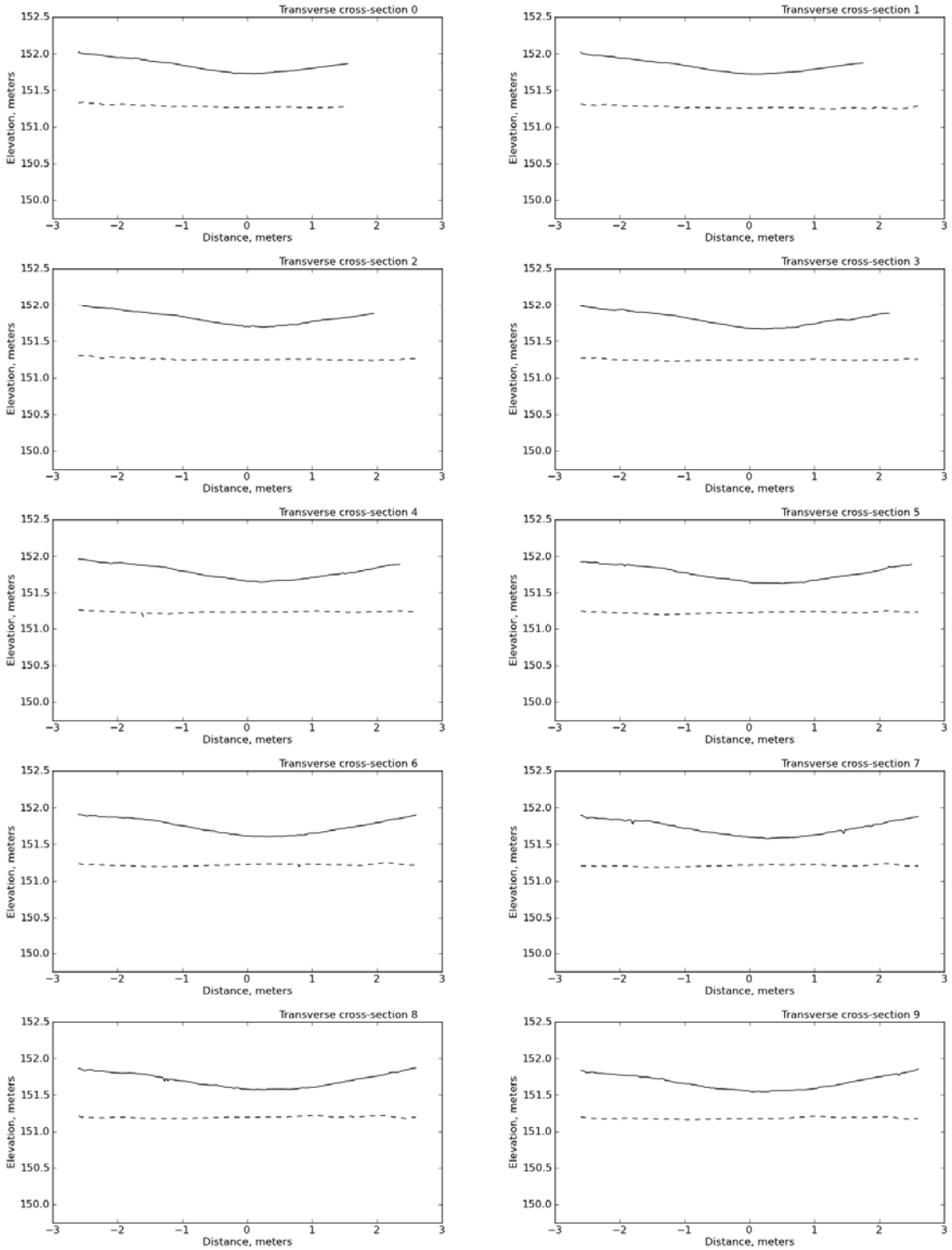

Figure A17. Transverse cross-sections 0 to 9 for SEP 3. Dashed line represents the clay layer and solid line represents the soil surface.

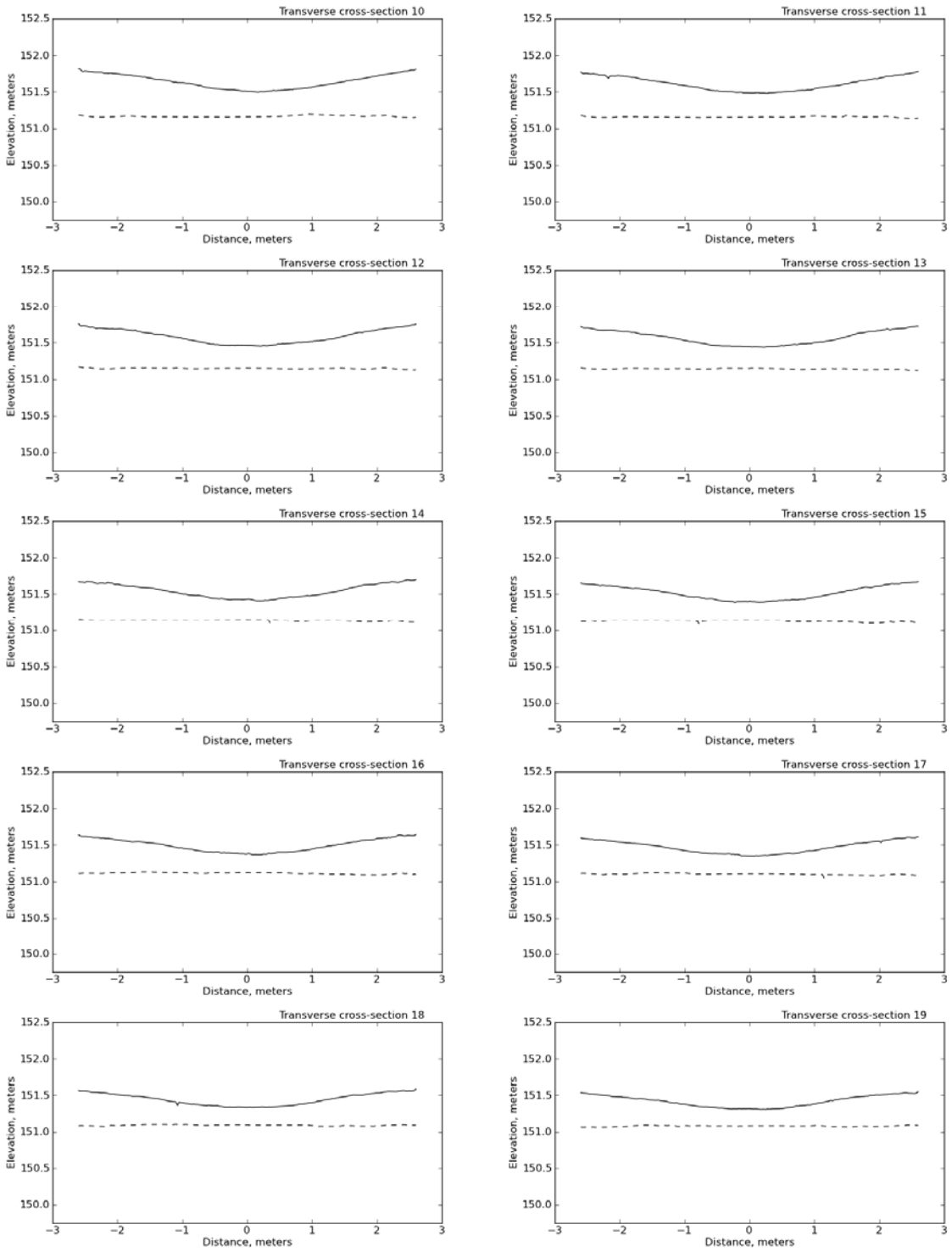

Figure A18. Transverse cross-sections 10 to 19 for SEP 3. Dashed line represents the clay layer and solid line represents the soil surface.

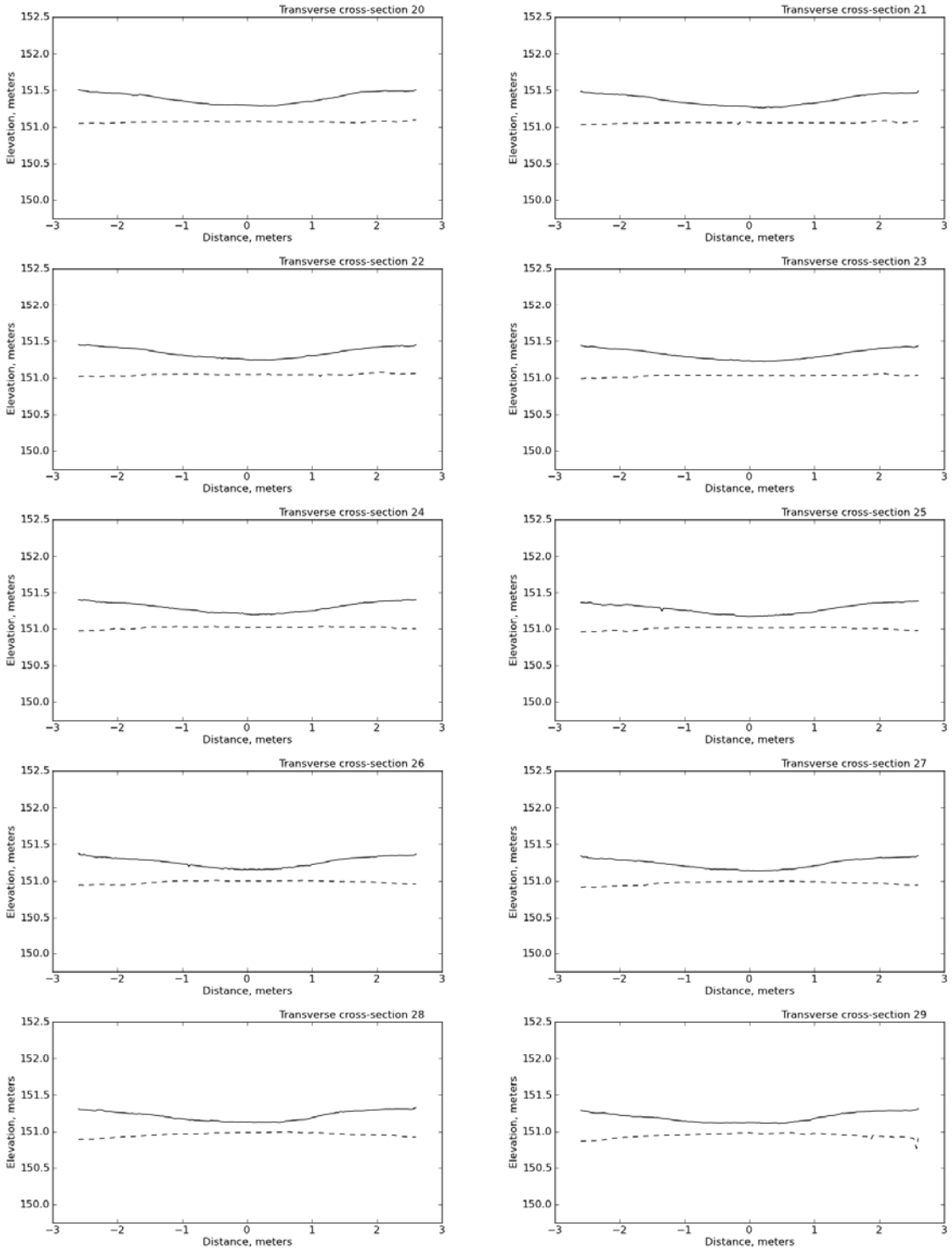

Figure A19. Transverse cross-sections 20 to 29 for SEP 3. Dashed line represents the clay layer and solid line represents the soil surface.

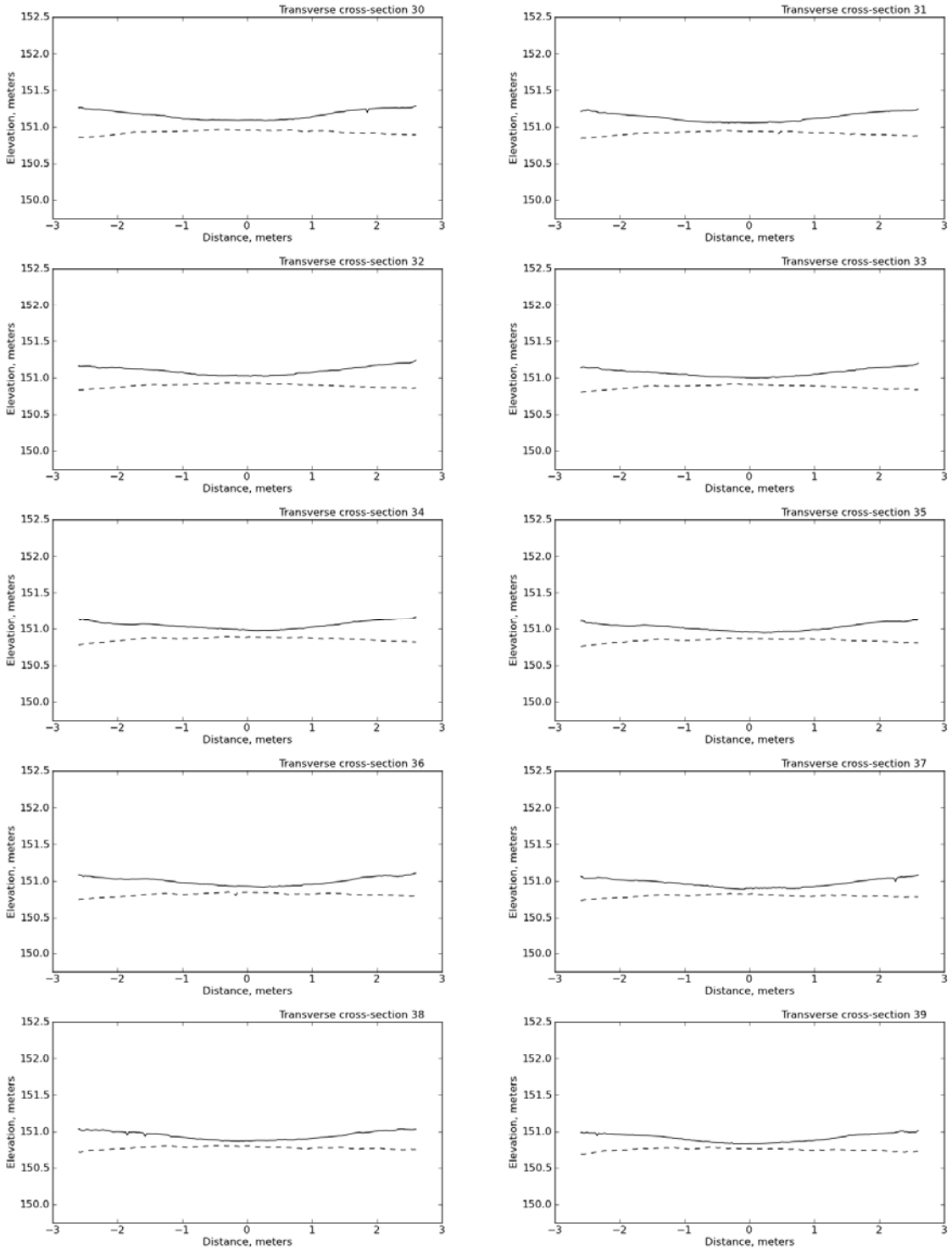

Figure A20. Transverse cross-sections 30 to 39 for SEP 3. Dashed line represents the clay layer and solid line represents the soil surface.

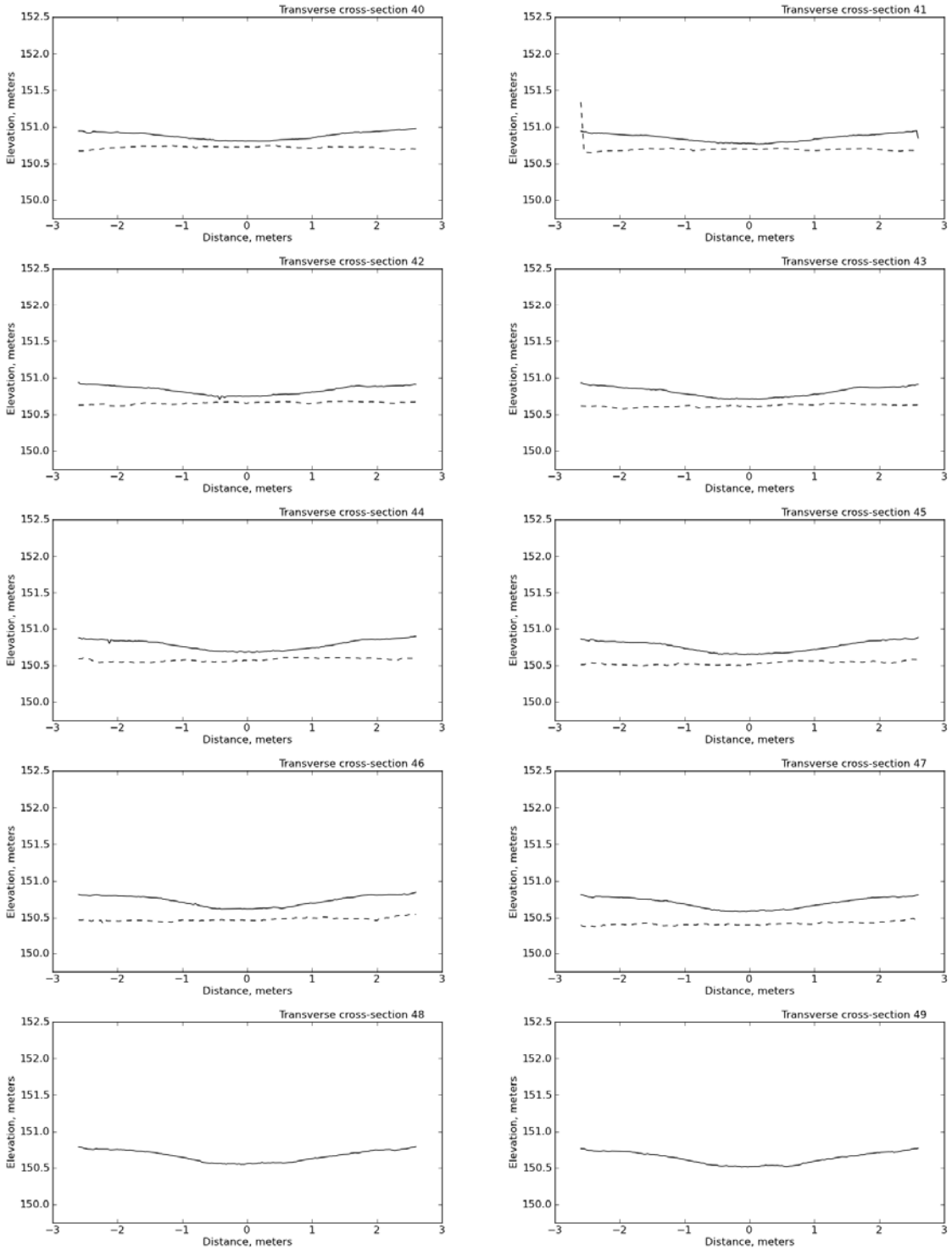

Figure A21. Transverse cross-sections 40 to 49 for SEP 3. Dashed line represents the clay layer and solid line represents the soil surface.

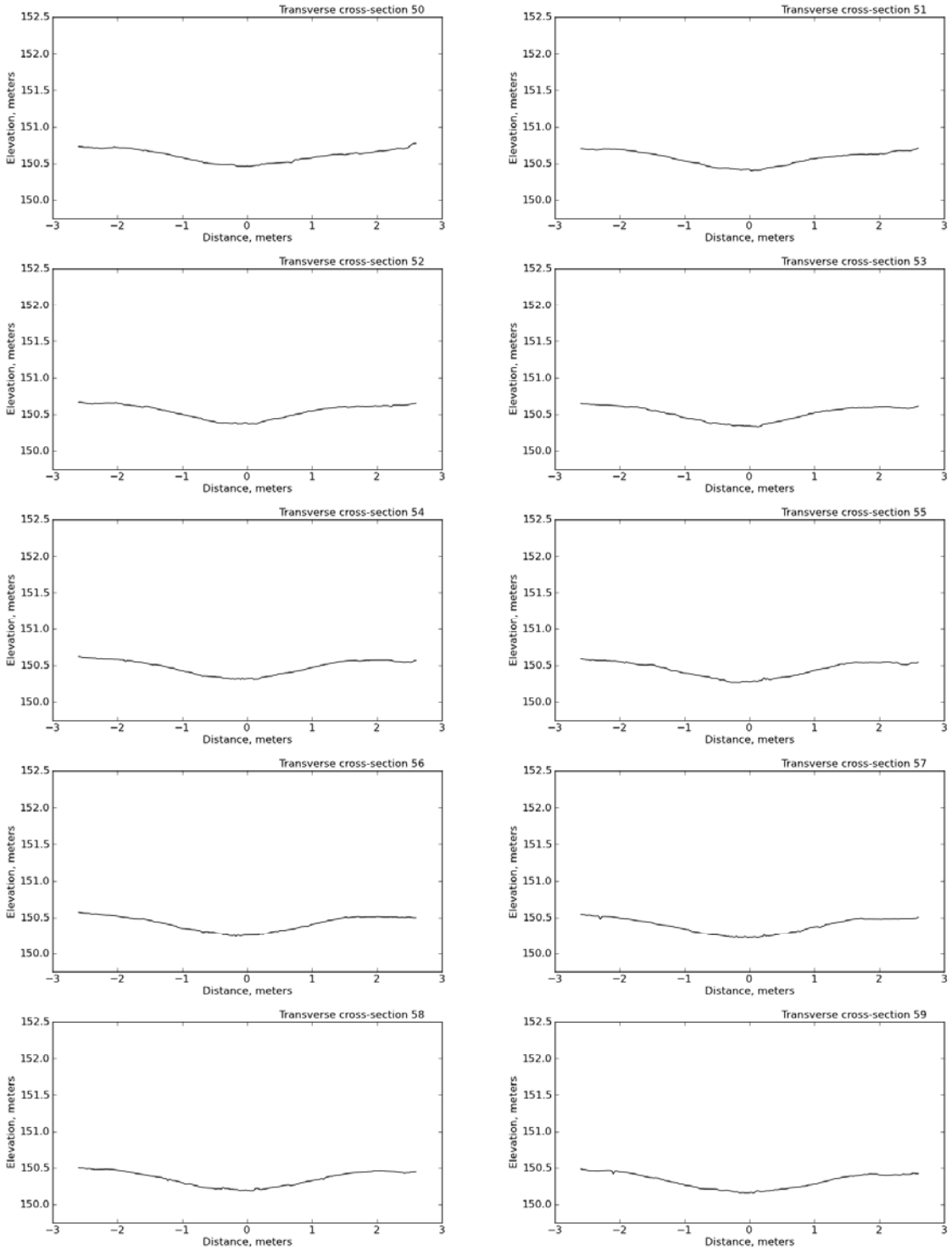

Figure A22. Transverse cross-sections 50 to 59 for SEP 3. Dashed line represents the clay layer and solid line represents the soil surface.

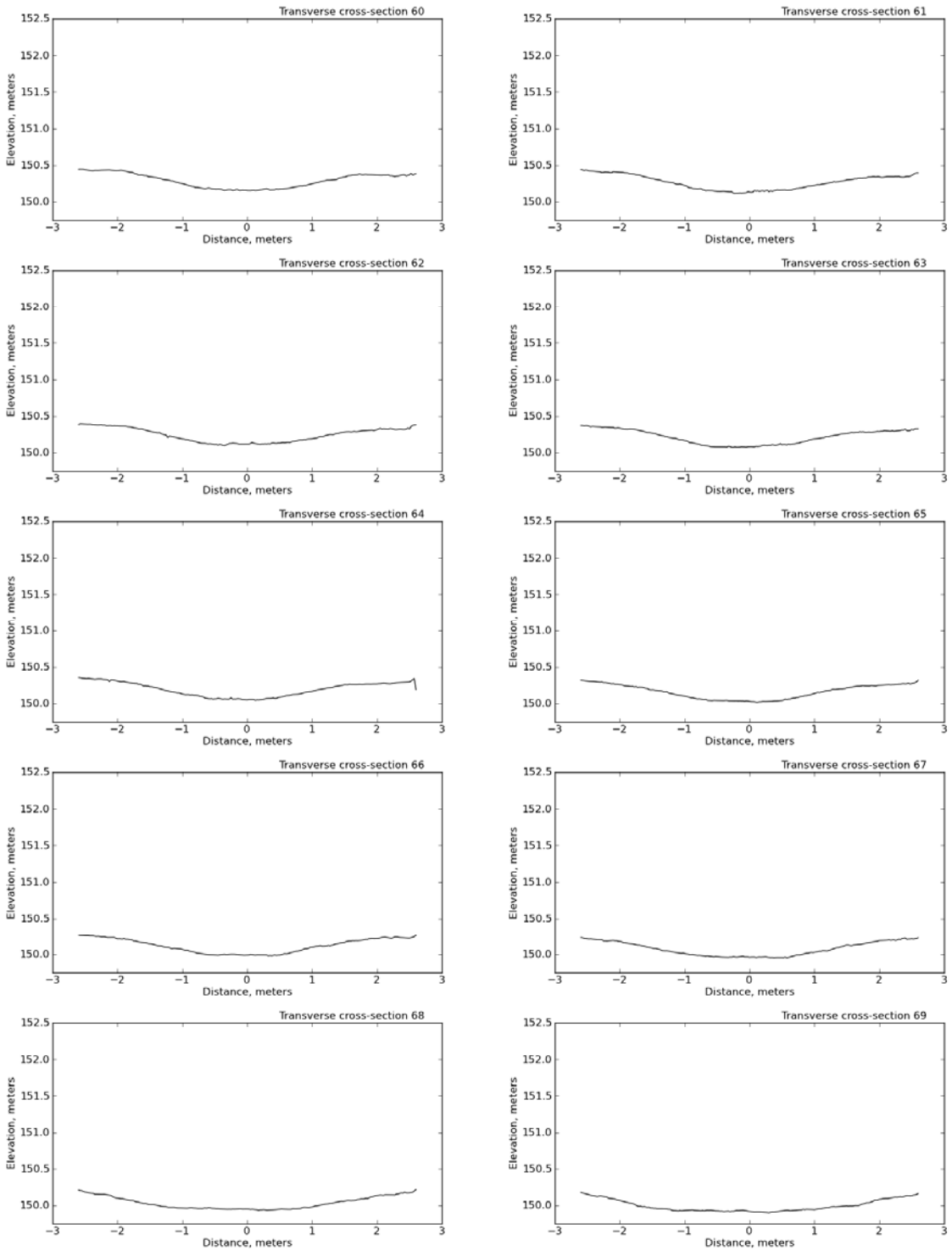

Figure A23. Transverse cross-sections 60 to 69 for SEP 3. Dashed line represents the clay layer and solid line represents the soil surface.

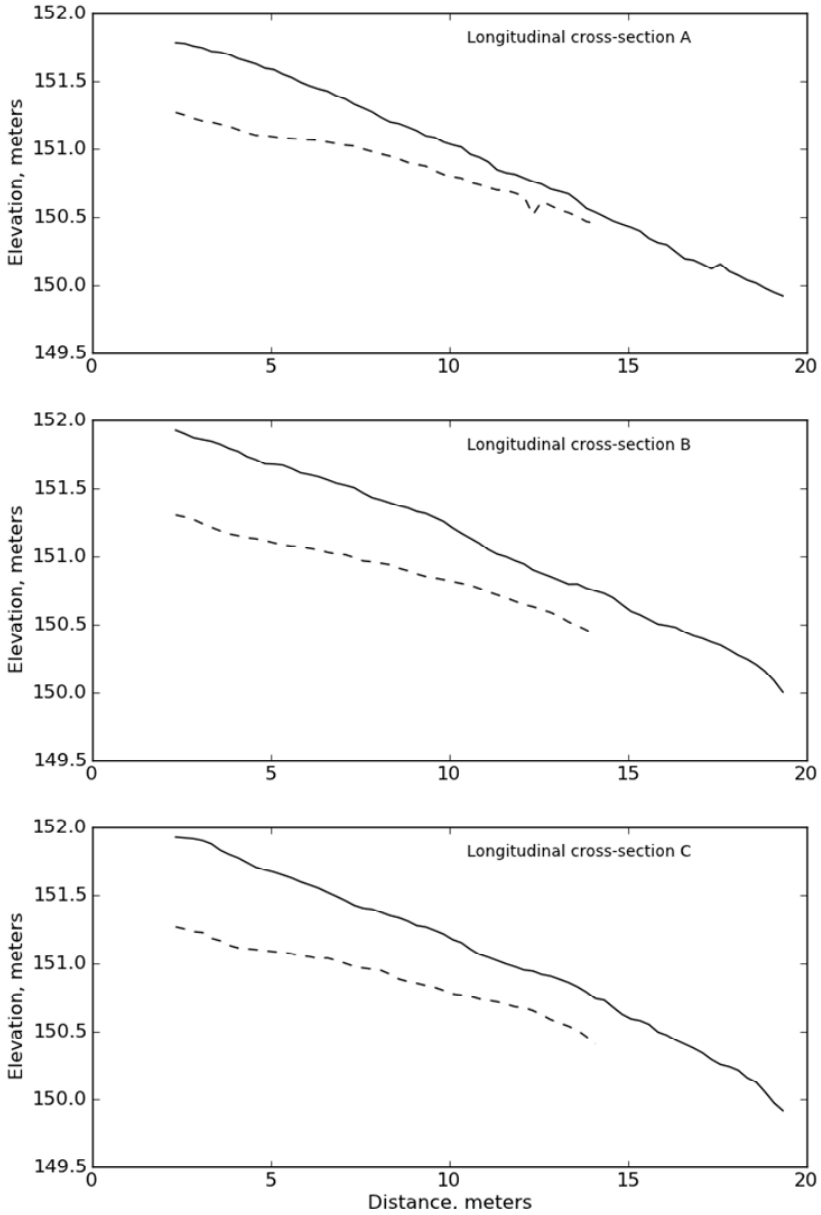

Figure A24. Longitudinal cross-sections for SEP 4.

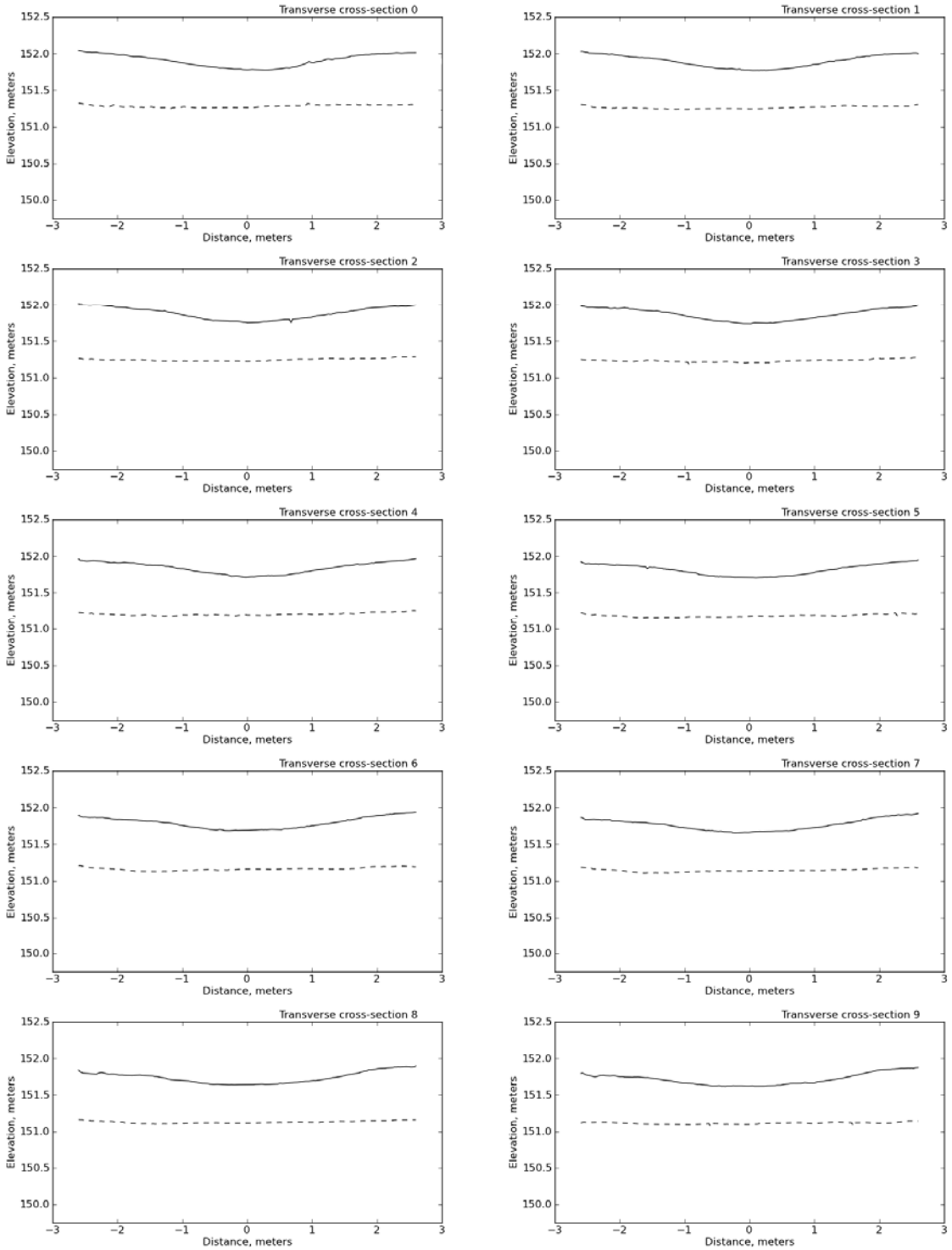

Figure A25. Transverse cross-sections 0 to 9 for SEP 4. Dashed line represents the clay layer and solid line represents the soil surface.

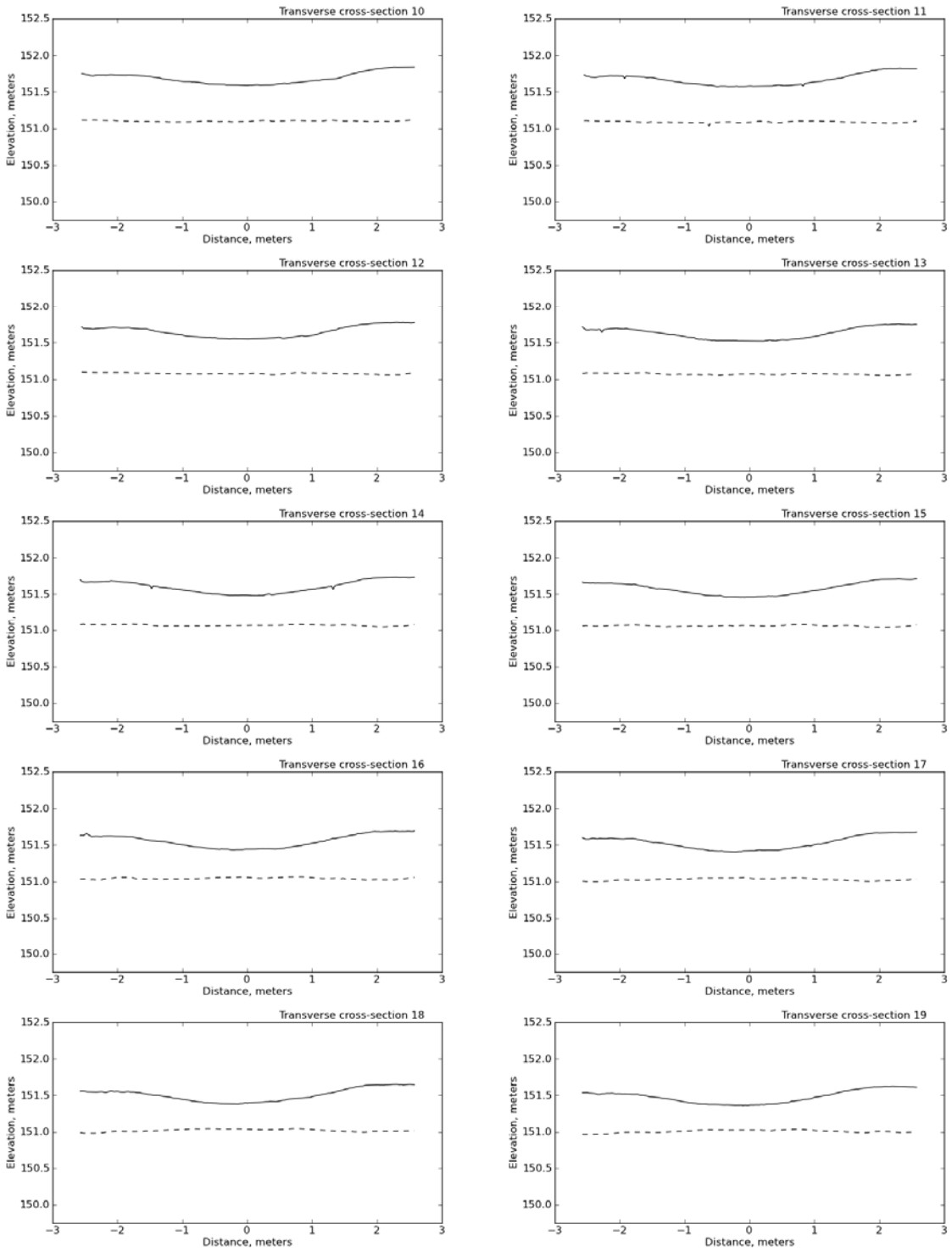

Figure A26. Transverse cross-sections 10 to 19 for SEP 4. Dashed line represents the clay layer and solid line represents the soil surface.

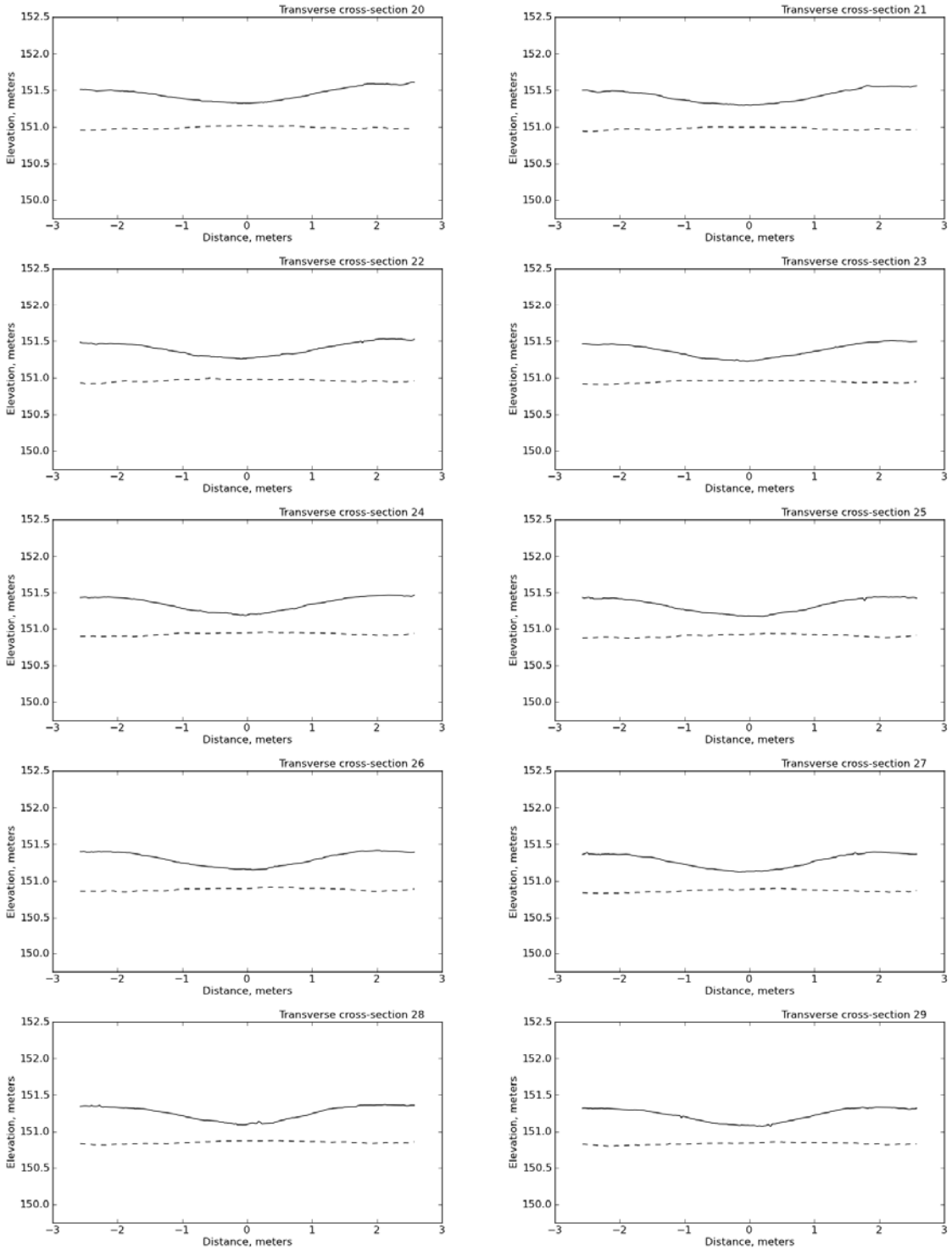

Figure A27. Transverse cross-sections 20 to 29 for SEP 4. Dashed line represents the clay layer and solid line represents the soil surface.

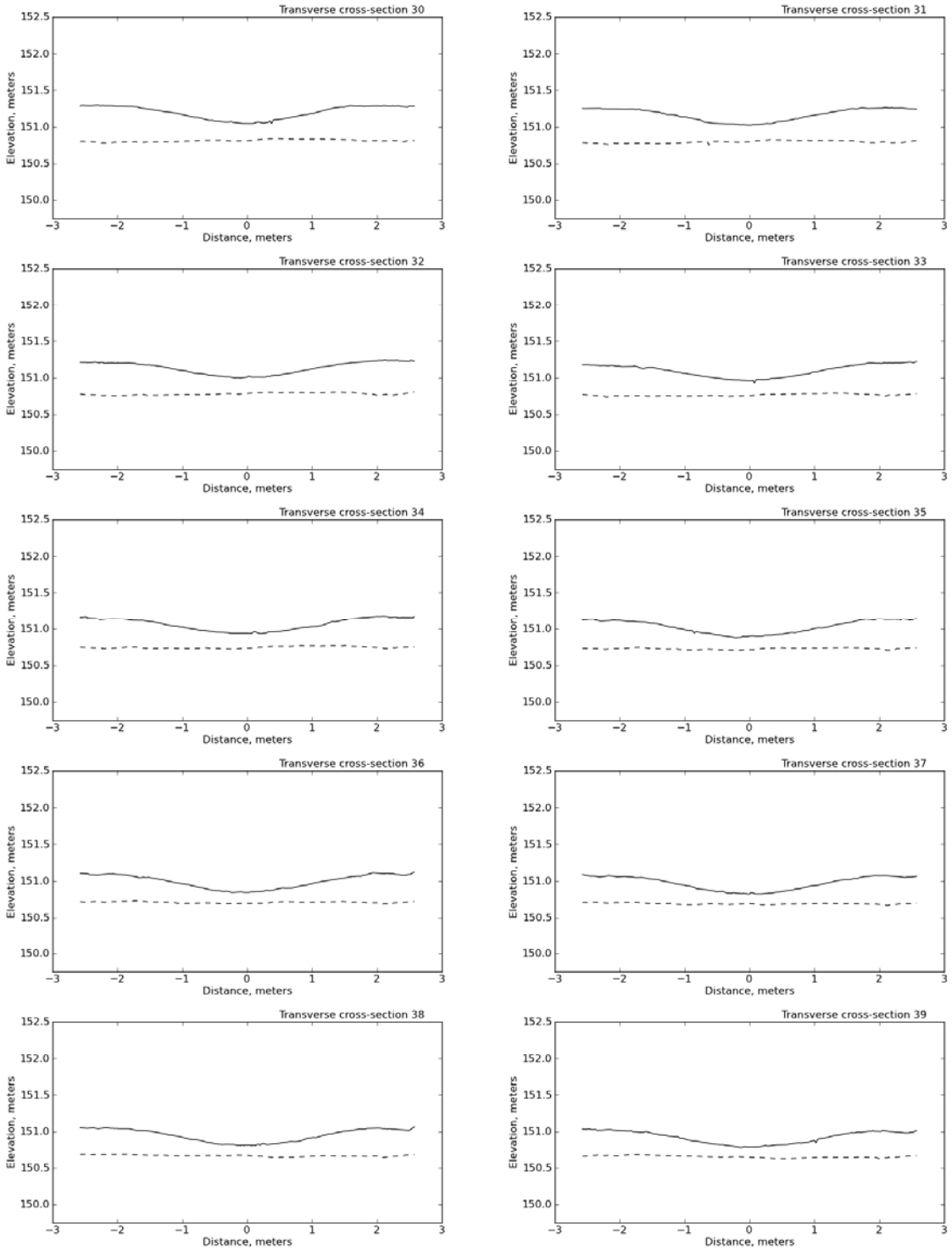

Figure A28. Transverse cross-sections 30 to 39 for SEP 4. Dashed line represents the clay layer and solid line represents the soil surface.

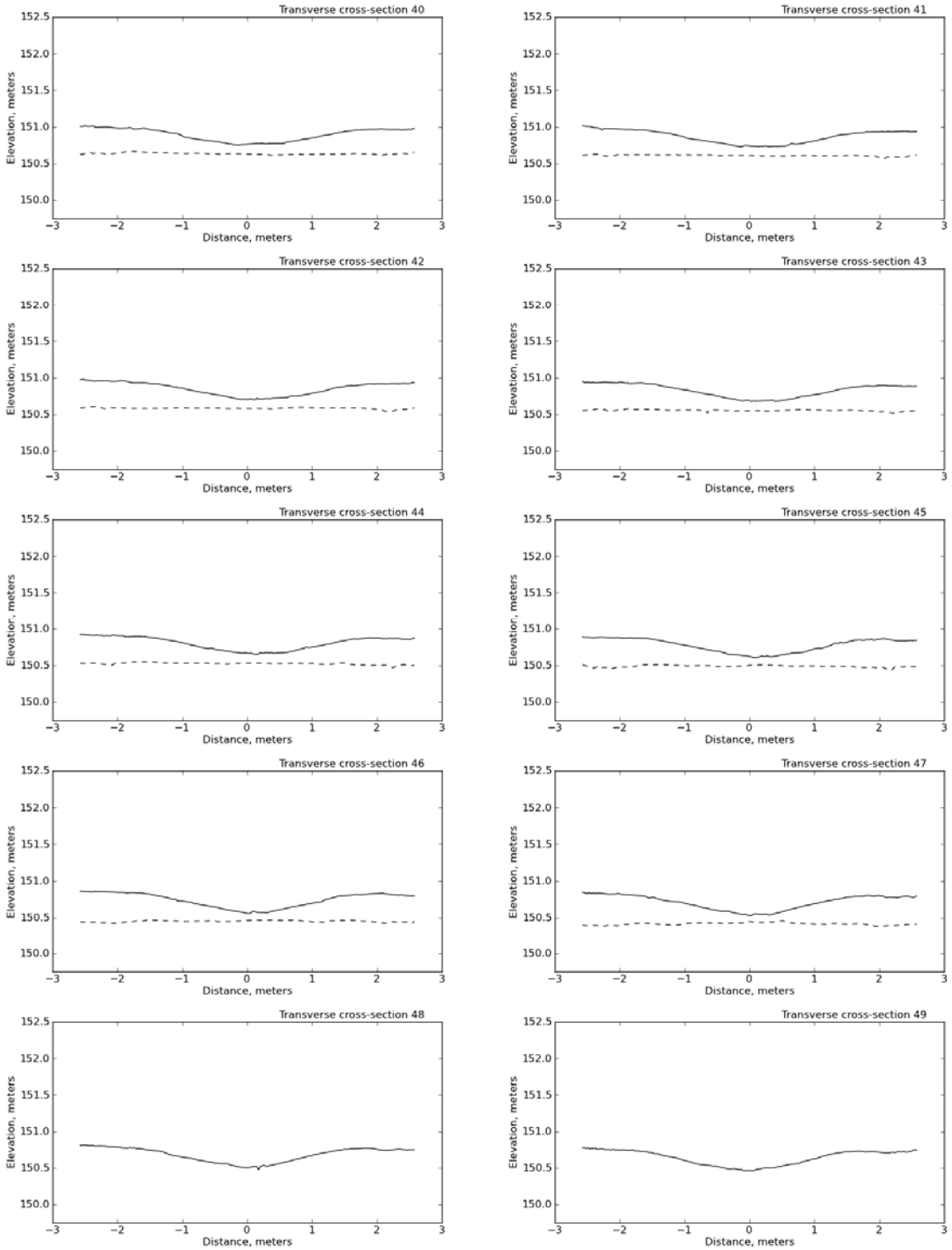

Figure A29. Transverse cross-sections 40 to 49 for SEP 4. Dashed line represents the clay layer and solid line represents the soil surface.

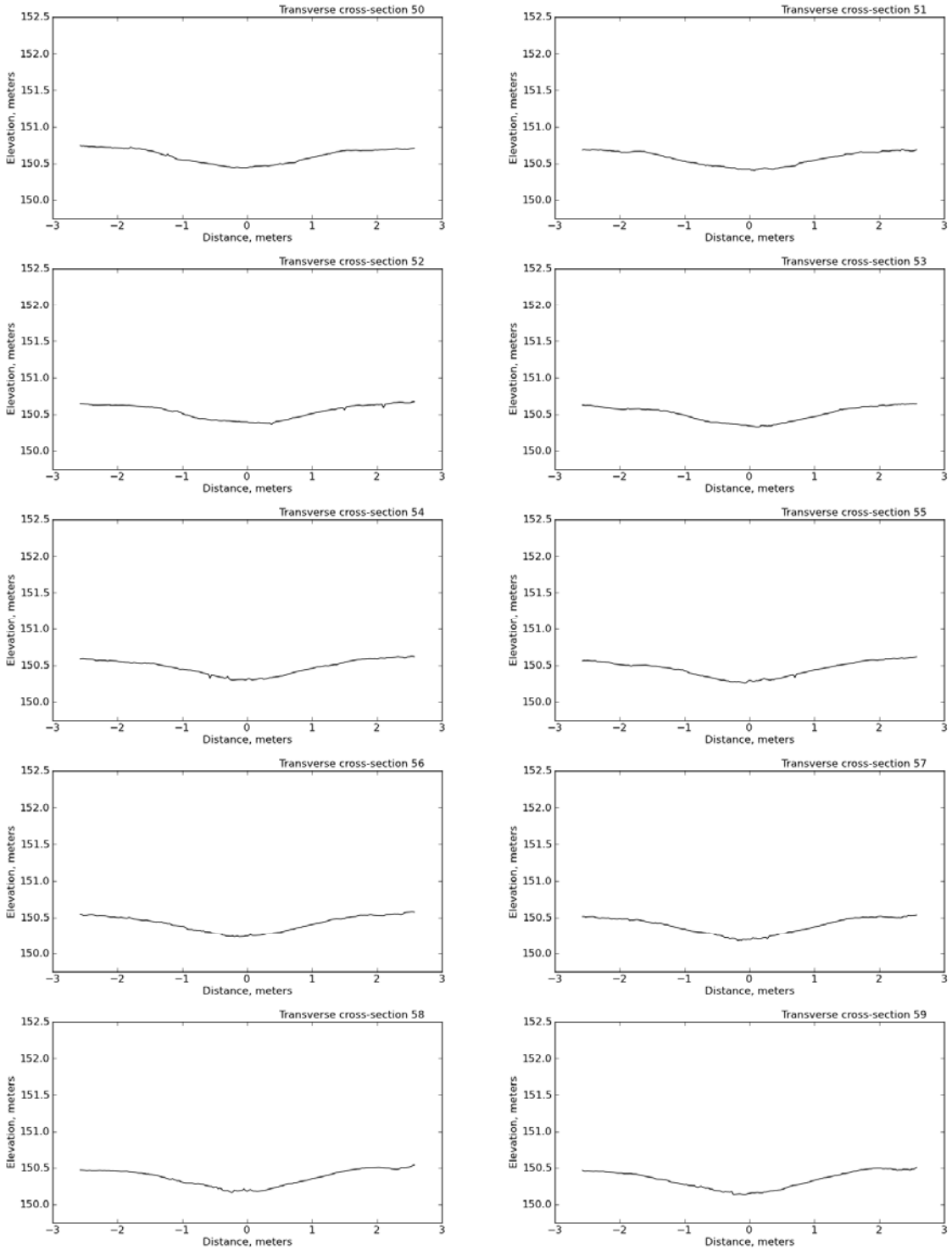

Figure A30. Transverse cross-sections 50 to 59 for SEP 4. Dashed line represents the clay layer and solid line represents the soil surface.

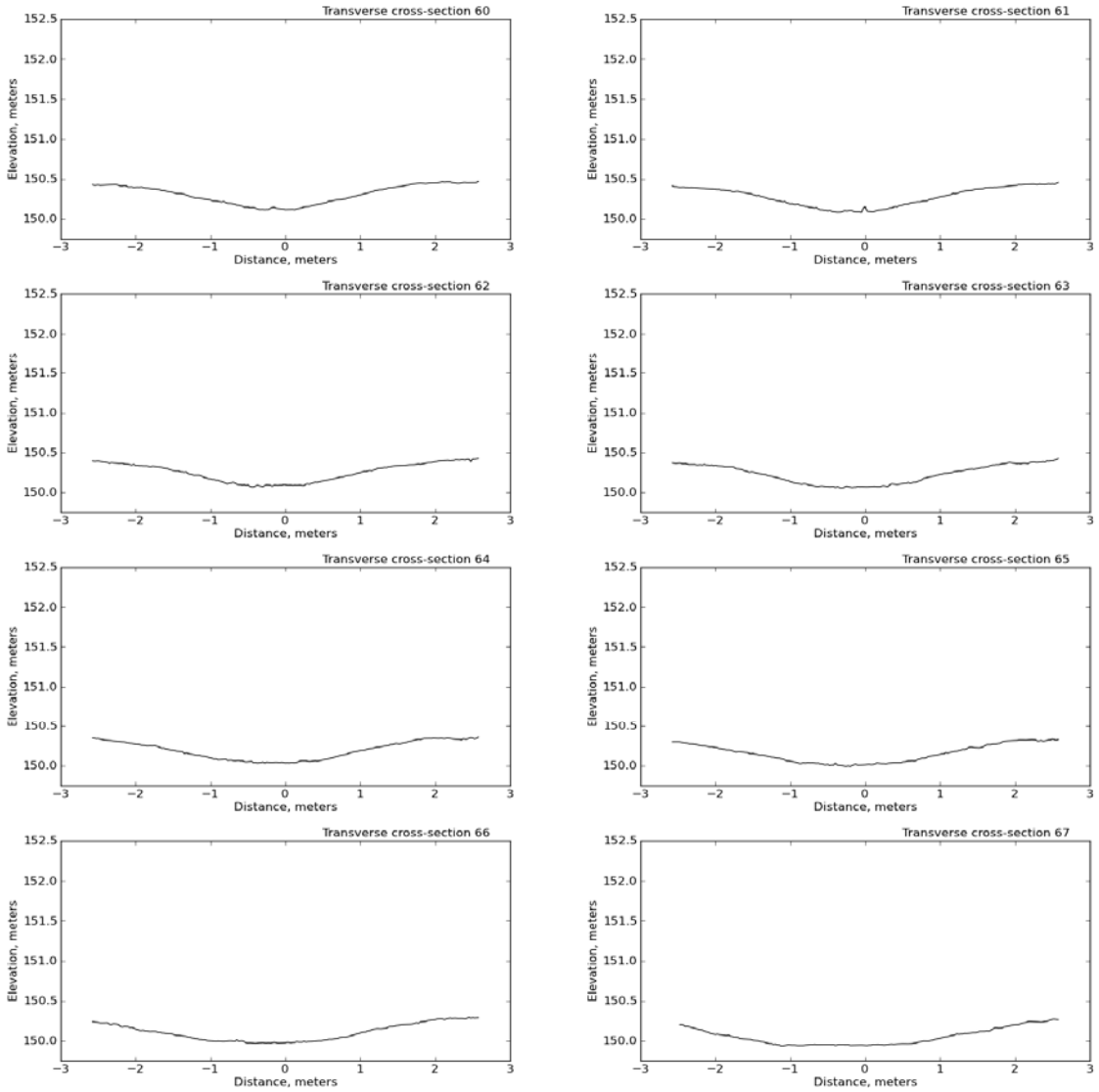

Figure A31. Transverse cross-sections 60 to 67 for SEP 4. Dashed line represents the clay layer and solid line represents the soil surface.

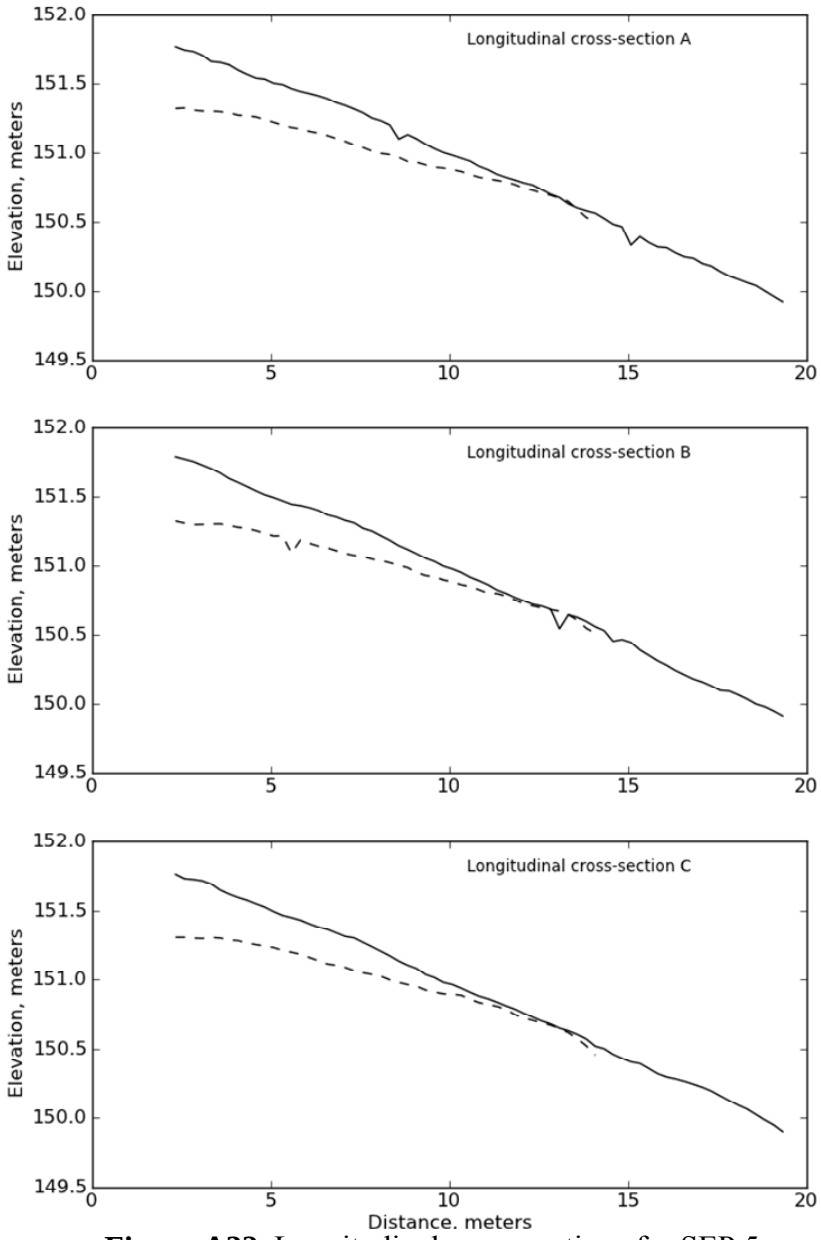

Figure A32. Longitudinal cross-sections for SEP 5.

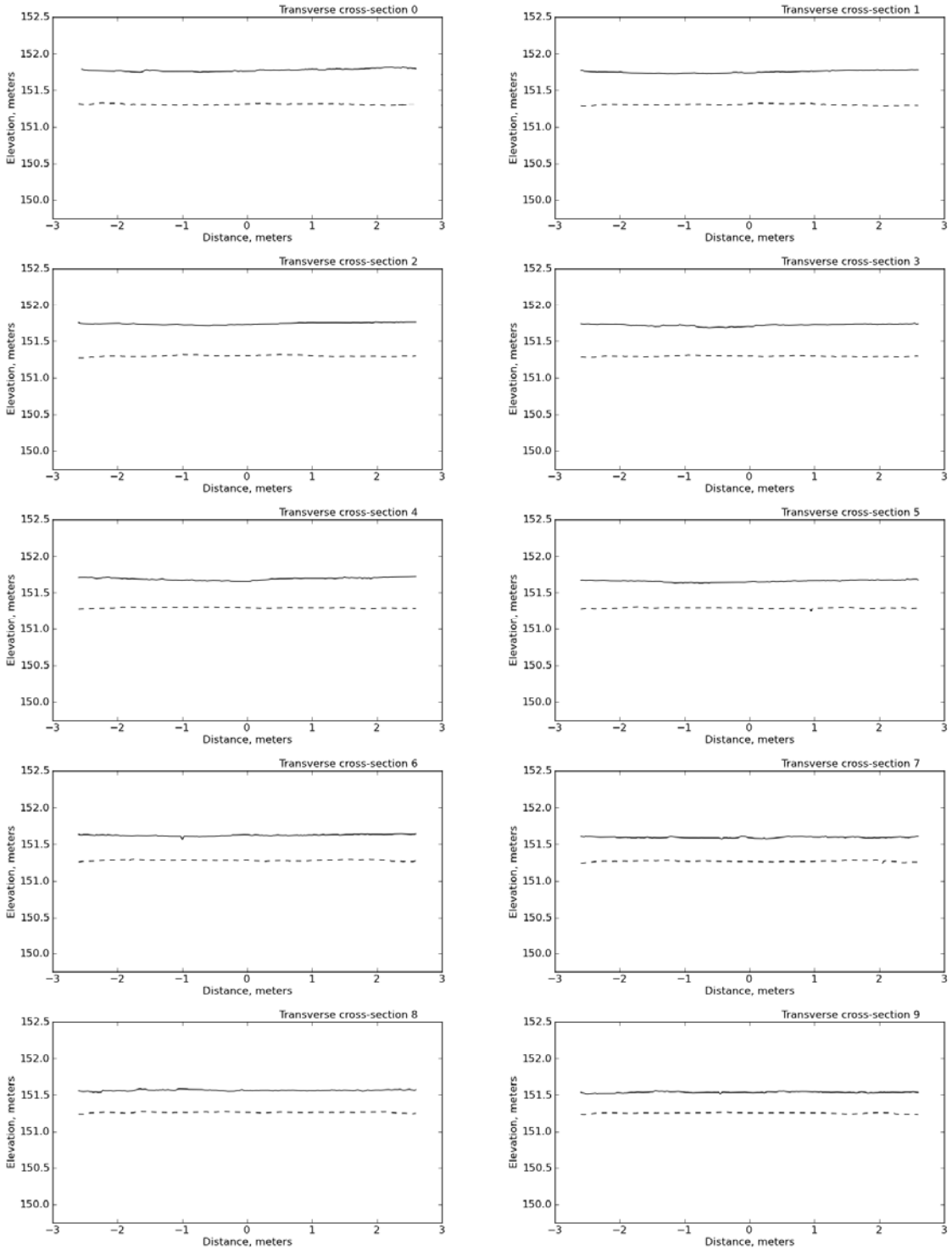

Figure A33. Transverse cross-sections 0 to 9 for SEP 5. Dashed line represents the clay layer and solid line represents the soil surface.

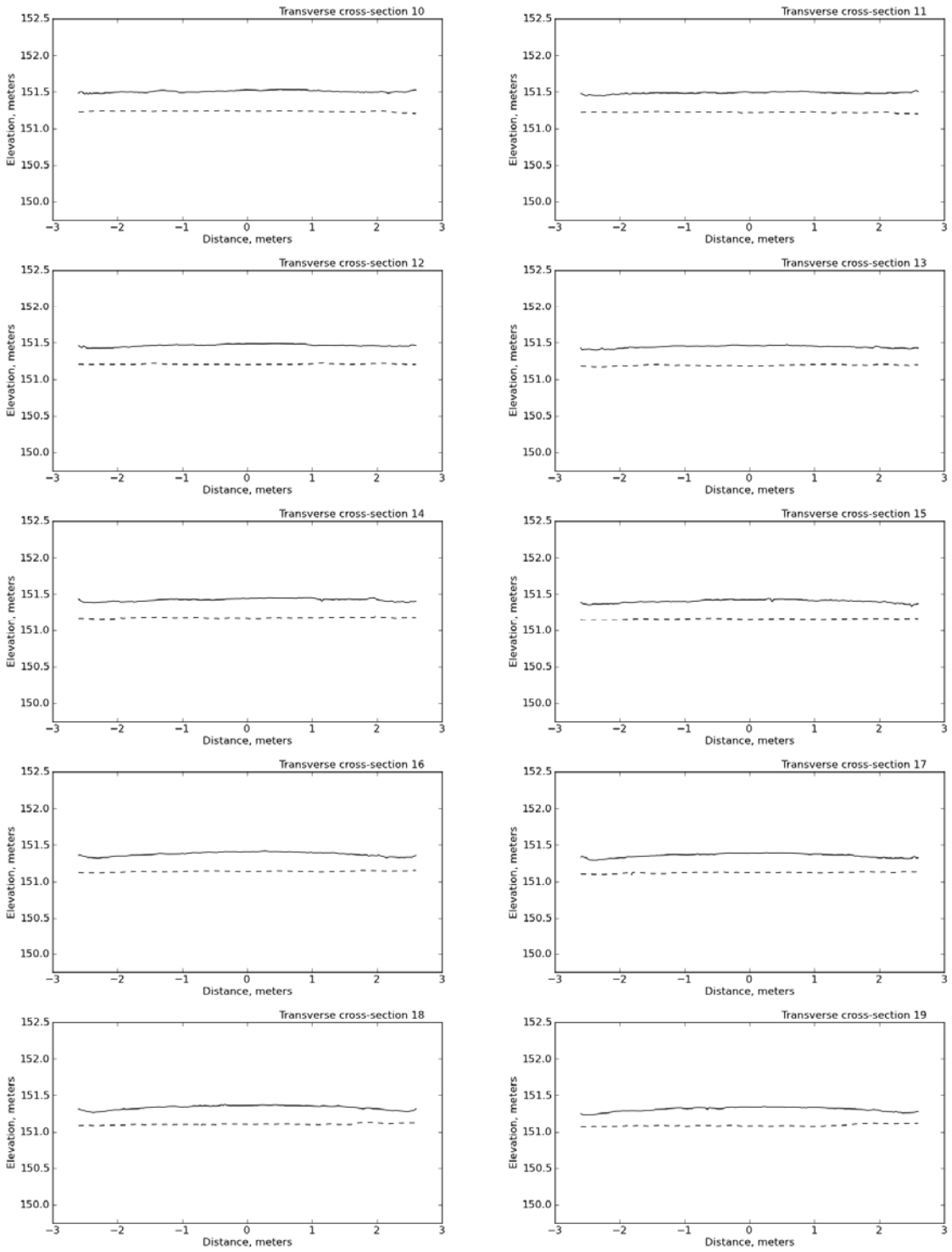

Figure A34. Transverse cross-sections 10 to 19 for SEP 5. Dashed line represents the clay layer and solid line represents the soil surface.

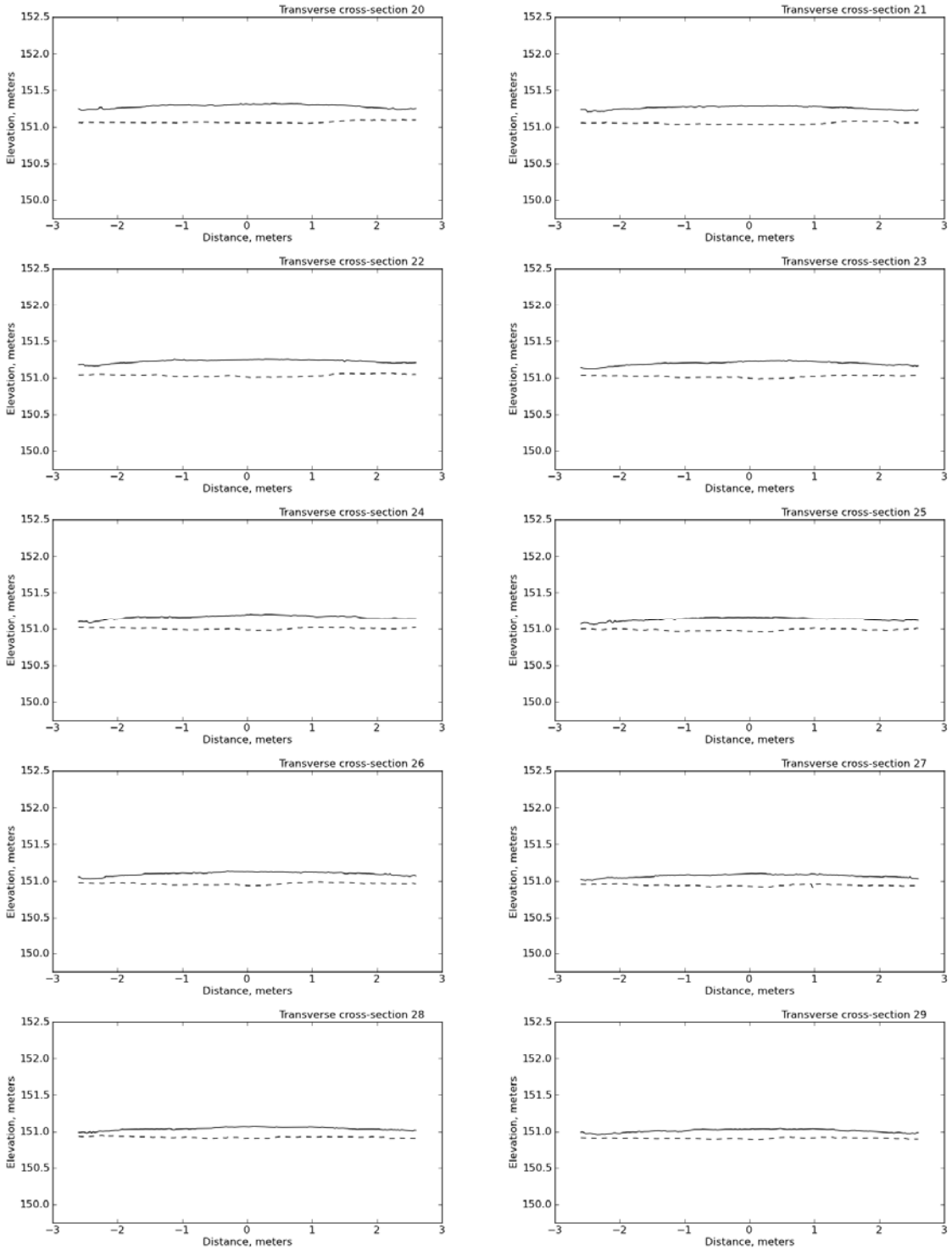

Figure A35. Transverse cross-sections 20 to 29 for SEP 5. Dashed line represents the clay layer and solid line represents the soil surface.

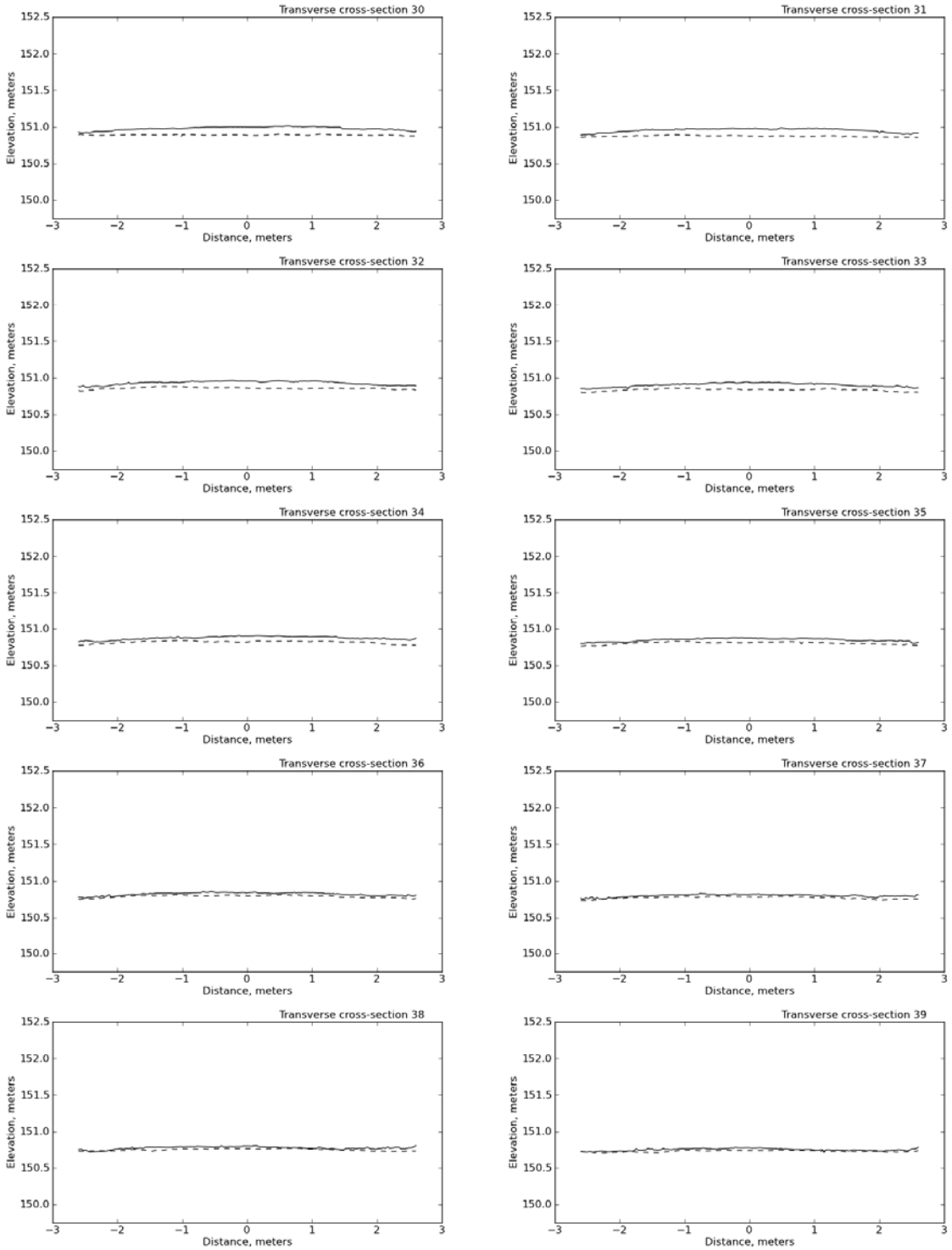

Figure A36. Transverse cross-sections 30 to 39 for SEP 5. Dashed line represents the clay layer and solid line represents the soil surface.

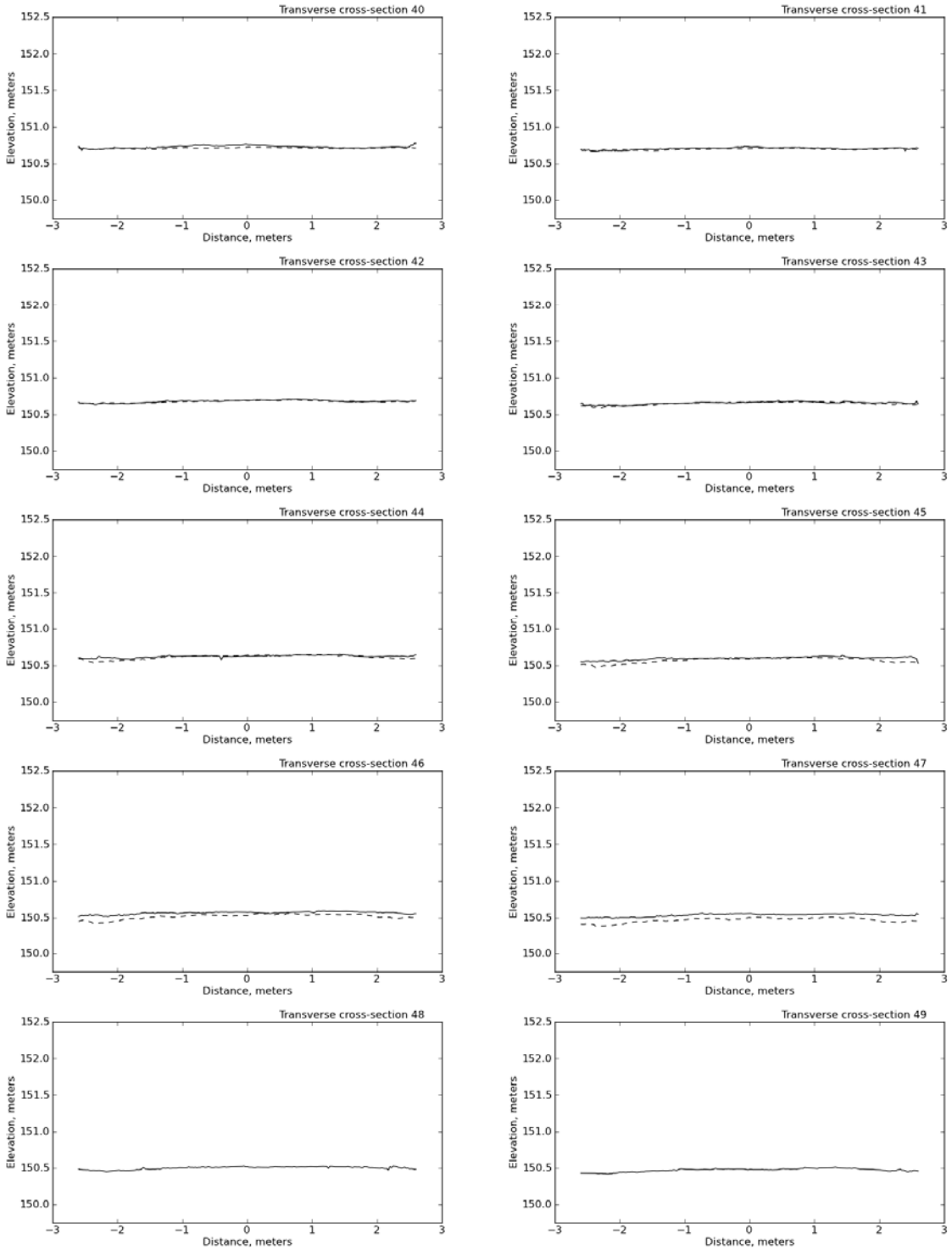

Figure A37. Transverse cross-sections 40 to 49 for SEP 5. Dashed line represents the clay layer and solid line represents the soil surface.

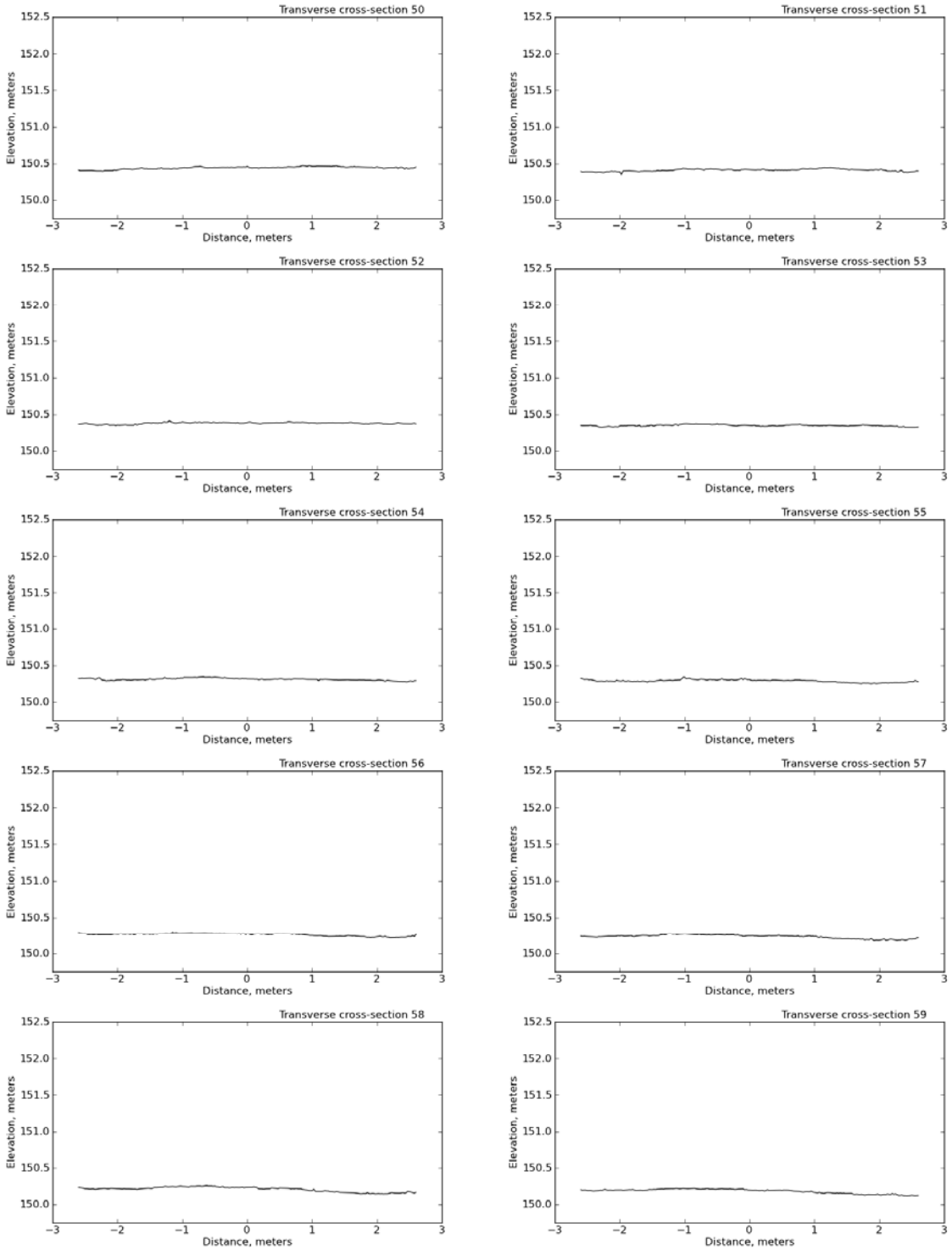

Figure A38. Transverse cross-sections 50 to 59 for SEP 5. Dashed line represents the clay layer and solid line represents the soil surface.

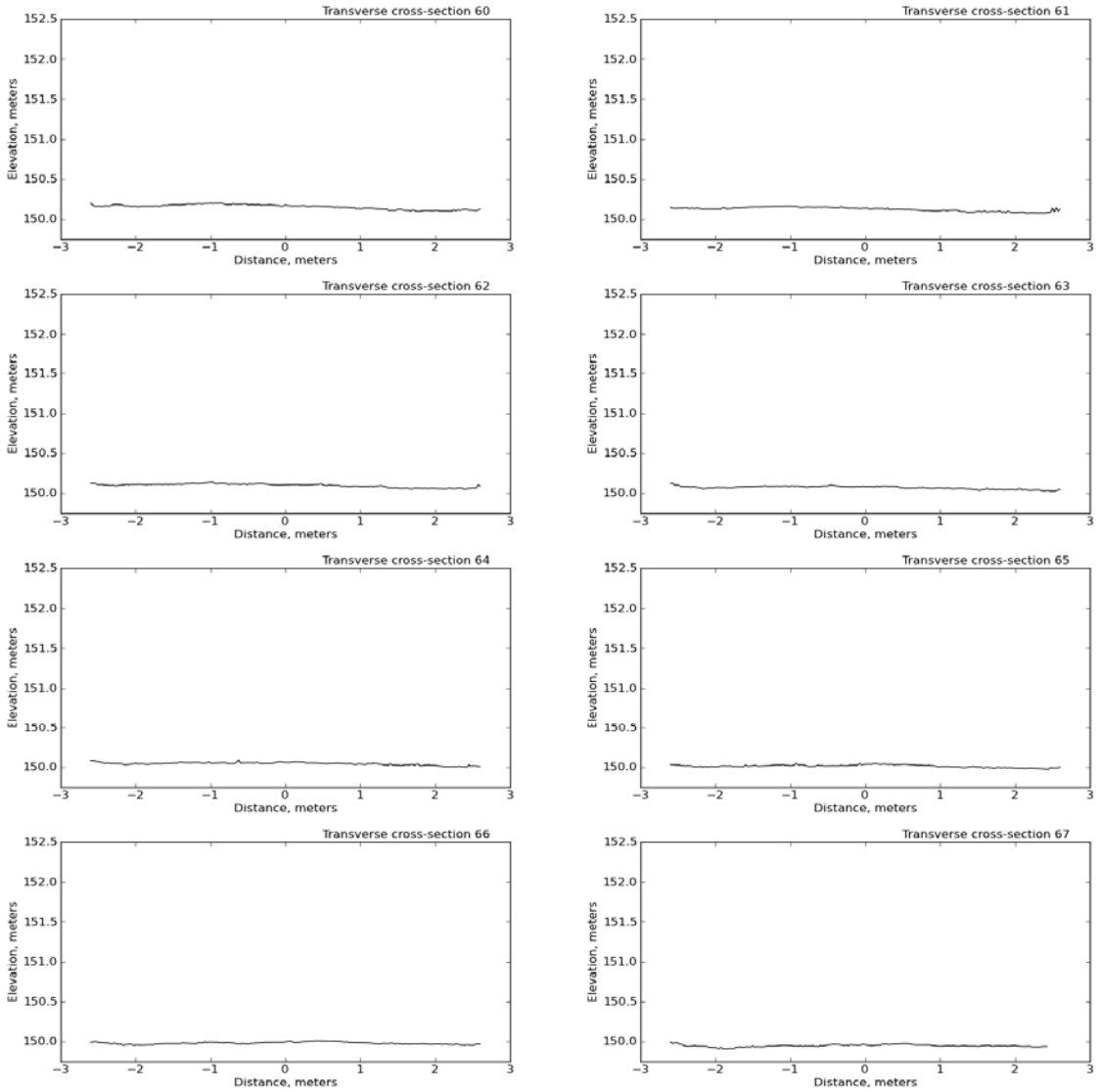

Figure A39. Transverse cross-sections 60 to 67 for SEP 5. Dashed line represents the clay layer and solid line represents the soil surface.

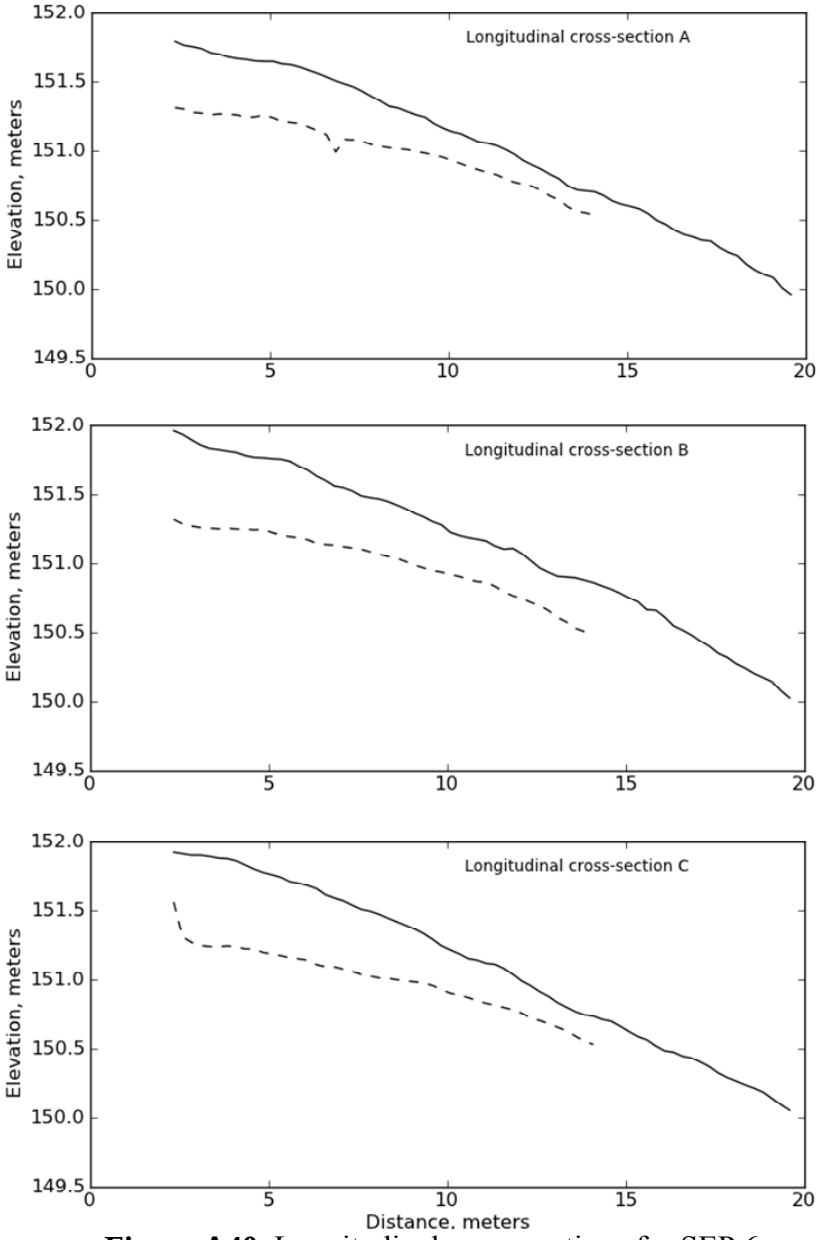

Figure A40. Longitudinal cross-sections for SEP 6.

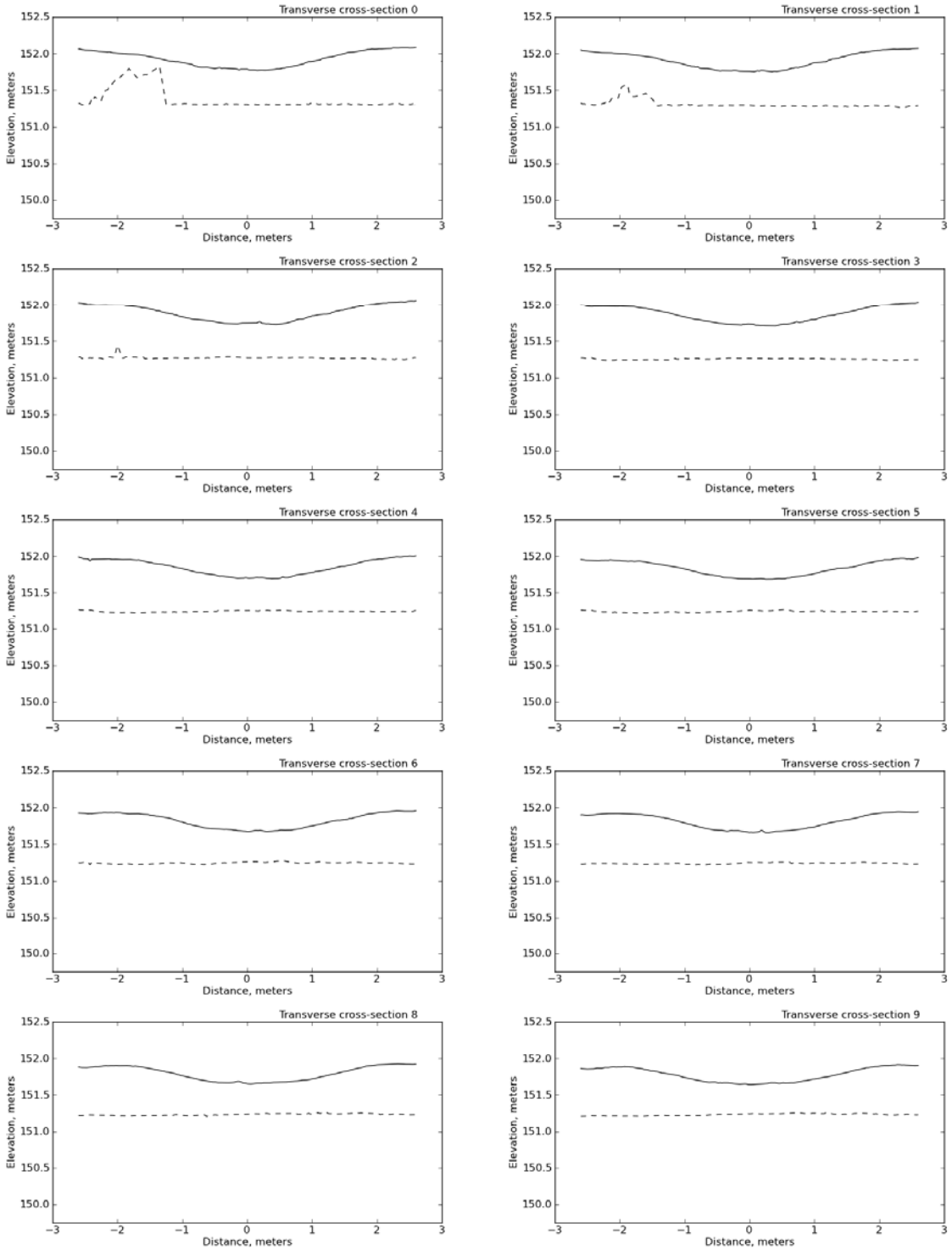

Figure A41. Transverse cross-sections 0 to 9 for SEP 6. Dashed line represents the clay layer and solid line represents the soil surface.

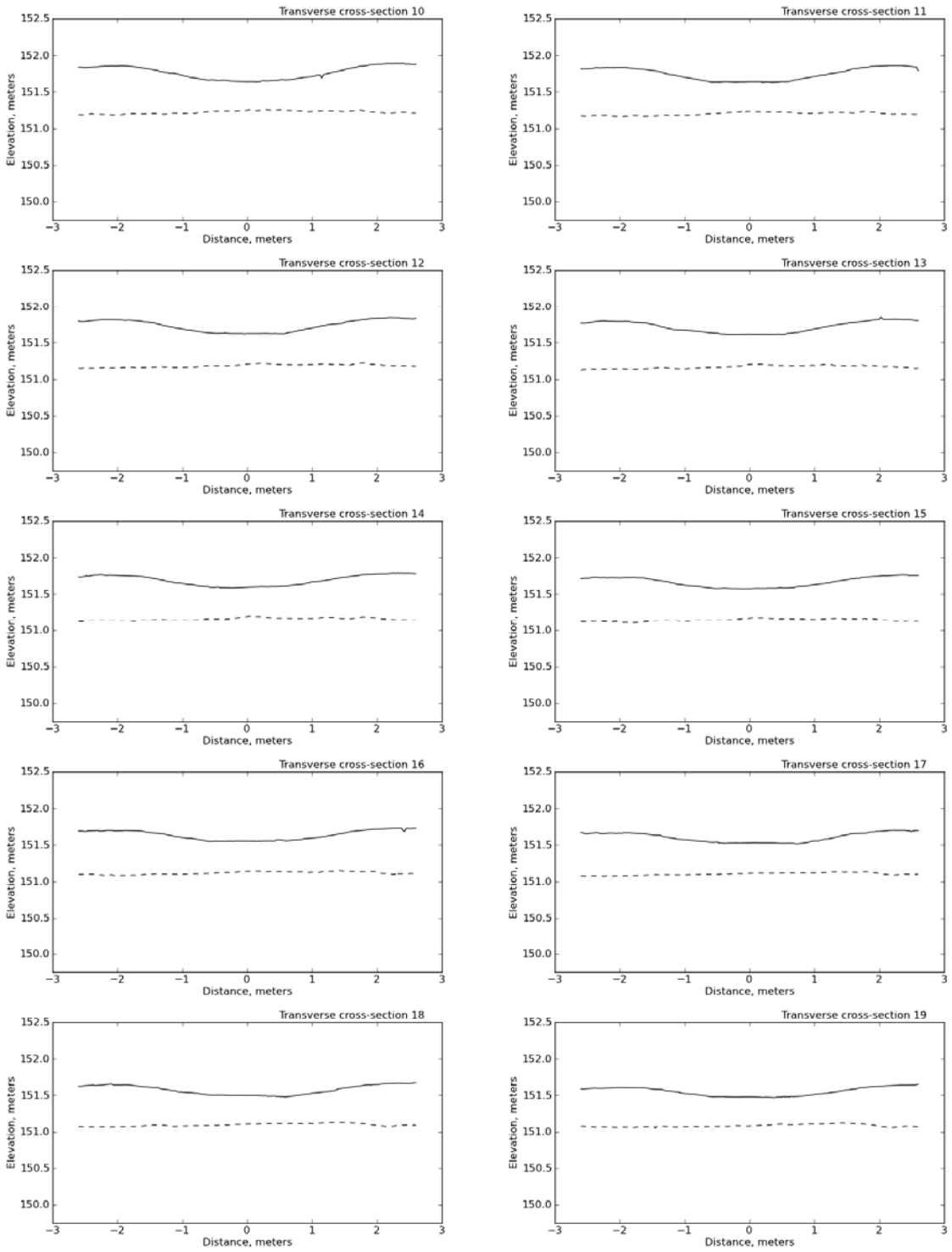

Figure A42. Transverse cross-sections 10 to 19 for SEP 6. Dashed line represents the clay layer and solid line represents the soil surface.

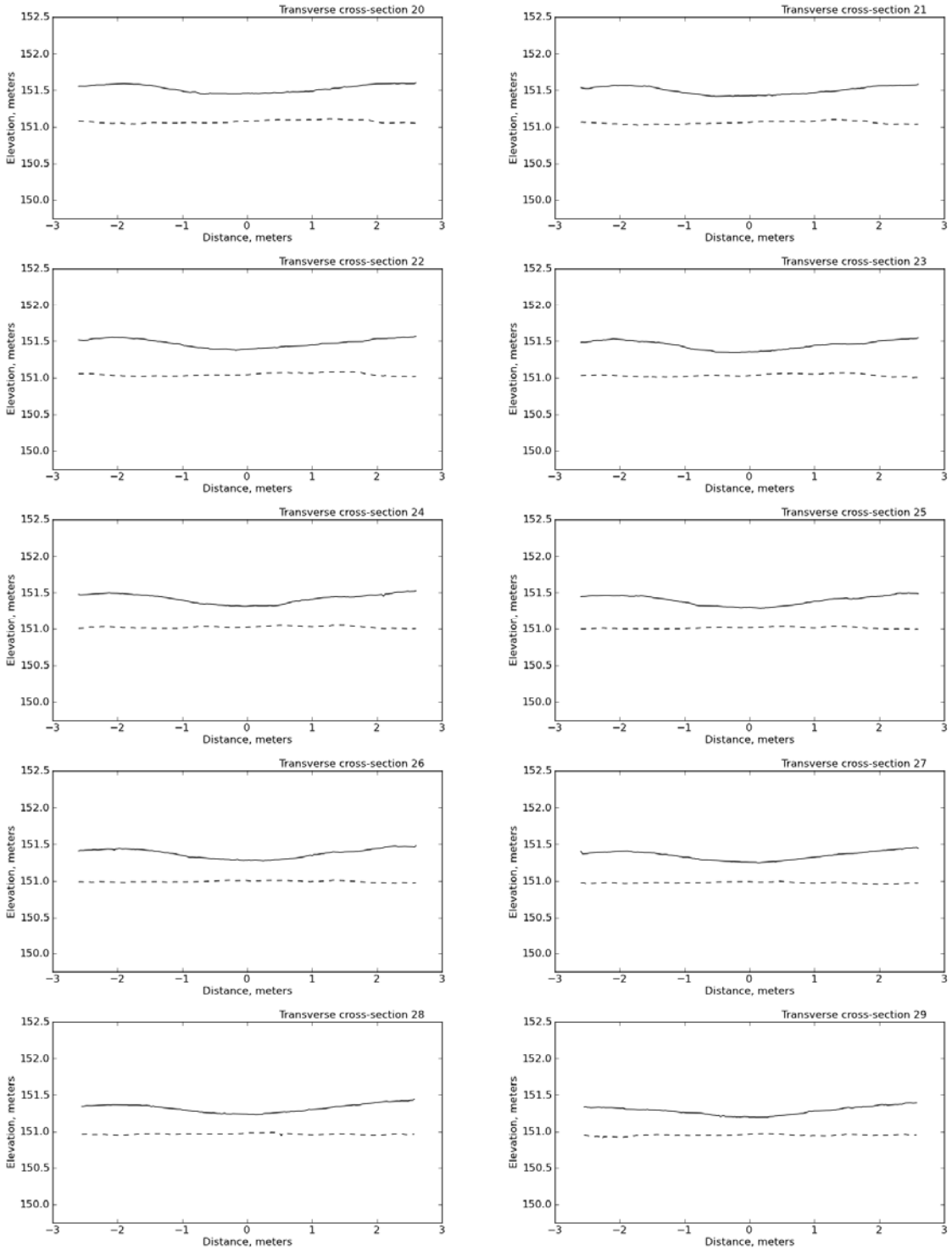

Figure A43. Transverse cross-sections 20 to 29 for SEP 6. Dashed line represents the clay layer and solid line represents the soil surface.

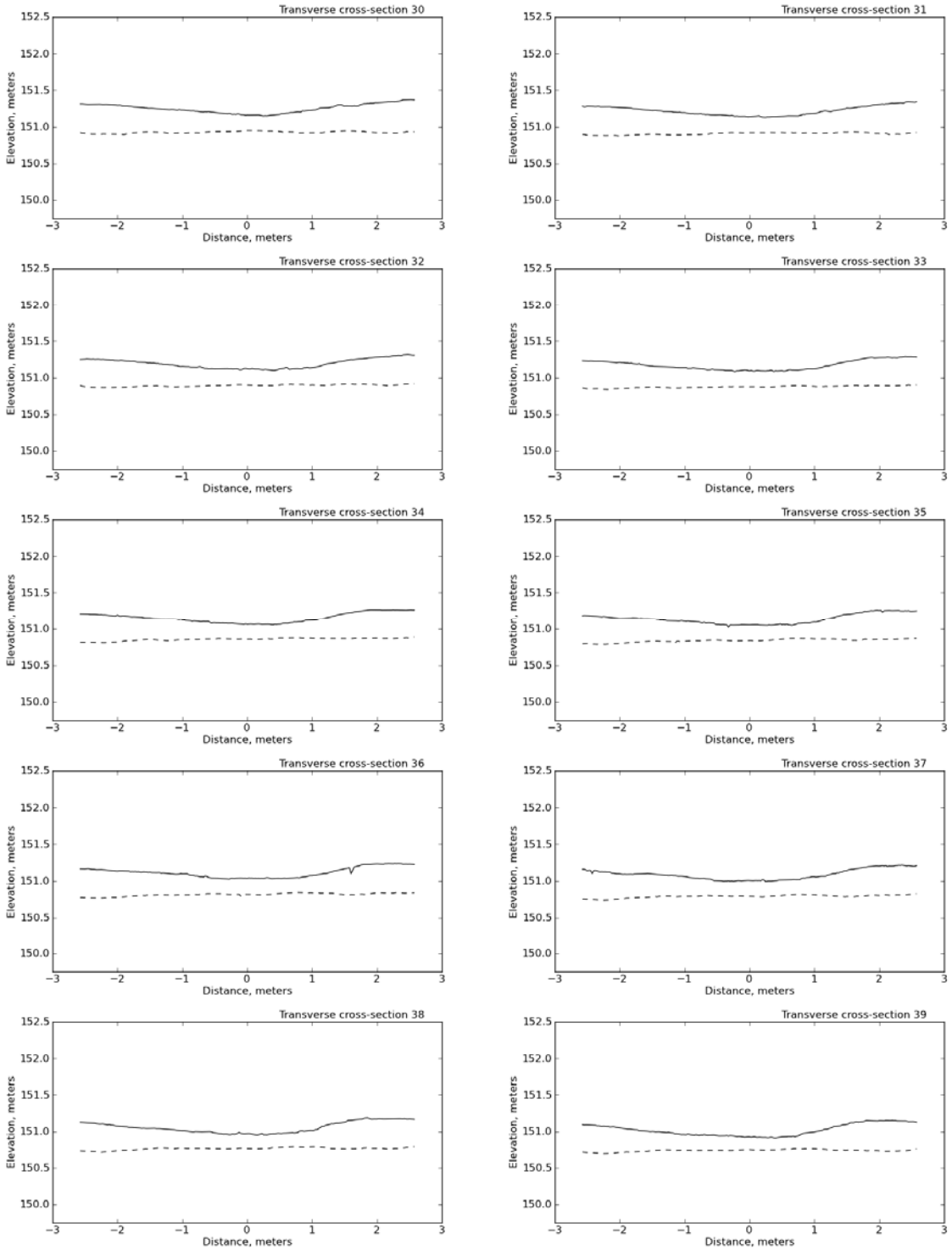

Figure A44. Transverse cross-sections 30 to 39 for SEP 6. Dashed line represents the clay layer and solid line represents the soil surface.

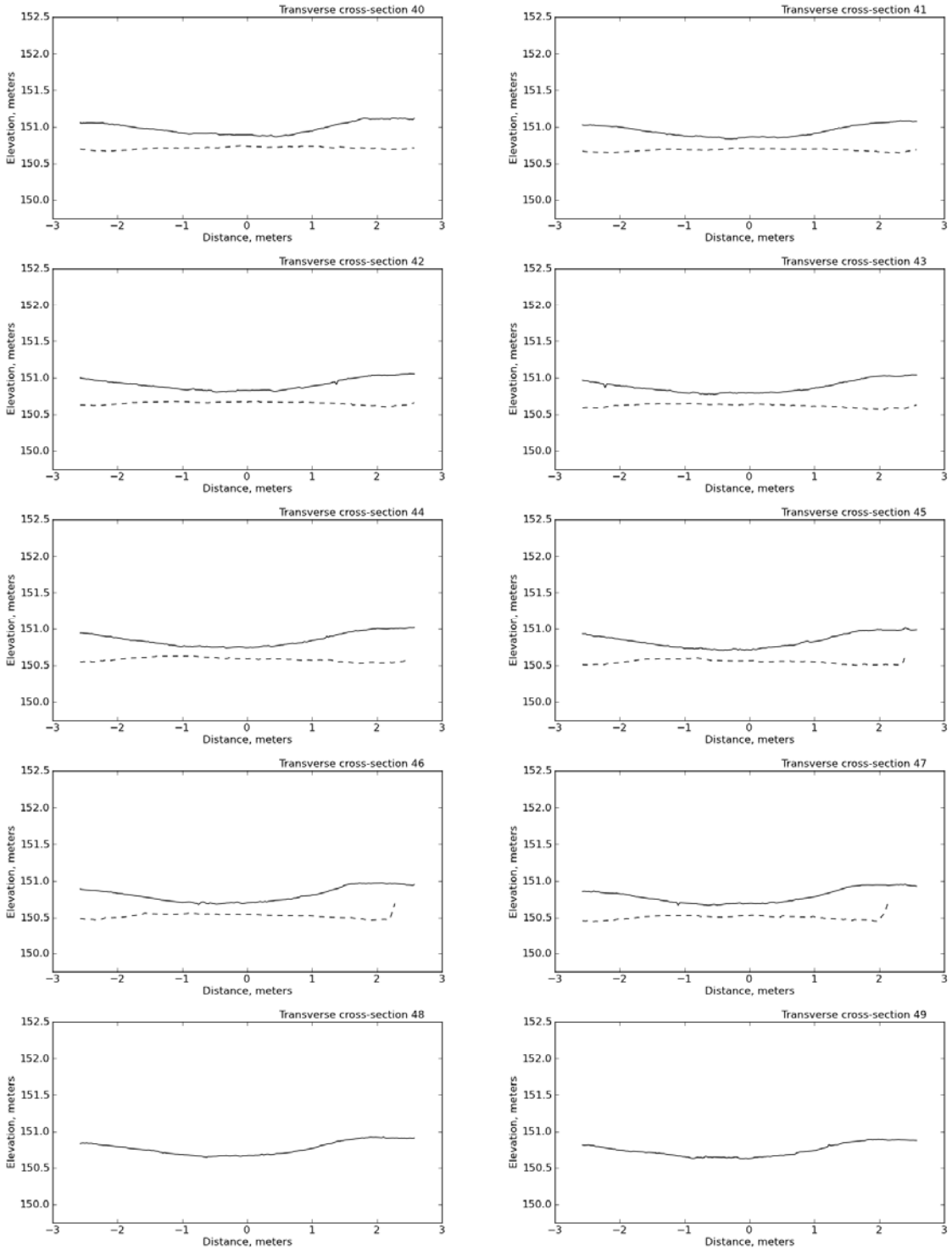

Figure A45. Transverse cross-sections 40 to 49 for SEP 6. Dashed line represents the clay layer and solid line represents the soil surface.

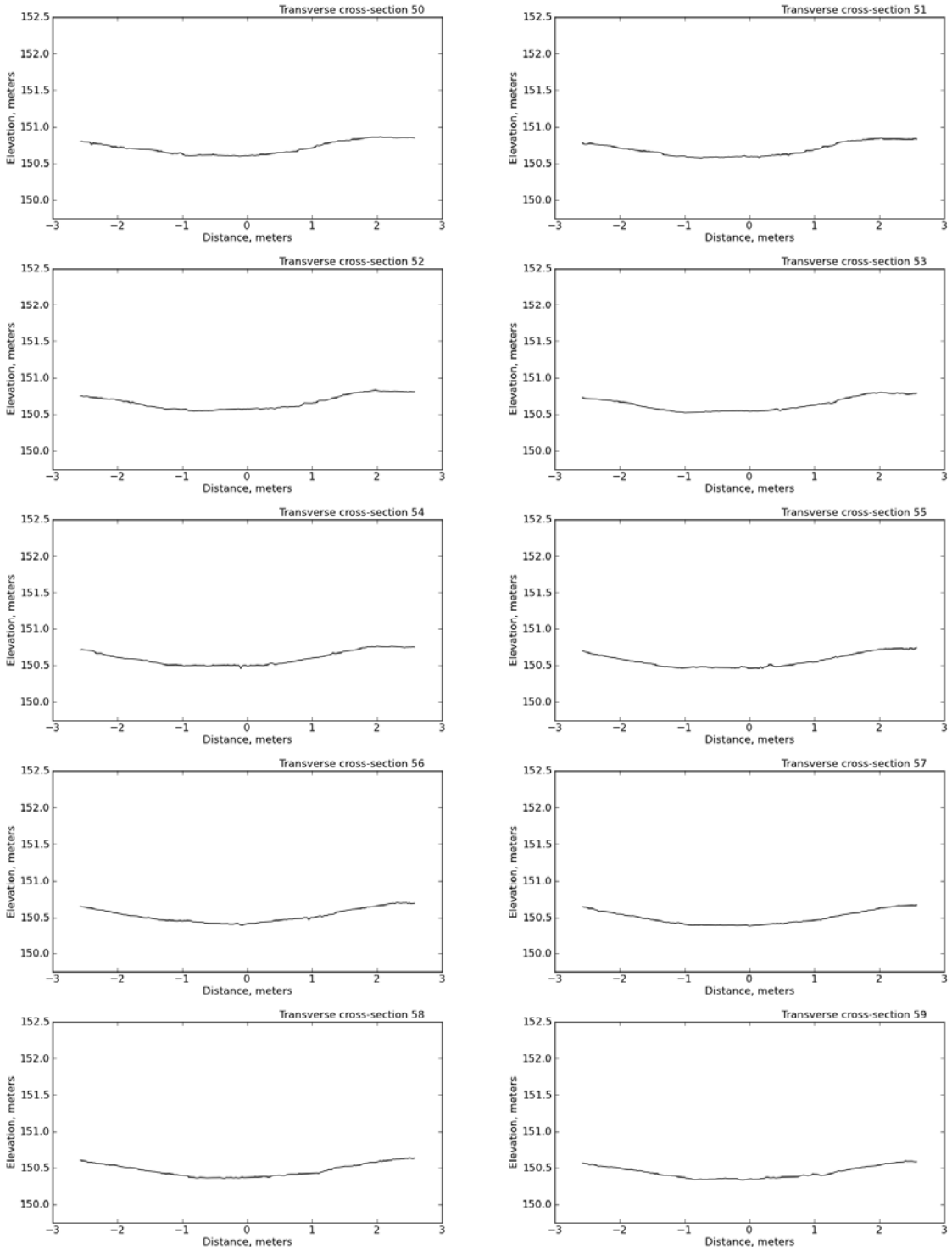

Figure A46. Transverse cross-sections 50 to 59 for SEP 6. Dashed line represents the clay layer and solid line represents the soil surface.

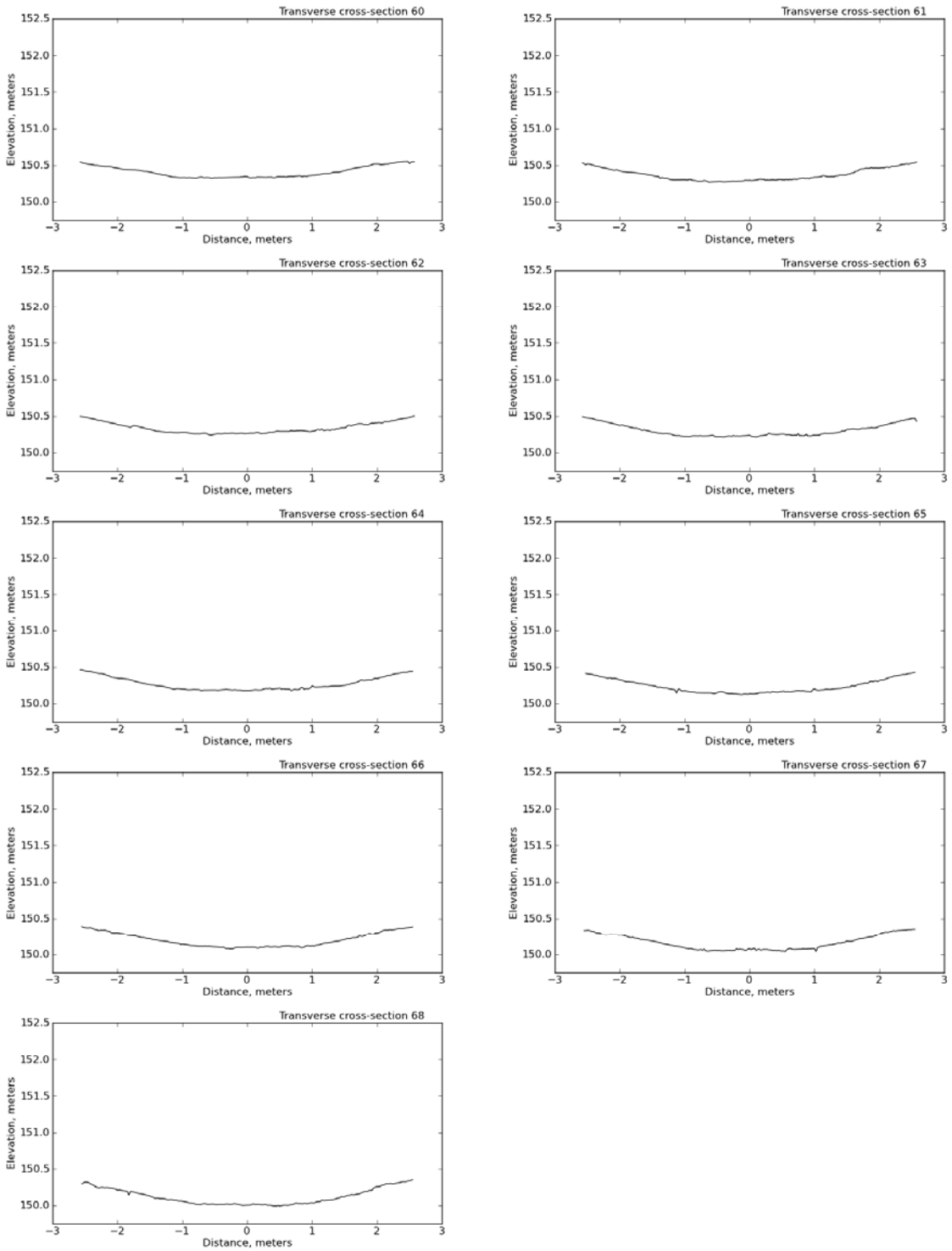

Figure A47. Transverse cross-sections 60 to 68 for SEP 6. Dashed line represents the clay layer and solid line represents the soil surface.